33

3-PHASE GATE-TURN OFF THYRISTOR INVERTER

by

D.A. KLEYN

Submitted to the

Department of Electrical Engineering

of the

University of Cape Town

in fulfilment of the requirements

for the Degree of M.Sc.(Eng.)

1986

INDEX

Page

ACKNOWLEDGEMENTS

I would like to express my appreciation to the following people for the help I have received during the course of the project:
K. Hoffman, M. Attfield, N. Wright, D. Kenyon, A. Meyer of GEC South Africa (Pty) Ltd, B. Wilson of GEC Projects (Pty) Ltd.

I would also like to thank my typist Mrs. I. von Bentheim for the work she has done typing this manuscript.

I would also like to express my sincere thanks to:

GEC South Africa (Pty) Ltd
GEC Projects (Pty) Ltd

who were the main sponsors of the project.

The following organisations also donated equipment, without which the project would not have been possible.

SEMIKRON SA ((Pty) Ltd
International Components (Pty) Ltd
Arthur Trevor Williams (Pty) Ltd
Cutler-Hammer SA Ltd
EDAC (Pty) Ltd

ABSTRACT

The requirements of a standard 3-phase Induction Motor driven by a Voltage Source Inverter (VSI) are studied. A full 3-phase Variable Speed Drive (VSD) and its controller have been designed, constructed and tested. Gate Turn-Off Thyristors (GTO's) are used as the main switching elements in the Inverter stage of the Drive. The drive requirements of GTO's are studied in detail.

NOMENCLATURE

VSI	Voltage Source Inverter
VSD	Variable Speed Drive
PWM	Pulse Width Modulation
GTO	Gate Turn-Off Thyristor
S.C.	Short-Circuit
O.C.	Open-Circuit
R1	Stator Resistance
$R2'$	Referred Rotor Resistance
X1	Stator Reactance
$X2'$	Referred Rotor Reactance
Rm	Magnetising Resistance
Xm	Magnetising Reactance
Z_s	Stator Impedance
T	Torque
T_{max}	Pull-Out Torque
S	Slip
S_{max}	Slip at Pull-Out Torque
ϕ	Airgap Flux
W_s	Synchronous Speed (Rad/Sec)
W_m	Mechanical Speed (Rad/Sec)
Cs	Snubber Capacitor
Rs	Snubber Resistor
P_{RS}	Power Rating of Snubber Resistor
Ds	Snubber Diode
DF	Freewheel Diode
B	Magnetic Flux Density
B_{SAT}	Saturated Magnetic Flux Density
H	Magnetic Field Strength
H_{SAT}	Saturated Magentic Field Strength
μ_0	Permeability of Free Space
μ_r	Relative Permeability
L_e	Effective Magnetic Length

A_e	Effecitve Magnetic Area
VCO	Voltage Controlled Oscillator
VCT	Voltage Clock Trigger
FCT	Frequency Clock Trigger
OCT	Output Clock Trigger
RCT	Reference Clock Trigger
F	Inverter Output Frequency
F_o	Maximum Inverter Switching Frequency
I_{ripple}	Ripple Current
I_A	Primary Anode Current
I_{TRMS}	Maximum Permissible RMS On-State Current
I_{TQRM}	Maximum Repetitive Controllabe On-State Current
I_{TQSM}	Non-repetitive Controllable On-State Current
I_{TSM}	Surge Current
I_{TQT}	Tail Current
I_H	Typical Holding Current
I_L	Typical Latching Current
I_{GT}	Maximum Gate Trigger Current
I_G	Gate Current
I_{RGM}	Typical Reverse Gate Current
PIV	Peak Inverse Voltage
U_{DRM}	Repetitive Peak Forward Off-State Voltage
Lg	Gate Circuit Inductance
t_{tmin}	Minimum Duration of On-State Current
t_{gd}	Typical Gate Controlled Delay Time
t_{dq}	Typical Gate Controlled Storage Time
t_{fq}	Typical Gate Controlled Fall Time
t_{gq}	Maximum Gate Controlled Turn-off Time
di/dt	Rate of rise of Turn-on Current
dv/dt	Rate of Rise of Turn-off Voltage
di_g/dt	Rate of Rise of Turn-on Gate Current
FET	Field Effect Transistor
BJT	Bipolar Junction Transistor

INTRODUCTION

The development of GTO's, particularly in the last 5 years, has made the switching of large currents at high voltages at relatively high frequencies possible.

Although conventional thyristors have similar voltage and current ratings, GTO's are particularly attractive because they are able to be turned off actively by the application of a negative current pulse to the gate of the device. This, in conjunction with their high switching frequency capability, makes them well suited to use in Pulse Width Modulation (PWM) Inverters.

The object of this thesis is to firstly develop a 3-phase VSD which will operate from a 380 Volt power reticulation system, then secondly to upgrade the system to 525 Volts. This will enable the system to be used in the South African mining industry. It should have a sufficient power rating so that it can drive a standard 22 kW Induction motor and also have an output frequency range of 10 to 50 Hz. GTO's are used as the main switching elements in the Inverter stage of the VSD.

A simple analogue PWM controller has been designed which incorporates the Philips HEF4752 integrated circuit. The controller includes the following features.

(1) Over current protection
(2) Over voltage protection
(3) Short-circuit protection
(4) Base-Boost (voltage boost at low output frequencies)
(5) Maximum switching frequency control
(6) Minimum pulse width
(7) Speed control using a potentiometer
(8) Controlled rate of acceleration/deceleration
(9) Interlock delay setting

After full design and testing of the individual sections of the VSD it was assembled and the complete unit tested.

1. GATE TURN-OFF THYRISTORS

1.1 Historical Review

The name "Gate Turn-off Thyristor" is relatively new in the Power Semi-conductor vocabulary. The principles of their operation and use have however been investigated since the early 1960's. One of the major pioneers in the field was the General Electric Company in America. Initially they were called "Gate Turn-off Switches"[1] but this was later changed to "Turn-off Silicon-Controlled Rectifiers"[2]. Early production of these devices, with current interruption capabilities of 1 to 2 amps at 500 volts, was undertaken by General Electric.

At this stage a number of other international companies started to develop these devices. However, it was not until the early 1970's that any really significant developments were made. RCA produced a device called a "Gate Turn-off Silicon Controlled Rectifier" which could interrupt currents of 8,5 amps at 600 volts[3]. They described these devices as, "fully regenerative switches that exhibit full gate control, as they can be turned on by a positive pulse of gate current and are capable of being turned off by application of a pulsed negative bias between the gate and cathode terminals".

By the mid 1970's General Electric started producing a device known as a "Latching Power Transistor" with a maximum current rating of 25 amps and a rated voltage of 800 volts[4]. This device could be latched on like a thyristor with a positive base current pulse and turned off with a short negative base current pulse.

From this stage a widescale interest was generated and development progressed rapidly. Most of the major Power Semi-conductor manufacturers in the U.S.A., Europe and Japan have produced devices now known as "Gate Turn-off Thyristors" with RMS current ratings of up to 200 amps and 1200 volts.

1.2 Switching Requirements

The main objective of this section is to give one a brief understanding of the operation of GTO's so as to be able to use them effectively. Full details of the operation of these devices can be found in references [5] and [6].

1.2.1 Turn-on

A GTO is similar to a conventional thyristor in that it can be turned on by a relatively small gate current. However, the Turn-on efficiency of the GTO can be improved by providing a relatively large gate current. This ensures that each element of the GTO structure can receive sufficient triggering current[7]. A recommended value of gate current for Turn-on is 3 to 8 times the maximum gate trigger current, I_{GT}, for a minimum duration of twice the gate controlled delay time, t_{gd}[8]. This is shown in Fig. 1.2.1(a).

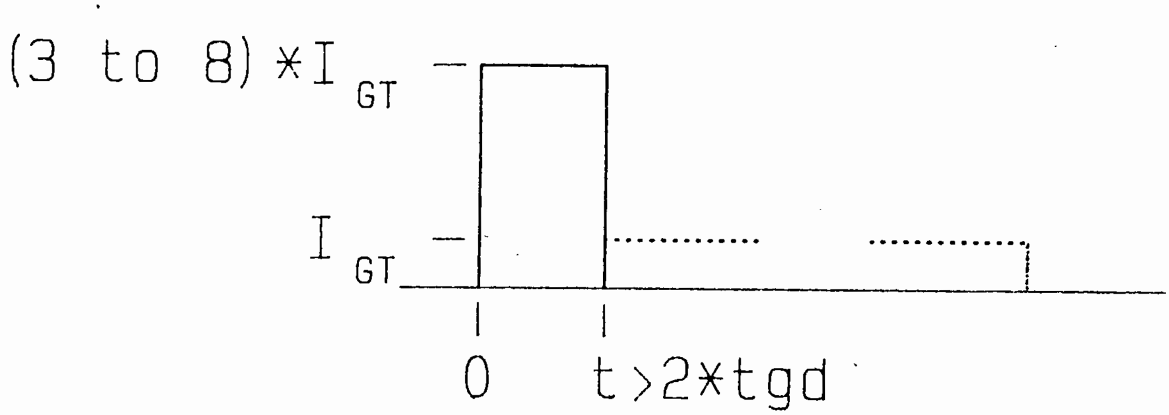

Figure 1.2.1(a) Turn-on Gate Current Waveform

It is not essential to provide gate current over the whole conduction period, but there are two major advantages if this is done,

(1) The on-state voltage drop across the GTO is decreased.

(2) The possibility of self extinguishment if the primary current through the GTO decreases below the Holding Current, I_H, is avoided.

1.2.2 Turn-off

The Turn-off process of a GTO is implemented by the application of a negative pulse to the gate. This causes a fast rising negative gate current which initially extracts the storage charge in the gate region and then starts to divert the anode current from the cathode to the gate[9]. The interdigitated gate structure pinches the diverted current into thin filaments and progressively reduces it, each filament of current extinguishing in turn. Finally, a small tail current persists for a few microseconds as some of the remaining recombining charge is removed.

It should be noted that the negative gate current is not of a predetermined magnitude as with Turn-on. The Turn-off gate current is dependant on the magnitude of the primary anode current through the GTO. A safe design parameter is that the Turn-off gain of a GTO, I_A/I_G, has a minimum safe value of 5[9] when the GTO is switching it's rated current.

A critical factor in switching a GTO off is the external Gate Circuit Inductance, L_G. In realizing the fast Turn-off of a GTO, inductance in the gate circuit is of no use as it limits the rate of rise of the Turn-off gate current, di_g/dt, which is necessary in the storage period t_{dq}. On the other hand gate current is required to flow until the GTO is completely turned off, so an inductor in the gate circuit ensures that the Turn-off gate current flows in the fall and tail period. By careful selection of this inductance the maximum repetitive controllable on-state current, I_{TQRM}, can be increased.

Figure 1.2.2(a) shows typical current waveforms in a GTO at Turn-off.

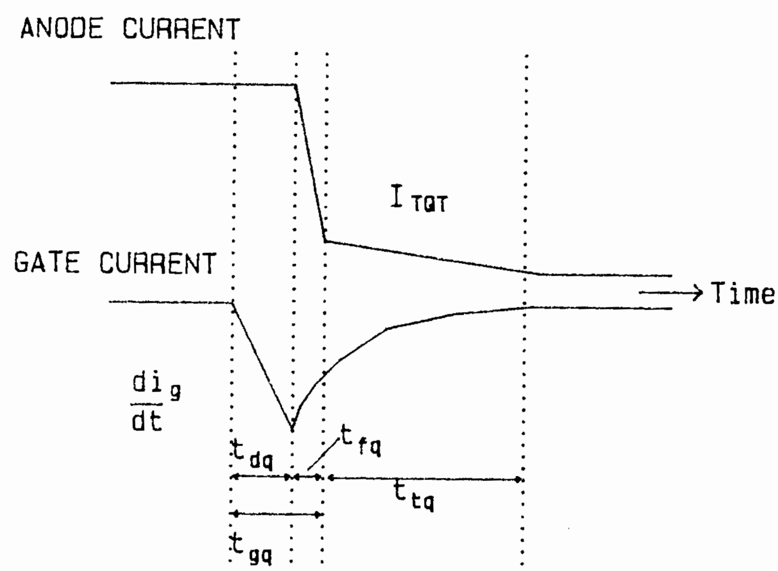

Figure 1.2.2(a) Typical Turn-off Current Waveforms

1.3. Advantages and Disadvantages of using GTO's

The major advantage of using a GTO is that it can be turned off under controlled conditions without any external circuitry, apart from the gate drive circuit. Thus all the commutation circuitry which is needed when using conventional SCR's is not required. The Gate Drive Circuit is however, more complicated as it has to be able to handle high currents when turning the GTO off. This obviously increases the cost of the driver. This cost is however, offset against commutation components which are no longer needed.

The switching frequency of GTO's is considerably higher than those obtainable with conventional SCR's which makes them particularly attractive in VSD applications. They also maintain superiority over Power Transistors and MOSFET's in high voltage and current applications, at present.

1.4 Manufacturers, Cost and Availability

Table 1 is a list of the major manufacturers of GTO's and a summary of some of their components. From the table it is clear that manufacturers have developed GTO's covering a wide range of ratings. Philips have a range of low power GTO's which are used principally in high frequency low current applications, such as television sets.

AEG-TELEFUNKEN and Hitachi GTO's are essentially the same devices, manufactured to the same specifications but marketed with a different trade name.

Toshiba and MEDL have a range of high current, high voltage GTO's which are particularly suitable for use in traction applications.

The remainder of the manufacturers have a range of GTO's which are most commonly used in VSD applications, both D.C. and A.C.

MANUFACTURER	PART NUMBER	VOLTS	AMP (RMS)	AMPS (MAX. CONTROLLABLE)	di/dt (A/μSec)	dv/dt (V/μSec)
Philips	BTI57-1500R	1500	3.2	10	--	10 000
	BTW58-1500R	1500	6.5	25	--	10 000
	BTW59-1500R	1500	13.5	50	--	10 000
	BTV60-1200R	1200	25	120	--	10 000
Hitachi/ AEG-TELEFUNKEN	G20	1200	10	20	150	1 000
	G50	1200	22	50	200	1 000
	G90	1200	40	90	200	1 000
	G200	1200	70	200	200	1 000
International Rectifier	81RDT	1200	125	350	400	600
	160PFT	1600	250	600	600	1 000
	350PJT	1600	550	1200	600	1 000
Westinghouse	GDM21210	1200	31	100	200	1 000
	GDM21220	1200	70	200	200	1 000
	GSD11245	1200	200	450	200	500
	GSD11260	1200	270	600	200	500
MEDL.	EG10	1200	35	150	250	1 000
	EG300	1200	250	600	500	500
	EG500-2500	2500	600	1400	250	500
	EG750	4500	800	2500	250	500
Toshiba	SG600R21	1300	400	600	100	250
	SG600EX21	2500	400	600	100	350
	SG800EX21	2500	400	800	100	350
	SG1400EX21	2500	700	1400	250	350

Table 1.4 The Major GTO Manufacturers and a Summarised List of Some of their Components

2. THEORETICAL ANALYSIS OF INDUCTION MOTORS

2.1 METHOD FOR DETERMINING THE EQUIVALENT CIRCUIT OF INDUCTION MOTORS.

The approximate equivalent circuit of an Induction motor is obtained with relative ease from Short-Circuit and Open-Circuit tests. The correlation of the theoretically calculated performance with the measured values is however, generally poor when using this circuit. Using a computer it is possible to disentangle the Short-Circuit results from the Open-Circuit ones using a numerical method[11].

Below is a method for obtaining the 'Exact' equivalent circuit of an Induction Motor, the principle of which is given by J. Hindmarsh in reference [12]. A flow diagram of this method is shown in Fig. 2.1(a). An important point to make at this stage is that for the Open-Circuit test the Induction Motor is driven at exactly synchronous speed. If the motor was not driven a modification must be made to the method described to take static losses and the small value of slip which would exist into account.

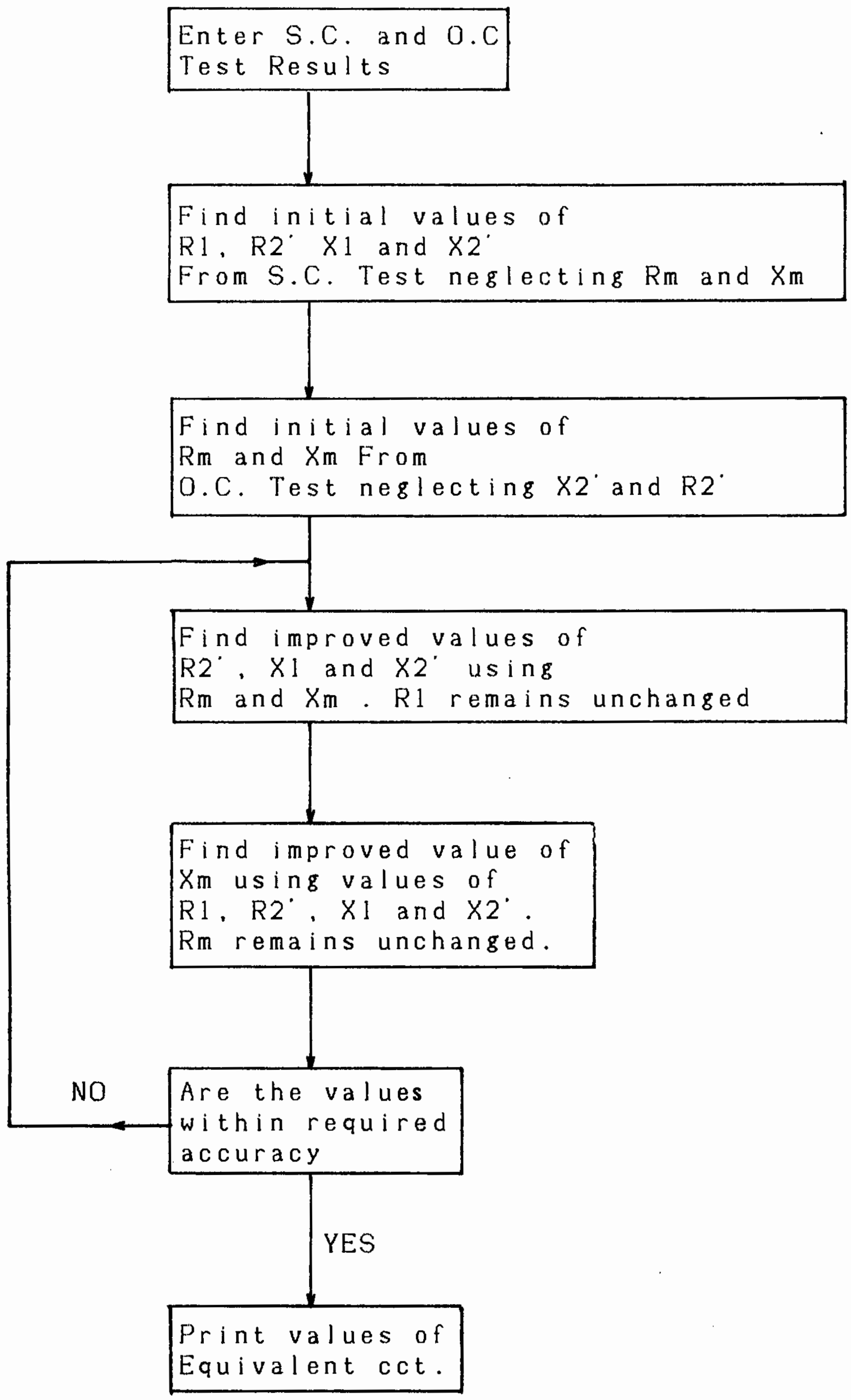

Figure 2.1(a) Flow Diagram for the Computation of Induction Motor Parameters

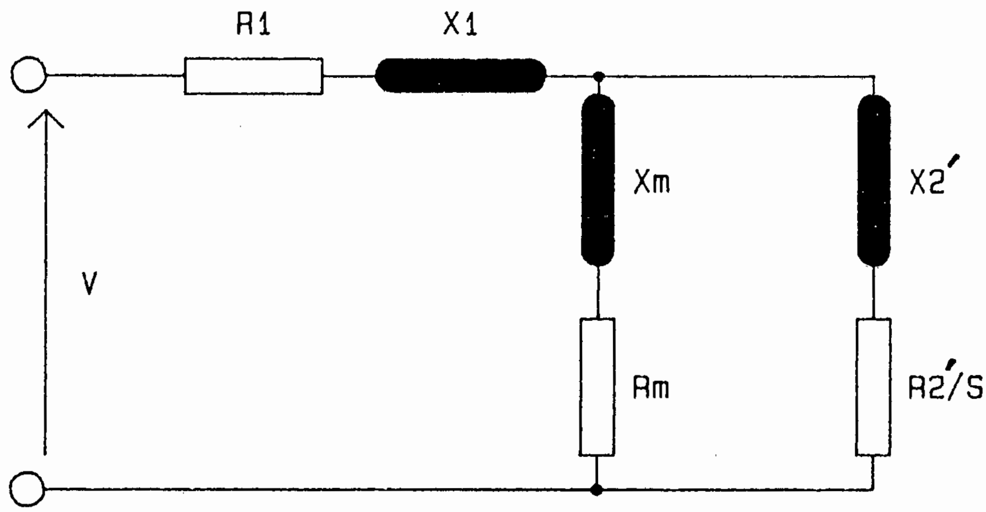

Figure 2.1(b) The Induction Motor Equivalent Circuit

Initially the values of R1, X1, X2' and R2' are calculated from the Short-Circuit test neglecting Xm and Rm. These equivalent circuit components are shown in Fig. 2.1(b) above. Using the Open-Circuit test and neglecting the rotor circuit the initial values of Xm and Rm are calculated. This now gives the complete first approximation to the equivalent circuit.

The new improved circuit can now be calculated by using an iterative numerical routine. The new improved values of X1, X2' and R2' can be calculated, this time incorporating Xm and Rm. An improved value of Xm is then calculated. The full mathematical details of this method are given in Appendix 2.1, as well as a computer program to implement it.

This method essentially determines the complex roots of a polynomial by a numerical method. The equation can have an oscillatory nature and converge to a fixed value. This is easily demonstrated by a slight modification to the program in Appendix 2.1., the results of which are shown in Fig. 2.1(c).

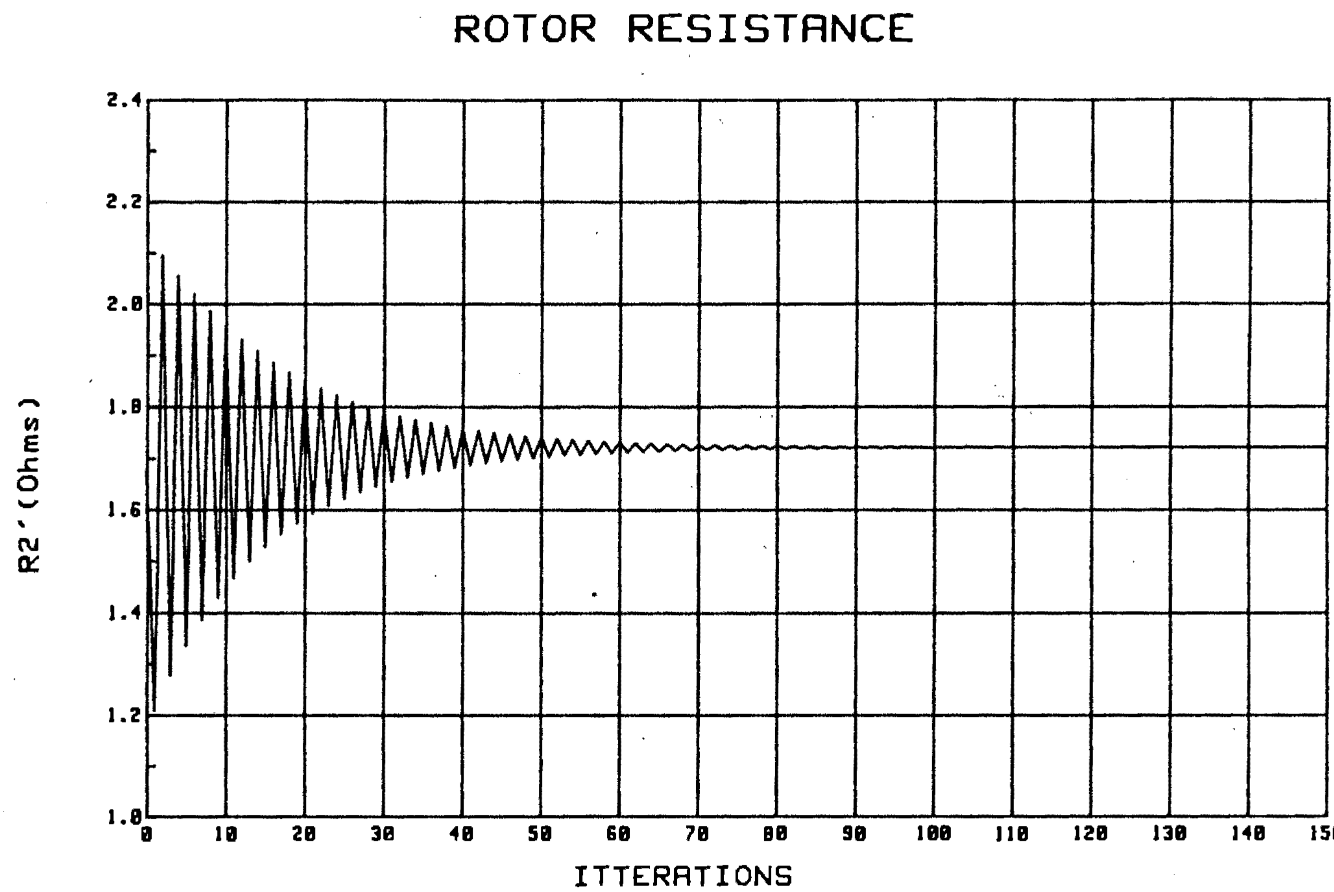

Figure 2.1(c) Graph demonstrating the oscillatory nature of R2' when using an iterative method for determining the equivalent circuit.

2.2 <u>TEST MOTOR AND EQUIVALENT CIRCUIT</u>

The motor which was tested was a standard GEC DZ160M with a full load current of 16.2A at 525 Volts. Full details of the test results are given in Appendix 2.2. Table 2.2 gives the equivalent circuit values for a given number of frequencies.

Component	Freq=50Hz	Freq=40Hz	Freq=30Hz	Freq=20Hz
R1(Ω)	2,0737	2,0737	2,0737	2,0737
R2'(Ω)	1,7272	1,4782	1,2664	1,0401
X1(Ω)	5,5279	4,6789	3,7792	2,7859
X2'(Ω)	5,5279	4,6789	3,7792	2,7859
Rm(Ω)	58,7067	36,1954	25,4745	33,8864
Xm(Ω)	213,5021	172,7872	131,3200	92,5984

Table 2.2 Equivalent circuit values for different frequencies

An important observation is that the value of R2' varies nearly linearly as a function of frequency. This fact must therefore be taken into account when analysing an Induction motor operating at variable frequencies. This is shown in Fig. 2.2(a). If R2' is not varied as a linear function of frequency the predicted slip window for normal operating conditions is increased.

All further results in this chapter will be given for this same GEC DZ160M Induction Motor.

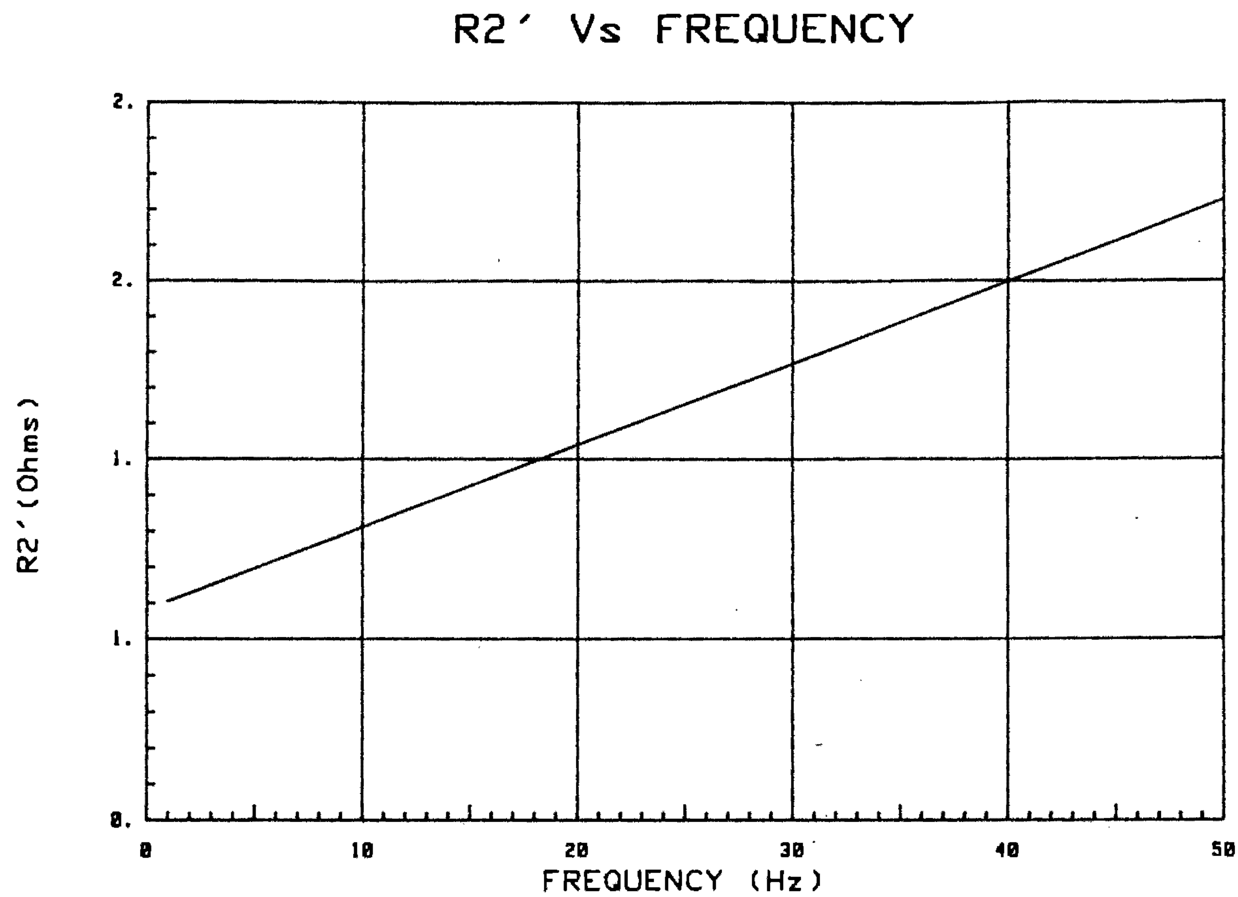

Figure 2.2(a) Rotor resistance as a function of frequency

2.3 THEORETICAL INDUCTION MOTOR CHARACTERISTICS

Now that the equivalent circuit of the motor has been obtained it can be used in certain theoretical predictions. A summary of induction motor theory is contained in Appendix 2.3. It is using this theory that the results in Fig. 2.3(a) were obtained with the aid of a computer. The software listing is also given in Appendix 2.3.

The development of this model is primarily for use in the next section in this chapter. It is not intended for it to be used as a detailed study between measured and predicted characteristics of induction motors. However, it should be noted that the measured and theoretical values of Pull-Out torque correlate accurately. Full details of these results are given in Chapter 8.7

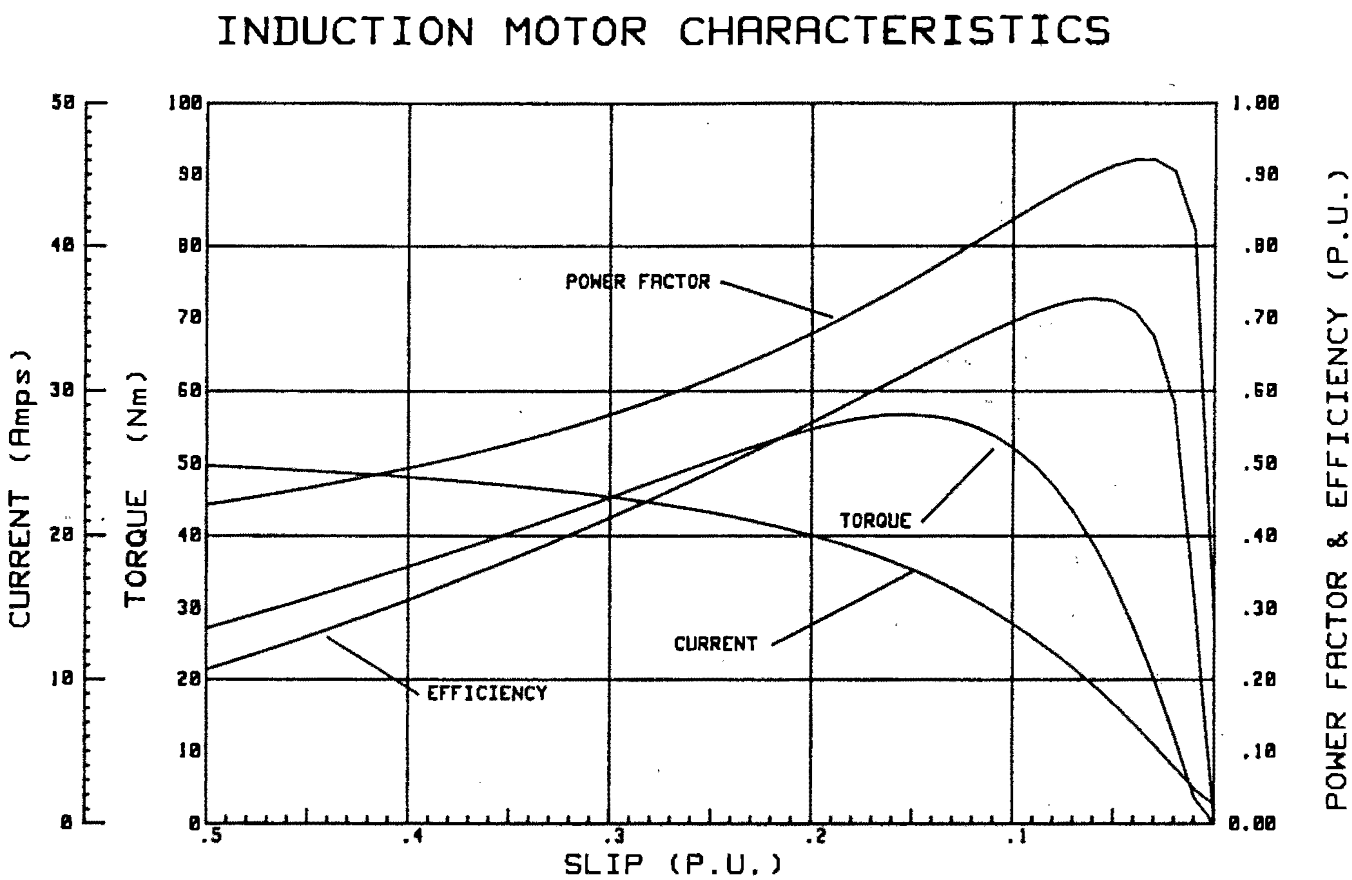

Figure 2.3(a) GEC DZ160M Induction Motor characteristics with V_{L-L} = 525 volts, frequency = 50Hz T_{max} = 63.7 Nm S_{max} = 0.16

2.4 VOLTAGE REQUIREMENTS OF AN INDUCTION MOTOR DRIVEN BY A VOLTAGE SOURCE INVERTER.

In an Induction motor drive it is generally desirable to have a constant torque output for a given current throughout its range of operating frequencies[15]. To achieve this it is necessary to produce a constant airgap flux ϕ in the motor[16] where,

$$\phi = \left[\frac{V_s - IZ_s}{f}\right] K$$

V_s = Terminal voltage

IZ_s = Stator impedance voltage drop

K = Constant for a particular machine

f = Frequency

For constant flux the ratio $\frac{V_s - IZ_s}{f}$ must also be kept constant.

However, as frequency is reduced, the term Z_s tends towards the value of the stator resistance R1.

Thus, if a constant Volts/Hz relationship, V_s/f, is used there is a decrease in airgap flux due to IZ_s. This causes drastic reductions in the torque at lower frequencies and is clearly shown in Fig. 2.4(a) where a linear Volts/Hz relationship has been used.

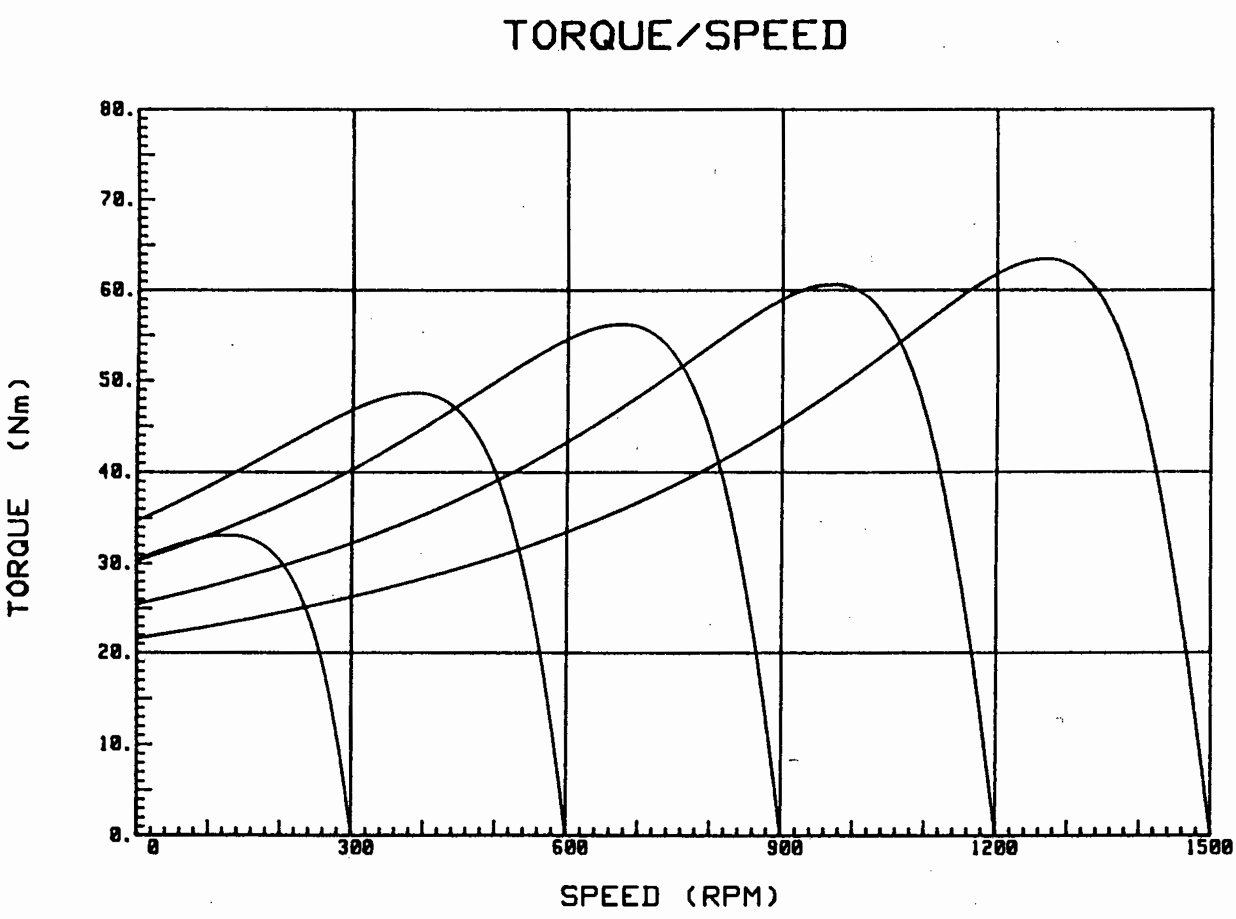

Figure 2.4(a) Torque/Speed Characteristics with no Base-Boost

By deviating from this linear relationship and increasing the value of applied voltage at low frequencies one can overcome this problem. A relatively simple method can be used to determine the amount of Base-Boost required. Once the Torque/Speed curve for the primary frequency, normally 50 Hz, of the machine has been obtained, it is only necessary to ensure that motor will have the same value of Pull-Out torque over its whole frequency range.

By using the linear approximation as a first estimate of required voltage and obtaining the Pull-Out torque one can compare the magnitudes of these torques. If the Pull-Out torque for the new frequency is less than the required value, the voltage can be incremented by a small value until the correct value is obtained. The result of using this method is shown in Fig. 2.4(b)

The computer program for determining the voltage corrections is listed in Appendix 2.4.

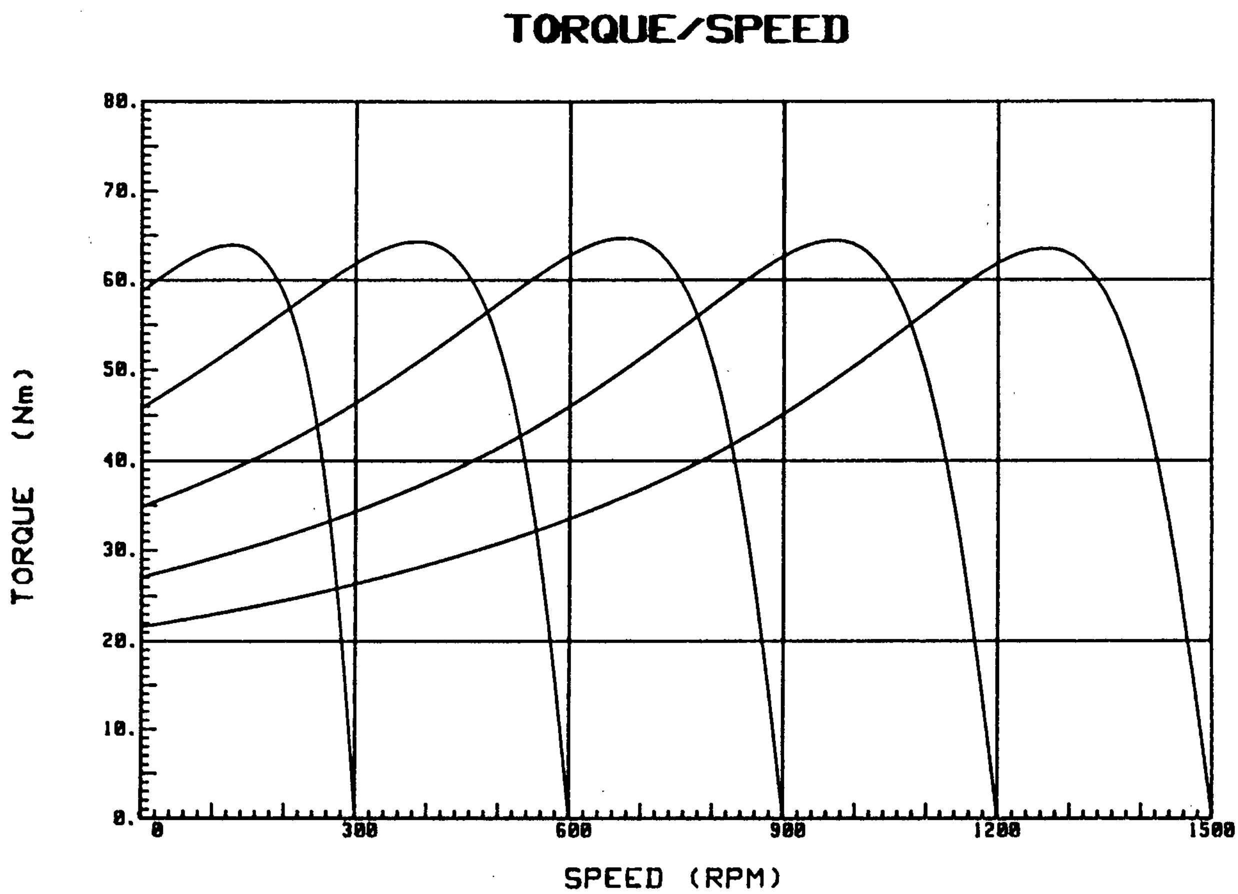

Figure 2.4(b) Torque/Speed Characteristics with Base-Boost

The program in Appendix 2.4 takes the fact that R2' varies as a function of frequency into account. The values of the reactive components of the impedence are also varied linearly as a function of frequency. The results of the graphs in Fig 2.4(b) are tabulated below in Table 2.4.

Applied Frequency (Hz)	Applied Voltage (Volts)	Rotor Resistance (Ohms)	T_{max} (Nm)
50	525	1,7277	63,5
40	431	1,4983	63,8
30	336	1,2691	64,0
20	240	1,0401	63,7
10	146	0,8111	64,0

Table 2.4 Optimised Volts/Frequency values and corresponding Rotor Resistance and Pull-Out Torque.

The values of Pull-Out Torque in Table 2.4 indicate that this method for obtaining the correct Volts/ Frequency relationship is very effective.

This optimisation program is easily modified so that the Volts/Frequency relationship is calculated for the complete operating Frequency range of the motor. These results are shown in Fig. 2.4(c) and the deviation from a linear relationship is clearly seen. However, care should be taken when specifying the amount of Base-Boost required. Excessive Base-Boost can cause saturation which in turn produces unacceptable losses and noise. Iron losses are usually of secondary importance however, because of the low stator frequency[18].

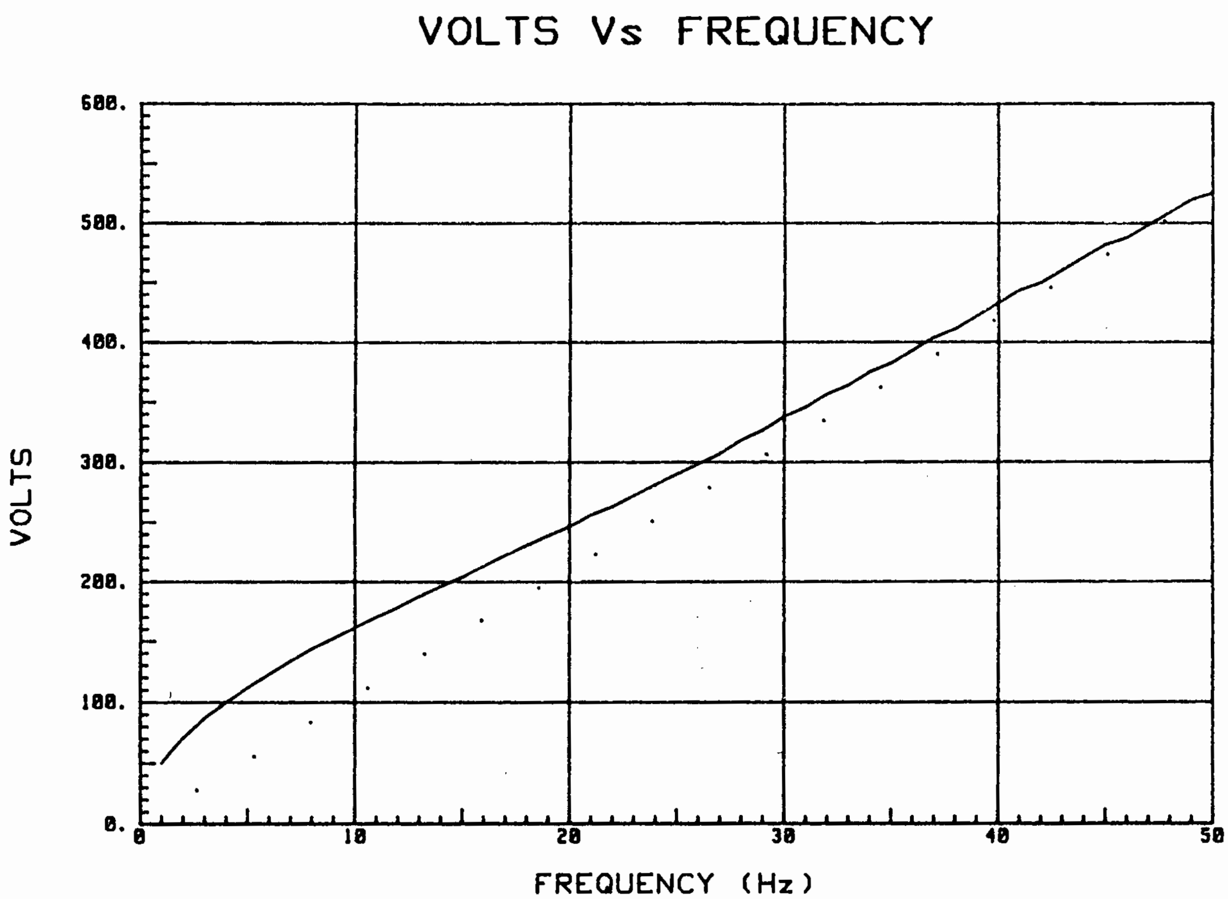

Figure 2.4(c) Voltage/Frequency relationship showing Base-Boost

3. SPECTRAL ANALYSIS OF SWITCHING WAVEFORMS

3.1 DISCRETE FOURIER TRANSFORM METHOD

This method enables one to determine the Fourier Series of any periodic waveform even though an analytic expression for it may not be known[17].

By definition the Fourier Series of any periodic waveform may be expressed in the form

$$Y = C_0 + C_1 \ Sin(\theta+\alpha_1) + C_2 \ Sin(2\theta+\alpha_2) + \ldots \quad (1)$$

By expanding this expression and substituting

$$a_i = C_i \ Sin \ \alpha_i$$
$$b_i = C_i \ Cos \ \alpha_i \quad \text{for } i = 1,2,3,\ldots\ldots\ldots$$

equation (1) becomes

$$Y = C_0 + \Sigma_{i=1}^{\infty} a_i \ Cos(i\theta) + \Sigma_{i=1}^{\infty} b_i \, Sin(i\theta) \quad (2)$$

$$\text{where } \frac{a_i}{b_i} = \tan \alpha_i \text{ and } C_i = \sqrt{a_i^2 + b_i^2}$$

By employing a method of numerical integration the Fourier coefficients for this expression can be obtained.

Therefore for a sampled data waveform

$$C_0 = \frac{1}{N} \Sigma_{i=0}^{N-1} M_i \quad (3)$$

$$a_i = \frac{2}{N} \Sigma_{i=0}^{N-1} M_i \ \cos \ \delta_i \quad (4)$$

$$b_i = \frac{2}{N} \Sigma_{i=0}^{N-1} M_i \ \mathrm{Sin}\delta_i \qquad (5)$$

where $\delta_i = \dfrac{360 \times N_i \times I}{N}$

and N = Number of sampled points in the waveform

N_i = i_{th} sample

M_i = Modulus of the sampled waveform at α_i

I = Harmonic number

Therefore by using the fact that

$$C_i = \sqrt{a_i^2 + b_i^2} \text{ and } \tan \alpha_i = \frac{a_i}{b_i}$$

the parameters of equation (1) can be calculated.

A computer program which implements this method is given in Appendix 3.1

3.2 THE SLONIM METHOD

This is a new method of calculating the Fourier Coefficients of a waveform developed by M.Slonim[18&19]. The coefficients are calculated as a function of the magnitude of the discontinuities in a waveform. This method is described below.

By definition the complex form of the Fourier Series is

$$F(k,t) = \frac{2}{T} \int_0^T f(t) \ e^{-jkwt} \ dt \qquad (6)$$

where k is the harmonic number

If $f(t)$ is a periodic function, of period T, and there are n discontinuity points in the function at t_0, t_1, t_2 .... t_{n-1}, then

$$F(k,t) = \frac{2}{T}\left[\int_{0}^{t_1} A_0 e^{-jk\omega t}\,dt + \int_{t_1}^{t_2} A_1 e^{-jk\omega t}\,dt \;....+\right.$$

$$\left.\int_{t_{n-1}}^{t_n} A_{n-1} e^{-jk\omega t}\,dt\right] \qquad (7)$$

where A_i is the magnitude of the function between t_i and t_{i+1}, as shown in Fig. 3.2.

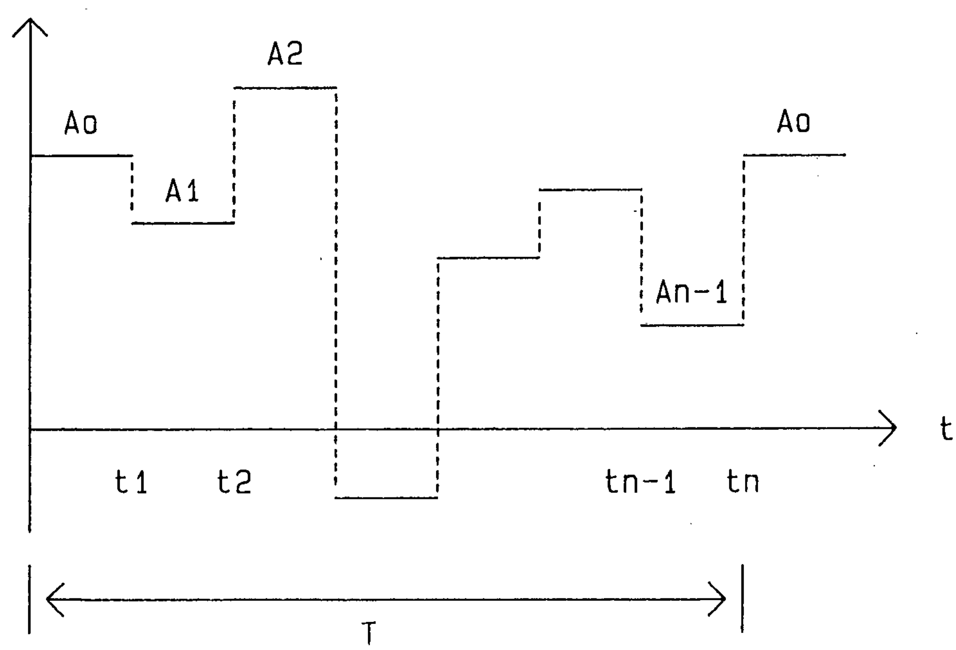

Figure 3.2 Staircase Function

$A_i(+)$ is the value of the function just after t_i
$A_i(-)$ is the value of the function just before t_i
$\Delta F(t_i) = A_i(+) - A_i(-)$

Integrating and rewriting (7) in the form

$$F(k,t) = \frac{2}{T} \cdot \frac{1}{jkw} \Big[-A_0(+)e^{-jkwt_0} + A(-)e^{jkwt_1}$$

$$- A_1(+)e^{-jkwt_1} + A_1(-)e^{-jkwt_2}$$

$$+ A_2(-)e^{-jkwt_3} + A_2(+)e^{-jkwt_2}$$

$$- A_3(+)e^{-jkwt_3} + A_3(-)e^{-jkwt_4}$$

$$\cdots\cdots\cdots\cdots\cdots\cdots\cdots\cdots\cdots\cdots$$

$$\cdots\cdots\cdots\cdots\cdots\cdots\cdots\cdots\cdots\cdots$$

$$+ A_{i-1}(-)e^{-jkwt_n} - A_{i-1}(+)e^{-jkwt_{n-1}} \Big]$$

$$= -\frac{2}{T} \cdot \frac{1}{jkw} \left[-\sum_{i=0}^{n-1} \Delta F(t_i)e^{-jkwt_i} \right] \qquad (8)$$

Hence

$$F(k,t) = \frac{1}{jk\pi} \Sigma_{i=0}^{n-1} \Delta F(t_i)e^{-jkwt_i} \qquad (9)$$

From equation (9) it is clear that the Fourier coefficients of a function are only dependent upon the magnitude of the discontinuities, and not on the function between these points.

Using the result in (9) an expression for any periodic function can now be found.

3.3 RESULTS

3.3.1 Square Wave Excitation

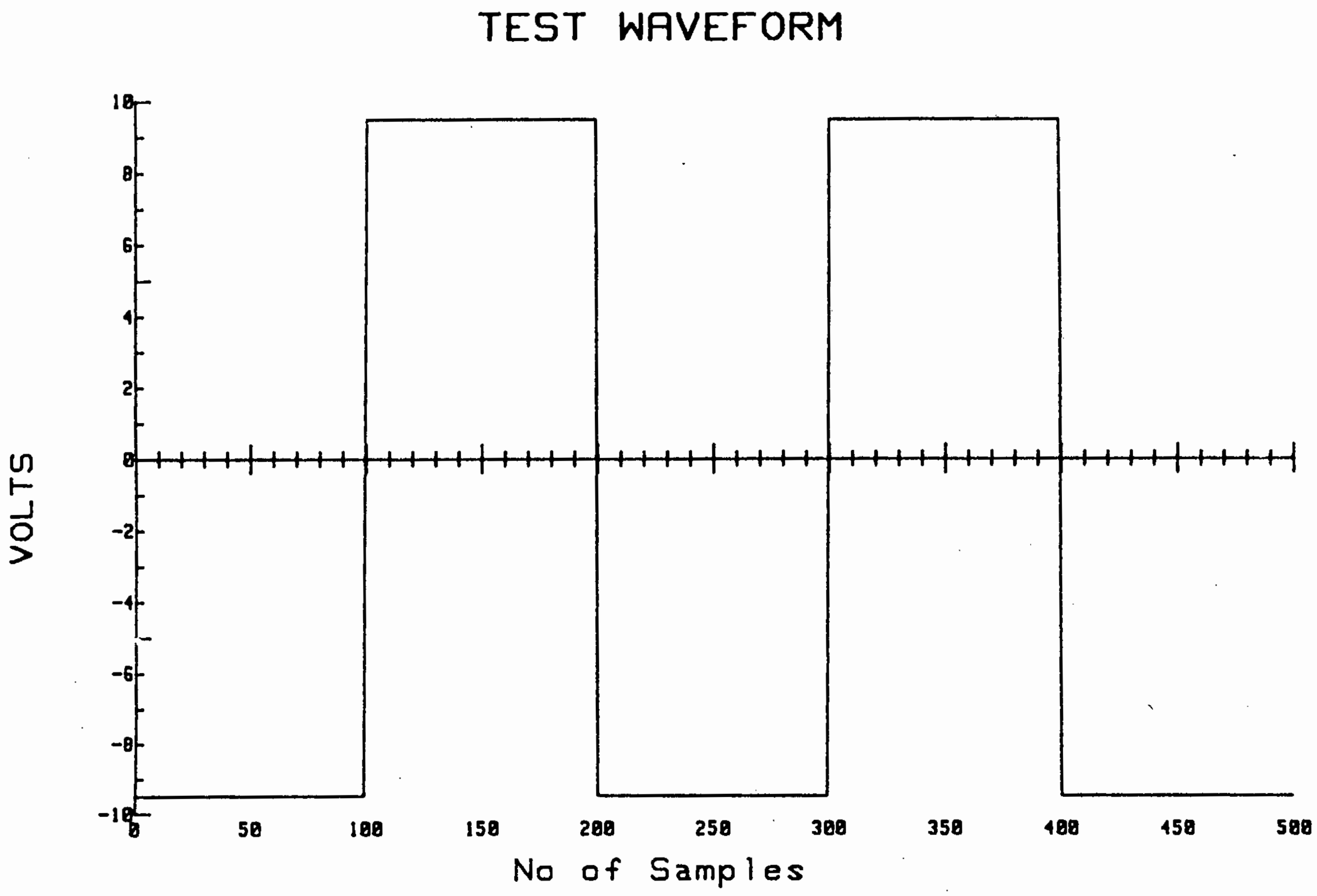

Figure 3.3.1(a) Square Wave Signal ± 9.5 Vpeak

The waveform in Fig. 3.3.1(a) was captured and stored using a fast A/D converter. A spectral analysis of this waveform using both the Discrete Fourier Transform and Slonim methods was performed and the results listed in Table 3.3.1.

Harmonic Number	Harmonic Magnitude		
	Slonim	Discrete Fourier	Analytic Fourier
1	12,0958	12,0959	12,0958
3	4,0319	4,0324	4,0319
5	2,4192	2,4199	2,4192
7	1,7280	1,7290	1,7280
9	1,3440	1,3454	1,3440
11	1,0996	1,1013	1,0996
13	0,9304	0,9324	0,9304
15	0,8064	0,8086	0,8064

Table 3.3.1. **The magnitude of the harmonic component of a ± 9,5 V square wave using**
(1) Slonim Method
(2) Discrete Fourier Transform method
(3) Analytic Fourier Series

From these results it is clear that the Slonim Method and the Analytic Fourier Series results correspond exactly. A maximum error of 0,27% occurs when comparing the results of the Discrete and Analytic Fourier methods. The difference between the results is caused by sampling errors at the exact points of discontinuity of the waveform. This error could be decreased if the sampling frequency of the captured waveform in Fig. 3.3.1(a) was increased.

Fig. 3.3.1(b) gives a plot of the spectrum of this waveform.

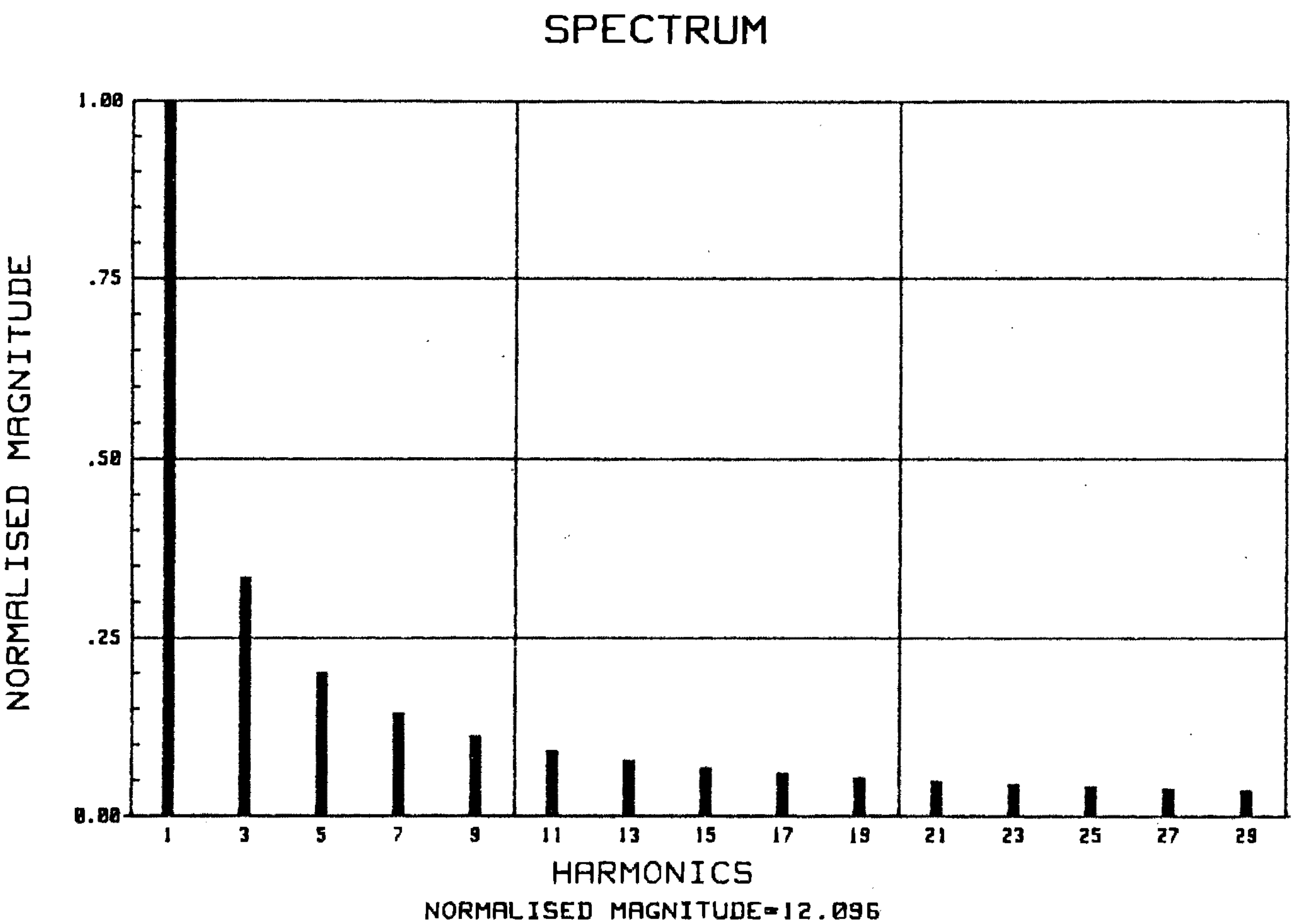

Figure 3.3.1(b) Spectrum of a ± 9,5 V Square Wave

3.3.2. Thyristor Inverter Current Waveform

A typical current, or voltage waveform for that matter, which is obtained from a thyristor inverter is shown in Fig. 3.2.2.(a). Once again the Slonim and Discrete Fourier Transform methods were used to obtain the spectrum of the waveform.

The equation $I(k) = \frac{4I}{k\pi}\left[\mathrm{Sin}k\phi_1 - \mathrm{Sin}k\phi_2 + \mathrm{Sin}k\phi_3\right]$

for $k = 2V + 1$

$V = 1, 2, 3, 4, \ldots\ldots$

k = Harmonic number

was used for the Slonim method. The derivation of this equation is given in Appendix 3.3.2.

In the evaluation of this waveform the following values were used

$$\phi_1 = 62°$$
$$\phi_2 = 67°$$
$$\phi_3 = 84°$$

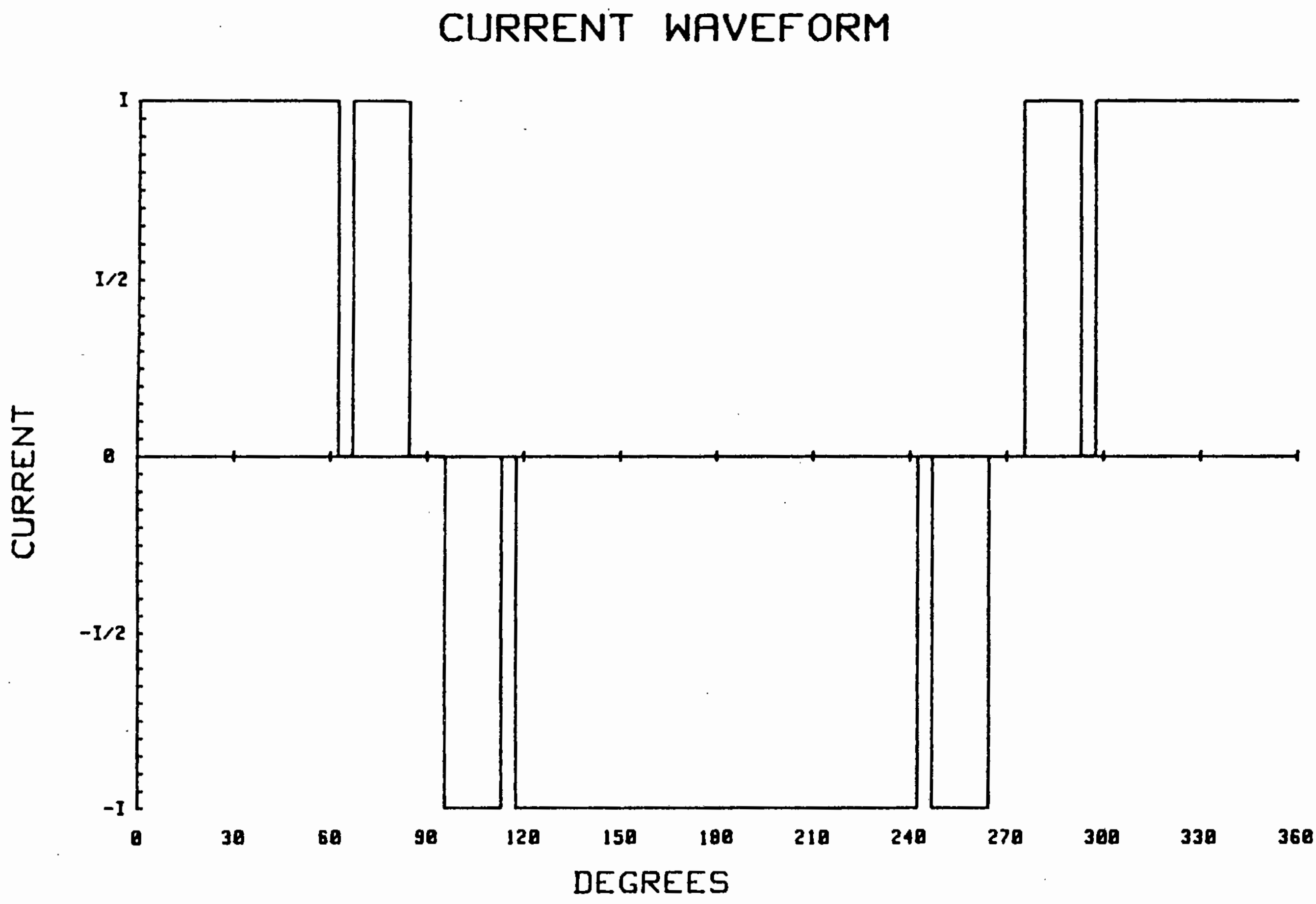

Figure 3.3.2(a) Current Waveform from a Thyristor Inverter

The results of the analysis using both the Slonim and Discrete Fourier Transform methods are given in Table 3.2.2. The maximum discrepancy between these two methods is 4,53%. The error would be less if the sampling frequency was increased. Fig.3.3.2(b) gives a plot of the spectrum of this waveform.

Harmonic Number	Magnitude	
	Discrete Fourier	Slonim
1	1,2190	1,2184
3	0,2926	0,2959
5	0,1358	0,1331
7	0,1359	0,1323
9	0,1699	0,1655
11	0,1573	0,1522
13	0,0760	0,0706
15	0,342	0,0395
17	0,1075	0,1126

Table 3.3.2 The Harmonic Components of a Waveform in Fig.3.3.2(a)

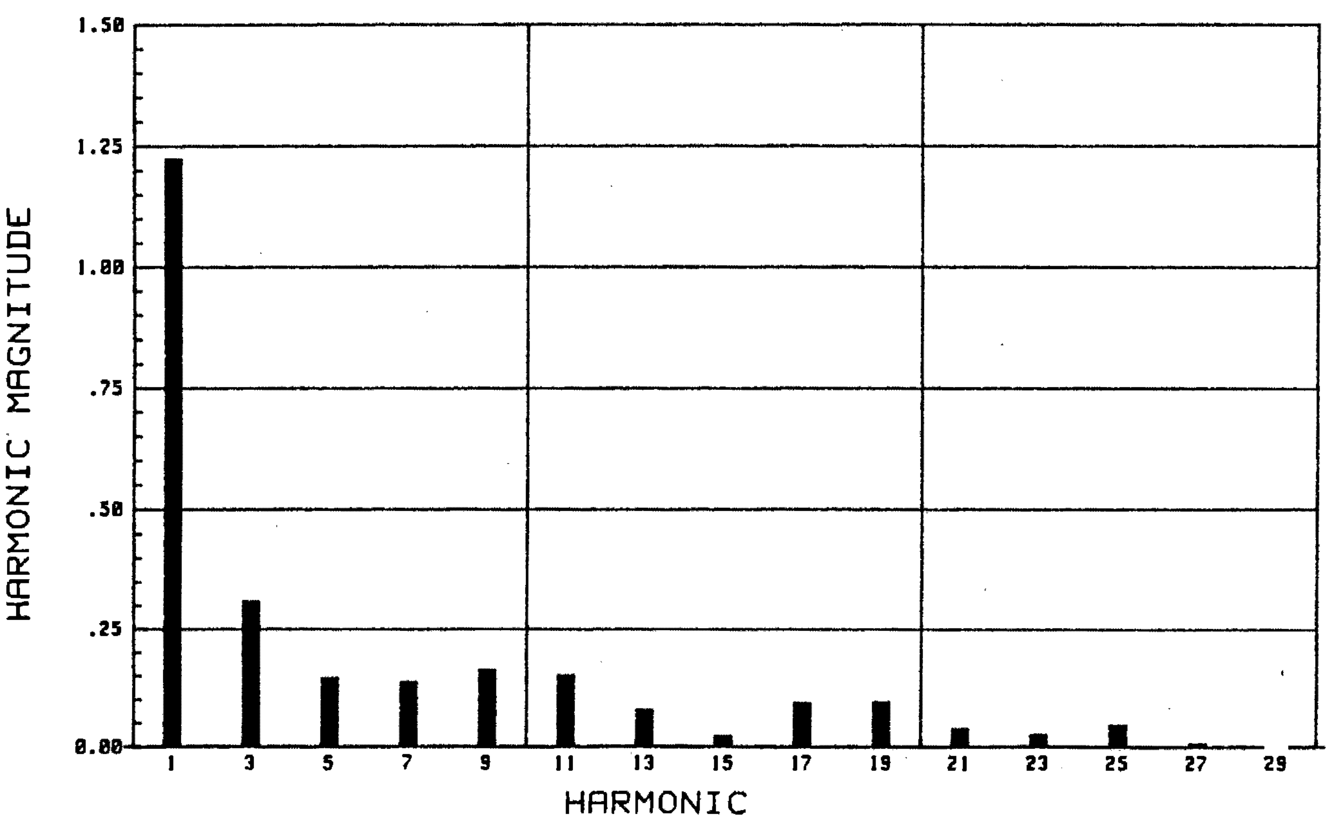

Figure 3.3.2(b) Spectrum of Thyristor Current Waveform

3.4 COMPARISON AND APPLICATION OF THE TWO METHODS

At this stage it is not very clear which of these two methods have advantages over each other.

The Slonim method has the advantage that the number of computations for each spectral component is greatly reduced. It does however, have the disadvantage that the points of discontinuity have to be located before computation can begin. This is not the case when Discrete Fourier Transforms are used. The method is relatively slow, but on the other hand its application is not dependant on the discontinuities of the waveform.

Both of these methods are ideally suited to spectral analysis of digitally captured waveforms but Discrete Fourier Transforms are best suited for applications where fast computation times are not necessary. The Slonim method is ideally suited to Real Time applications where fast computation speeds are necessary. It is however, very effective in applications where speed is not a necessity.

4. GENERAL DESCRIPTION AND SPECIFICATIONS OF VSD

4.1 GENERAL DESCRIPTION

The VSD can be divided up into a number of distinct circuits. A block diagram showing these sections is given in Fig. 4.1.

The 380/525 volt 50 Hz, 3 phase input is converted to 540/750 volts D.C. by a 3 phase bridge rectifier. The rectified waveform is smoothed by an effective capacitance of 4000 μF. This reduces the ripple content of the D.C. Link to less than 20 volts under full load conditions. A fully controlled 3 phase PWM Inverter, using GTO's as the main switching elements, is fed from the D.C. Link.
The output frequency range of the Inverter is 10 to 50 Hz.

The controller and it's hard wired relay interlock circuit are supplied by a common -15,0,+15 and 0, +5 volt power supply which is fed from the 3 phase 50 Hz input. Local pushbutton stations enable or disable the controller via it's interlock. A local 10k potentiometer is used to set the speed of the motor. Automatic slip compensation within the controller is used to maintain closer speed control without feedback.

Six gate drive control signals are generated within the controller. These are fed via opto-isolators to floating Gate Drive Circuits. Each Gate Driver has its own floating power supply which is supplied by an isolated winding on Transformer 2. Cooling fans are also driven off Transformer 2.

There are other feedback and control signals to the controller. Connected to the output of the Inverter is a DCCT which enables the Controller to monitor the output current to the load and take corrective action if an overcurrent condition occurs. Short-Circuit current is sensed by a shunt in the D.C. Link which causes the controller to fire a crowbar thyristor connected across the input of the Inverter. This, besides removing the voltage from the output and the shorting current away from the GTO's, also blows a fuse isolating the D.C. Link.

Over voltage in the D.C. Link, caused by regeneration from the load, is sensed by monitoring the voltage across the D.C. Link smoothing capacitors.

The general layout is shown in Fig. 4.1 while Appendix 4.1 contains a detailed circuit diagram and component listing.

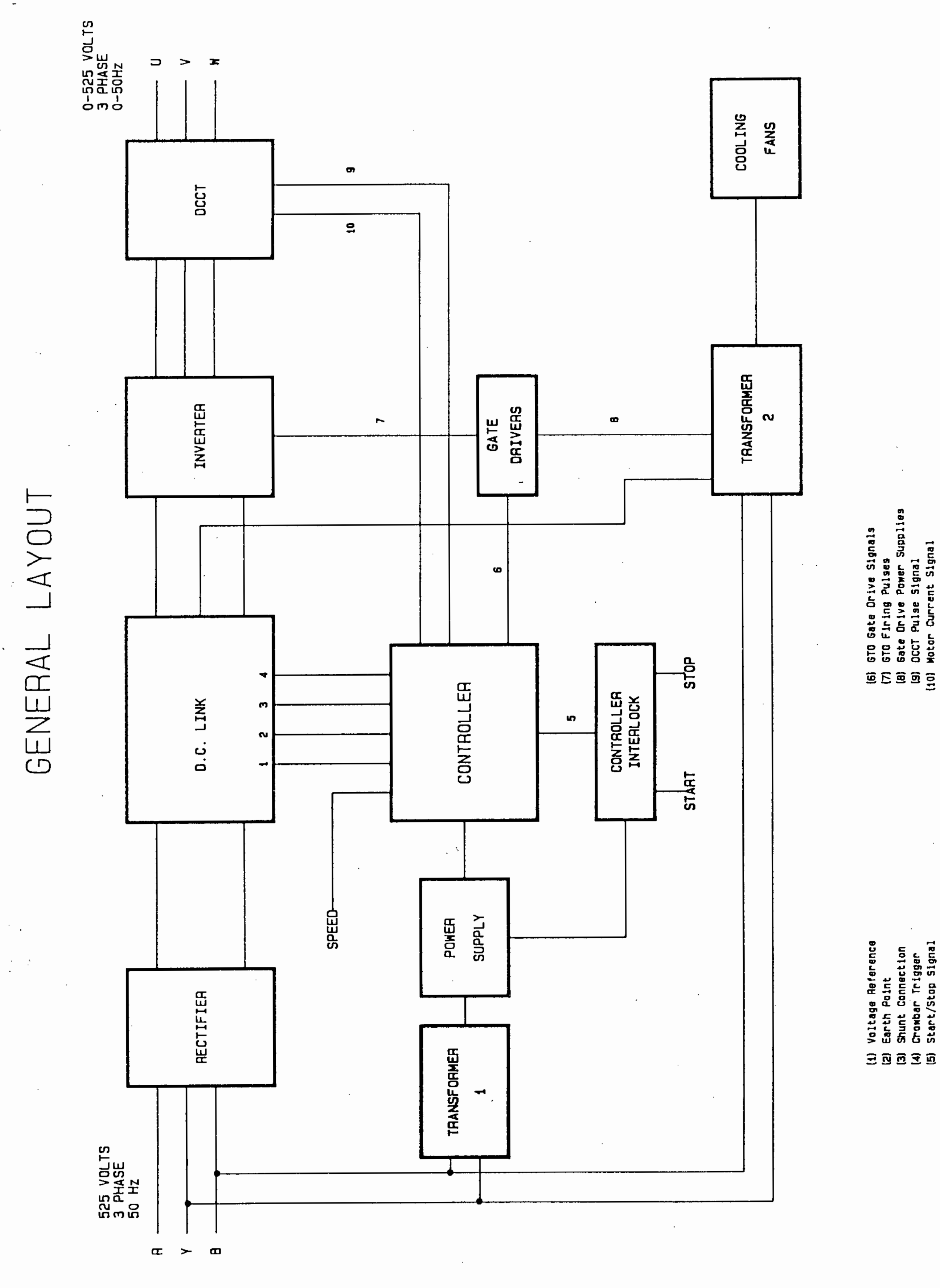

Figure 4.1 General Layout

4.2 POWER REQUIREMENTS OF CONTROL SECTIONS AND COOLING FANS

The Power Supply for the Controller and the Controller Interlock has the following specifications.

-15,0,+15 Volts 500 mA

0,+5 Volts 1 Amp

These voltage rails have a common reference point of 0 volts

Technical details of the Power Supply and Transformer 1 are shown in Appendix 4.2.

Transformer 1 supplies the 110 V_{RMS} required by the cooling fans and the contactors used in the controlled voltage build up of the D.C. Link at "Power Up". The latter is covered in detail in Chapter 5.

4.3 PULSE WIDTH MODULATION FIRING SEQUENCE

The fundamentals of PWM are discussed in detail by B Kliman and A Plunkett in reference [20] and state that certain different methods of implementing PWM are available although the pros and cons of each method are generally avoided. Fig. 4.3(a) shows typical voltage and current waveforms for a PWM Inverter, where V(t) is a sinusoidal approximation of the voltage across the load and I(t) the current in the load. It can be seen that the current lags the voltage which is the case for an inductive load. This immediately gives rise to the problem of generating positive voltage and negative current or negative voltage and positive current simultaneously. This condition is clearly shown in Fig. 4.3(a) in Regions (1) and (3).

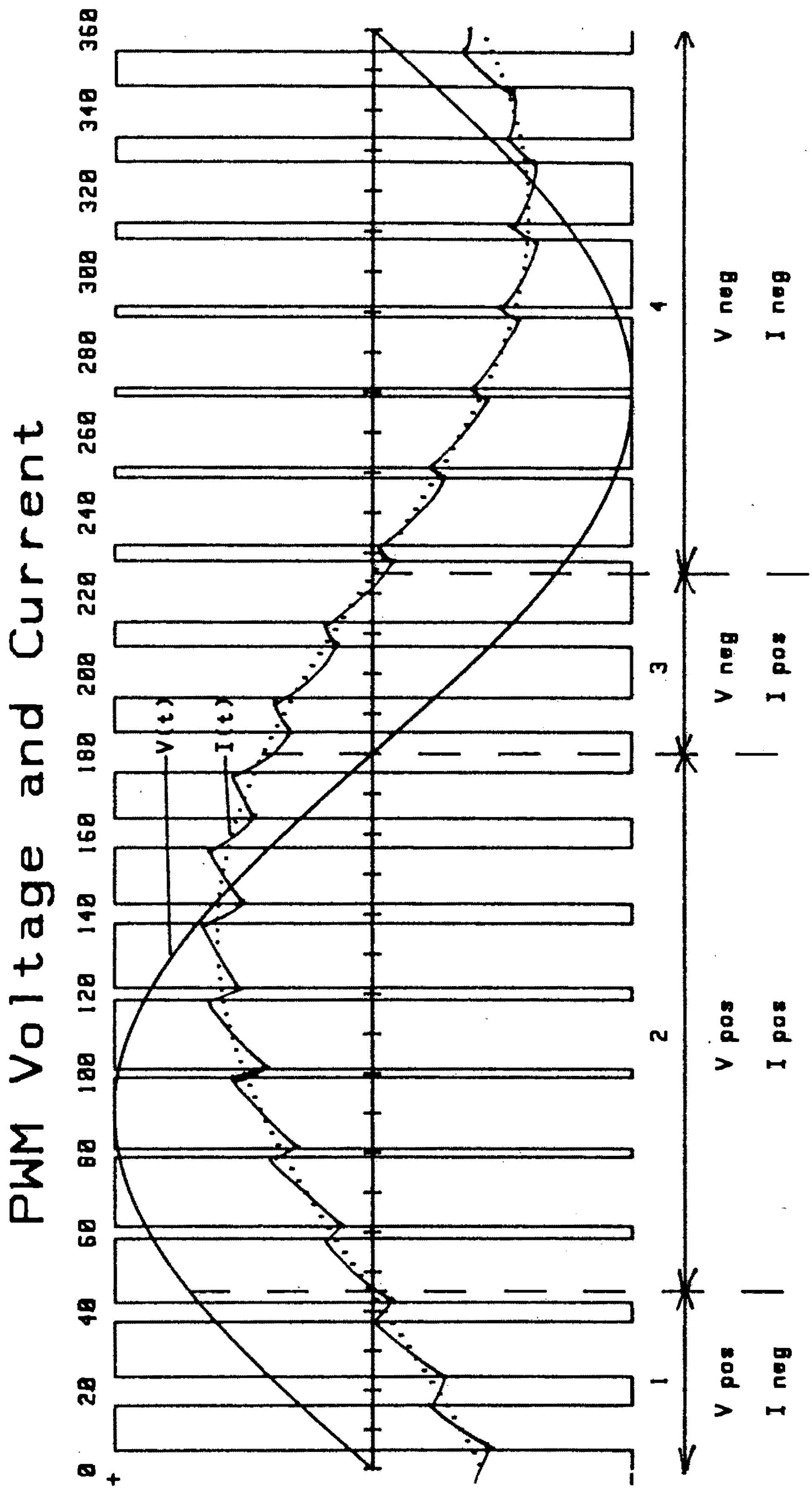

Figure 4.3(a) PWM Voltage and Current Waveforms

Fig. 4.3(b) shows a single Phase-Arm of an inverter showing the current directions used. If GTO1 is fired for the positive half-cycle and GTO2 for the negative half cycle it would mean that the lagging current would have to flow through the freewheel diode during the initial off period of each GTO. When the GTO turns on this current in the Freewheel diode will be extinguished, which can lead to a serious distortion of the current waveform[21].

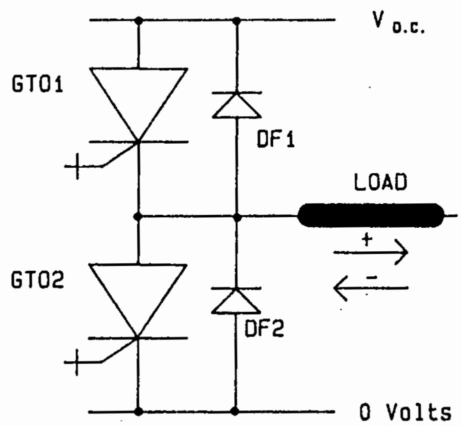

Figure 4.3(b) Load Current in a Phase-Arm

A method known as 2-Level PWM solves this problem. By firing GTO1 and GTO2 in a complementary sequence a conduction path for lagging current during period 1 and 3 now exists. During periods 2 and 4 this complimentary firing is still maintained, but it does not affect the output of the Inverter as no current flows in the complementary GTO.

A typical complimentary set of PWM firing signals for a full 3-phase bridge Inverter are shown in Fig. 4.3(c).

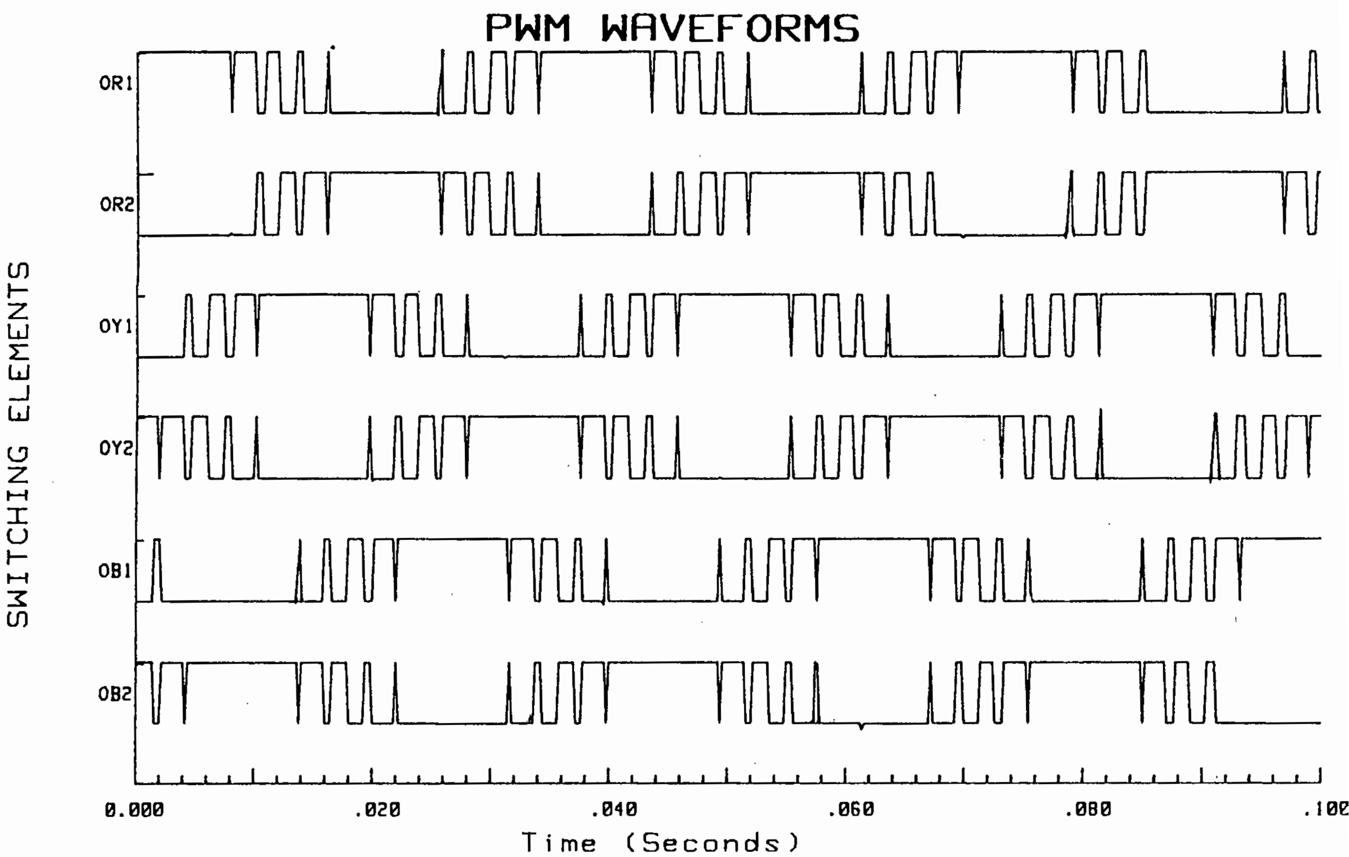

Fig. 4.3(c) PWM Waveforms for a Full 3-phase Bridge Inverter

4.4 SPECIFICATIONS OF THE CONTROLLER

4.4.1 Firing Signals for a Bridge Inverter

The controller supplies 6 independent firing signals, one to each GTO in the Inverter.
They are complimentary PWM signals for each of the two GTO's in each Phase-Arm. The signals from the controller for each Phase-Arm are phase displaced by 120° as required by a 3-phase Inverter.
Each output firing signal is capable of delivering 100 mA at 5 volts.

4.4.2 Minimum and Maximum Output Frequency

The minimum and maximum values are preset in the controller to 10 and 50 Hz respectively.

4.4.3 Maximum Switching Frequency

This is an adjustable feature of the controller. It can be adjusted over in the range 500 Hz to 1kHz using a trimpot, depending on the specifications of the GTO's being used and the requirements of the user.

4.4.4 Minimum Pulse Width

The minimum pulse width of a firing pulse to a GTO is fixed at 30 μSec, but can easily be changed by altering the value of one resistor. The duration of this minimum pulse width can thus be set to the manufacturers specifications.

4.4.5 Short-Circuit Latching

This is an essential feature of the controller even though it may not be evident at this stage. In the event of a short-circuit the existing firing conditions of the GTO's are maintained until the fault has been cleared, after which all GTO's are disabled and cannot fire again until the whole system is re-powered up.

5. POWER SWITCHING UNIT

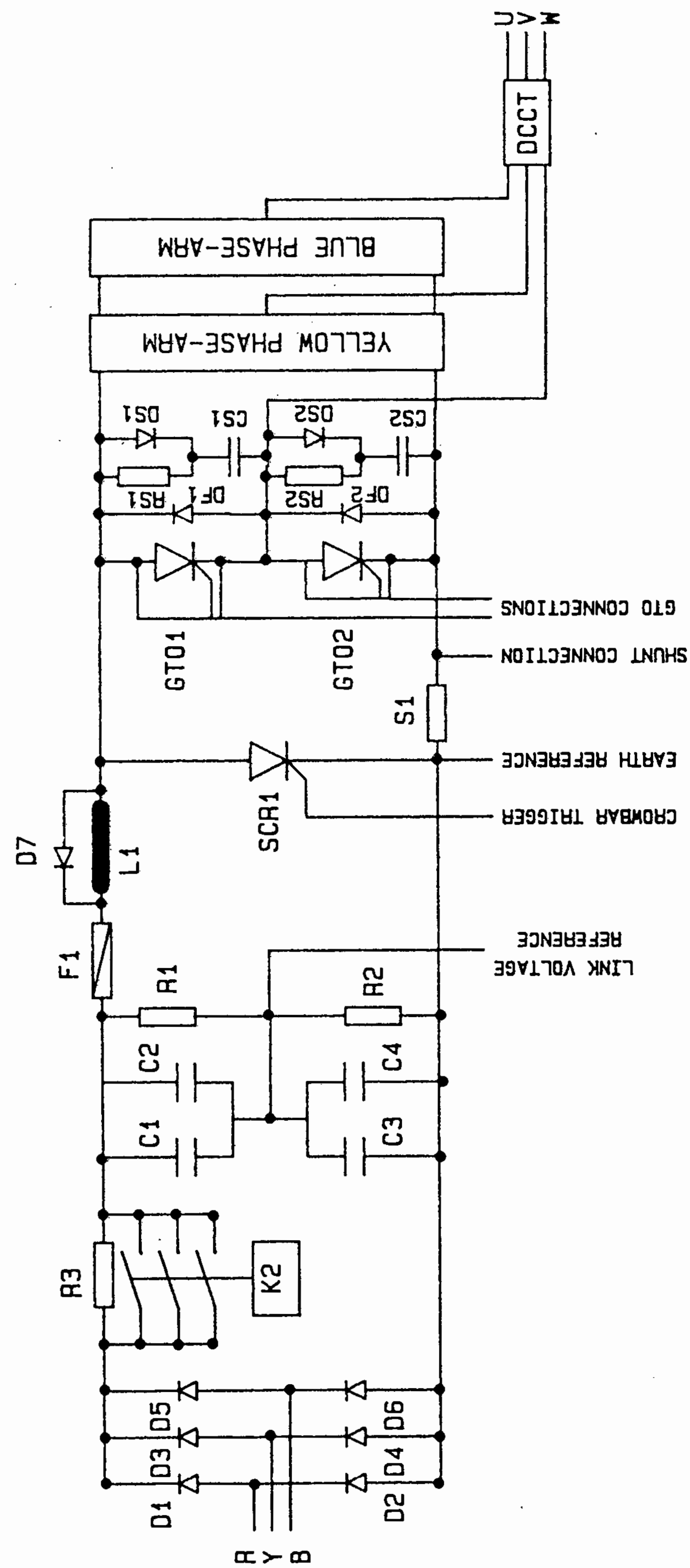

Figure 5. The Complete Power Switching Unit

5.1 BRIDGE RECTIFIER

The Bridge Rectifier consists of 6 diodes connected as shown in Fig. 5. If a 3-phase voltage is supplied to the input of the bridge, the peak D.C. output voltage is

$$V_{D.C.\ peak} = \sqrt{2} \times V_{RMS}$$

If V_{RMS} is 525 volts $V_{D.C.\ peak}$ = 743 volts

If V_{RMS} is 380 volts $V_{D.C.\ peak}$ = 537 volts

SKKD81-4 Powerblock diode modules were used to implement the bridge rectifier. There are 2 diodes in each module, therefore only 3 modules were used.

The SKKD81-4 devices have the following specifications:

PIV	1400	volts (Peak Inverse Voltage)
I_{TRMS}	140	amps (Maximum permissible RMS on-state current)
T_{TSM}	2000	amps (Maximum rated surge current)

Also, according to the manufacturers specifications, the D.C. current which these devices can safely carry when connected in a bridge configuration is 180 Amps. The module should be mounted on Semikron Heatsink (P3/180) and force cooled to meet the higher losses at the increased rating.

5.2 LINK SMOOTHING AND CONTROLLED VOLTAGE BUILD-UP

Smoothing of the D.C. Link voltage is achieved by using 4 polarised electrolytic capacitors. These capacitors have the following ratings

C = 4000 μF
V_{MAX} = 450 $V_{D.C.}$
I_{Ripple} = 16 A ripple current at 100 Hz
I_{Ripple} = 25 A ripple current at 10 kHz

When they are connected as shown in Fig. 5 they have a combined rating of

C = 4000 μF
V_{MAX} = 900 $V_{D.C.}$
I_{Ripple} = 32 A ripple current at 100 Hz
I_{Ripple} = 50 A ripple current at 10 kHz

"Sharing resistors" are connected in parallel with the capacitors to prevent unequal voltage sharing across them. The value of these resistors is 7k5 allowing adequate sharing current between the capacitors to ensure that an equal voltage occurs across them.

The combined power loss in the resistors is given by

$$P_{Loss} = \frac{V_{D.C.}^{2}}{2R} \approx 40 \text{ watts total}$$
(20 watts/resistor)

Using components which were readily available, the ratings of the sharing resistors are

7k5 , 25 watts

At switch on controlled voltage build-up of the D.C. Link is used, which serves a number of purposes.

(1) It limits the inrush current into the smoothing capacitors

(2) It controls the rate of rise of voltage, $\left(\frac{dv}{dt}\right)$, across the GTO's in the inverter section

(3) It allows the control logic to stabilise before any significant voltage exists across the GTO's

(4) In the event of spurious firing of the GTO's at power-up it limits the short-circuit current through them.

Controlled voltage build-up is achieved by inserting a limiting resistor in the D.C. Link for the duration of the link voltage build-up and then bridging it out after 1 or 2 seconds. This is achieved by connecting a normally open contactor in parallel with the limiting resistor. The contactor is controlled by an adjustable timer which brings it in after a preset time. The contactor and timer are supplied from the 110 V winding on Transformer 2. The details of their interconnection are given in Appendix 4.1.

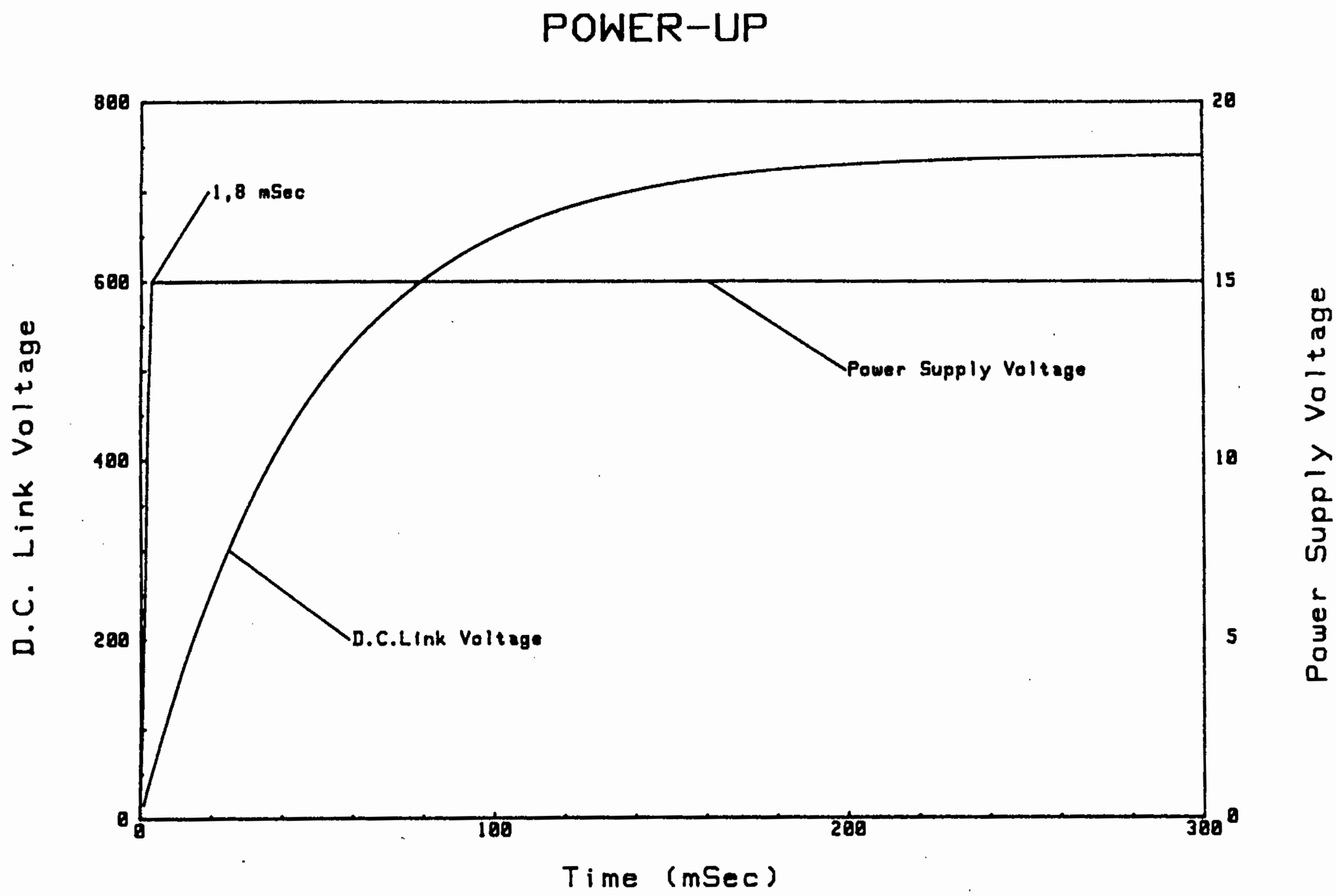

Figure 5.2(a) Power Supply and D.C. Link Voltage at Turn-on.

Fig. 5.2(a) shows the comparison between the voltage build-up of the D.C. Link and the Controller power supply. This shows that the logic voltage supply stabilises in 1,8 mSec, indicating that the TTL Logic I/O will have settled within 3 mSec of switching the system on.

5.3 SHORT-CIRCUIT PROTECTION COMPONENTS

The Short-Circuit protection circuitry shown in Fig. 5 consists of the following components

(1) D.C. Link inductor
(2) Freewheel diode
(3) Fuse
(4) Crowbar Thyristor
(5) Shunt

When a Short-Circuit occurs in the inverter the voltage across the shunt rises. If this voltage rises above a threshold limit set in the controller the crowbar thyristor is fired. This immediately reduces the voltage across the Inverter, hence limiting the Short-Circuit current through the GTO's. This causes the fuse to blow in the D.C. Link and the Short-Circuit is removed[22]. An extra fast SIEMENS Silized 50A 5SD fuse is used.

The D.C. Link inductor simultaneously limits the rate of rise of Short-Circuit current until the fault is cleared.

The rate of rise of this Short-Circuit current is given by

$$\frac{di}{dt} = \frac{V_{D.C.}}{L1}$$

L1 is 500 μH which gives

$$\frac{di}{dt} \approx 1{,}49 \text{ A}/\mu\text{Sec}$$

The freewheel diode across the inductor prevents an excessive voltage spike due to the fast interruption of the current through the inductor.

5.4 THE INVERTER BRIDGE

The Inverter Bridge consists of 6 GTO's, each of which has its own Freewheel diode and Snubber circuit. These components are shown in Fig. 5.

5.4.1 Gate Turn-off Thyristors

As a result of the unfavourable economic situation in South Africa at present the choice and supply of GTO's was found to be severely restricted. All the major manufacturers and their agents were investigated. The majority of the devices were prohibitively expensive due to the international exchange rate, or there was a 3 to 4 month supply delay. Other manufacturers could not supply certain devices advertised as they were having technical problems in their production.

The only suitable GTO available locally at a reasonable price was

AEG-TELEFUNKEN G200A 1200

The device has the following ratings

PIV	1200 Volts	(Peak Inverse Voltage)
I_{TRMS}	80 Amps	(Maximum permissible RMS on-state current)
I_{TQRM}	200 Amps	(Repetitive controllable on-state current)
I_{TQSM}	280 Amps	(Non-Repetivive controllable on-state current)
I_{TSM}	330 Amps	(Maximum rated surge current)

Also available after a 9 month supply delay were the AEG Power Block module

AEG-TELEFUNKEN GG90R 1100

These devices consist of 2 GTO's and 2 freewheel diodes in a Phase-Arm configuration.

They have the following ratings

PIV	1100	Volts (Peak Inverse Voltage)
I_{TRMS}	22	Amps (Maximum permissible RMS on-state current)
I_{TQRM}	90	Amps (Repetitive controllable on-state current)
I_{TQSM}	180	Amps (Non-Repetitive controllable on-state current)
I_{TSM}	270	Amps (Maximum rated surge current)

The recommended maximum switching frequency, F_o, for AEG-TELEFUNKEN GTO's is 1 kHz, even though the minimum duration of on-state current is 30 μSec. Full technical specifications are given in Appendix 5.4.1. for both G200 and GG90R GTO's.

GTO's with a PIV of 1600 Volts and similar current ratings to those required were promised by both Brown Boveri Corp and AEG-TELEFUNKEN but are now not available due to technical production problems.

5.4.2 Freewheel Diode and Snubber Circuit

Generally speaking the ratings of the Freewheel diodes should be similar to the current and voltage ratings of the GTO's. On recommendation from AEG-TELEFUNKEN in Germany D52SR1200 fast recovery diodes were used. These have the following ratings

PIV	1200 Volts	(Peak Inverse Voltage)
I_{TRMS}	120 Amps	(Maximum permissible RMS on-state current)
I_{TSM}	850 Amps	(Maximum rated surge current)

Obviously these are not necessary if the GG90R Powerblock devices are used.

A simple RCD snubber circuit is connected in parallel across each GTO. On the advice of AEG-TELEFUNKEN in Germany D21S1200 fast recovery diodes were used in the snubber circuit. The details of the snubber action are not discussed here, but are covered in most texts on Power Electronic switching.

To calculate the value of snubber capacitance required[8]

$$C_s \geq \frac{I_{TQSM}}{dv/dt}$$

Therefore for I_{TQSM} = 280 Amps and $\frac{dv}{dt}$ = 1000 Volts

$$C_s \geq 0,28\ \mu F$$

The value of snubber resistance is given by[23]

$$R_s \geq \frac{t_{tmin}}{4.C_s}$$

Therefore for $t_{tmin} = 30\mu Sec$

$$R_s \geq 26.8 \text{ ohms}$$

The power dissipation in the snubber resistor can be calculated using a good approximation from the value of the snubber capacitor[8].

$$P_{RS} = \frac{1}{2} C_S \times V_{D.C.}{}^2 \times F_o$$

Therefore for $V_{D.C.} = \sqrt{2} \times 525$ and $F_o = 1kHz$

$$P_{R.S} = 77 \text{ watts}$$

It should be noted that these values of capacitance and resistance are theoretical values derived for ideal circumstances and they should therefore only be used as a guideline. The nature of the Turn-on current and Turn-off voltage across the GTO should be investigated practically and the snubber components optimised.

Certain practical considerations must be taken into account.

- Low inductance capacitors should be used

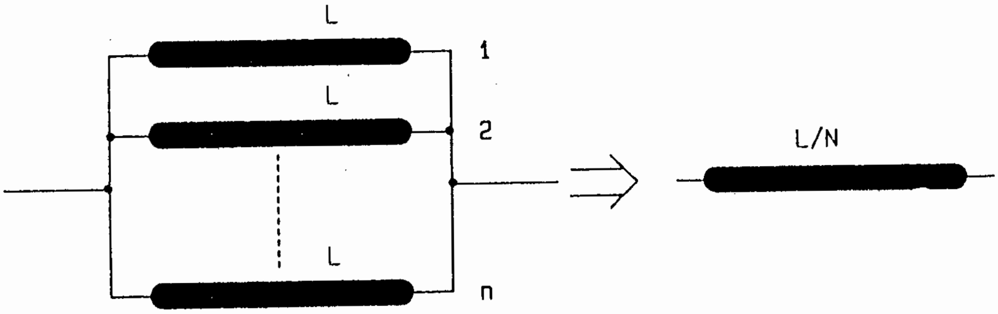

- Rather than using a single capacitor a number of smaller capacitors in parallel can be used causing an even greater decrease in the snubber capacitor inductance as shown above.

- A low inductive mechanical assembly must be used i.e. short leads between components.

- C_s should not be chosen larger than necessary as it increases the power loss in the snubber resistor

- R_s should be as large as possible to limit the discharge current of the snubber capacitor at Turn-on.

A very important factor to note is that these calculations are for a single GTO in a chopper configuration and not for 2 GTO's in a Phase-Arm configuration as in Fig. 5.4.2.

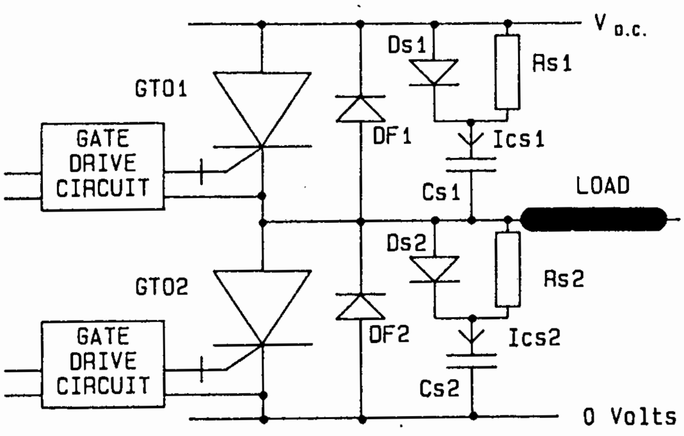

Figure 5.4.2. 2 GTO's in a Phase-Arm

Considering the case when GTO2 is ON and the voltage across C_{S2} is zero. When GTO2 turns off the voltage could rise to between 0 volts and $V_{D.C.}$, depending on the current through the load. Therefore when GTO1 turns on an instantaneous Short-Circuit path exists from $V_{D.C.} \rightarrow D_{S2} \rightarrow C_{S2}$ to 0 volts. A high spike of current will flow through GTO1 when it is turned on[24]. The same sequence of events also occurs with GTO2 receiving a high spike of current when it is turned on.

To avoid this "Snubber Shoot Through" the value of the snubber capacitor must be minimised and the snubber resistor maximised. Other more complicated snubber configurations avoid this problem[25]. These were not used as a large number of extra components are required which makes them unnecessarily expensive.

The new component values used after snubber optimisation are given in Chapter 8.

5.5 DIRECT CURRENT CURRENT TRANSFORMERS (DCCT's)

DCCT's are devices which are able to measure the output current in a 3-phase PWM system[26]. The details of the theoretical operation and design of the DCCT are given in Appendix 5.5. The basic circuit diagram for a single-phase DCCT is shown in Fig. 5.5(a).

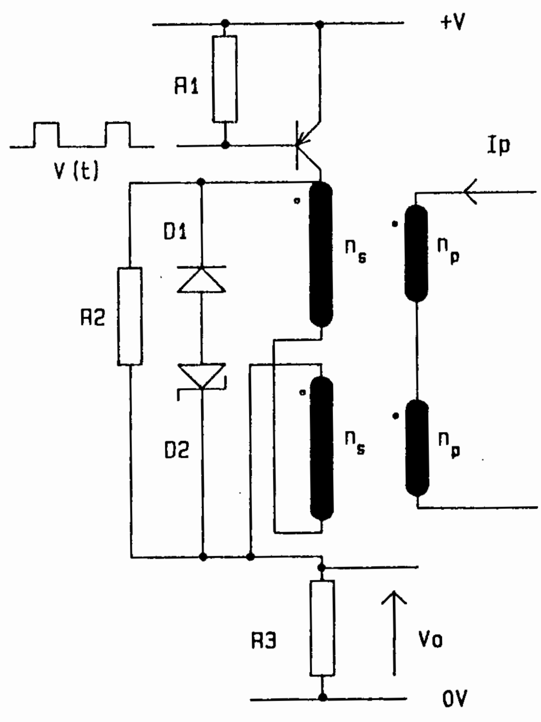

Figure 5.5(a) Basic Circuit Diagram of a Single Phase DCCT

The transformer consists of a pair of identically wound ferrite toroids with their secondary windings connected in anti-phase series as shown in Fig. 5.5(a). A common primary winding passes through the centre of both toroids. To measure the current in the primary winding, a pulsed voltage waveform is applied across the secondary windings.
This produces a voltage signal V_0 across sensing resistor R_3, proportional to the current in primary.

For a 3-phase current measurement, 3 pairs of toroids are used to sense the current in the 3 load conductors. They are connected with a common sensing resistor and switching stage. The output voltage from the sensing resistor is passed through a fast active rectifier. This 3 phase DCCT circuit provides an isolated output voltage which is proportional to the sum of the moduli of the current in the three phases. This gives

$$V_0 \ \alpha \ (|I_R| + |I_Y| + |I_B|)$$

A schematic of a full 3-phase DCCT is shown in Fig. 5.5(b). A detailed circuit diagram is given in Appendix 5.5(b).

D_1, D_2 and D_3 prevent inductive circulating currents. This DCCT is particularly useful in 3-phase A.C. motor control where accurate, high bandwidth, isolated current measurement is required.

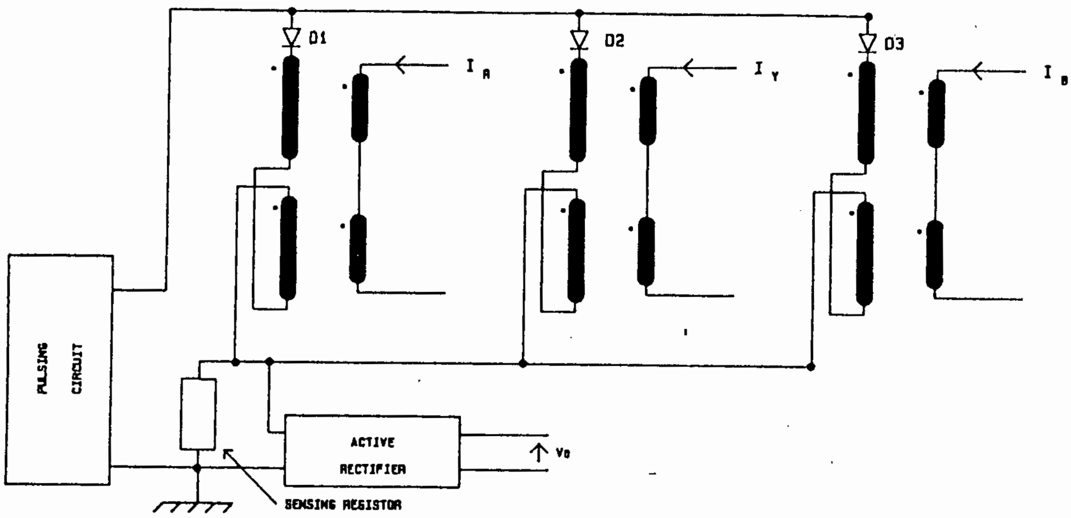

Figure 5.5(b) Three phase DCCT Schematic

A three phase DCCT was constructed using Philips Grade 3E2 toroids. This circuit was tested on a 3-phase load and the results tabulated in Table 5.5 and graphed in Fig 5.5(c) .

I_{RMS}/Phase	V_o(peak) (mV)
0	0
4	40
8	150
12	430
16	700
20	900
25	1050
30	1080

Table 5.5 DCCT Output Voltage

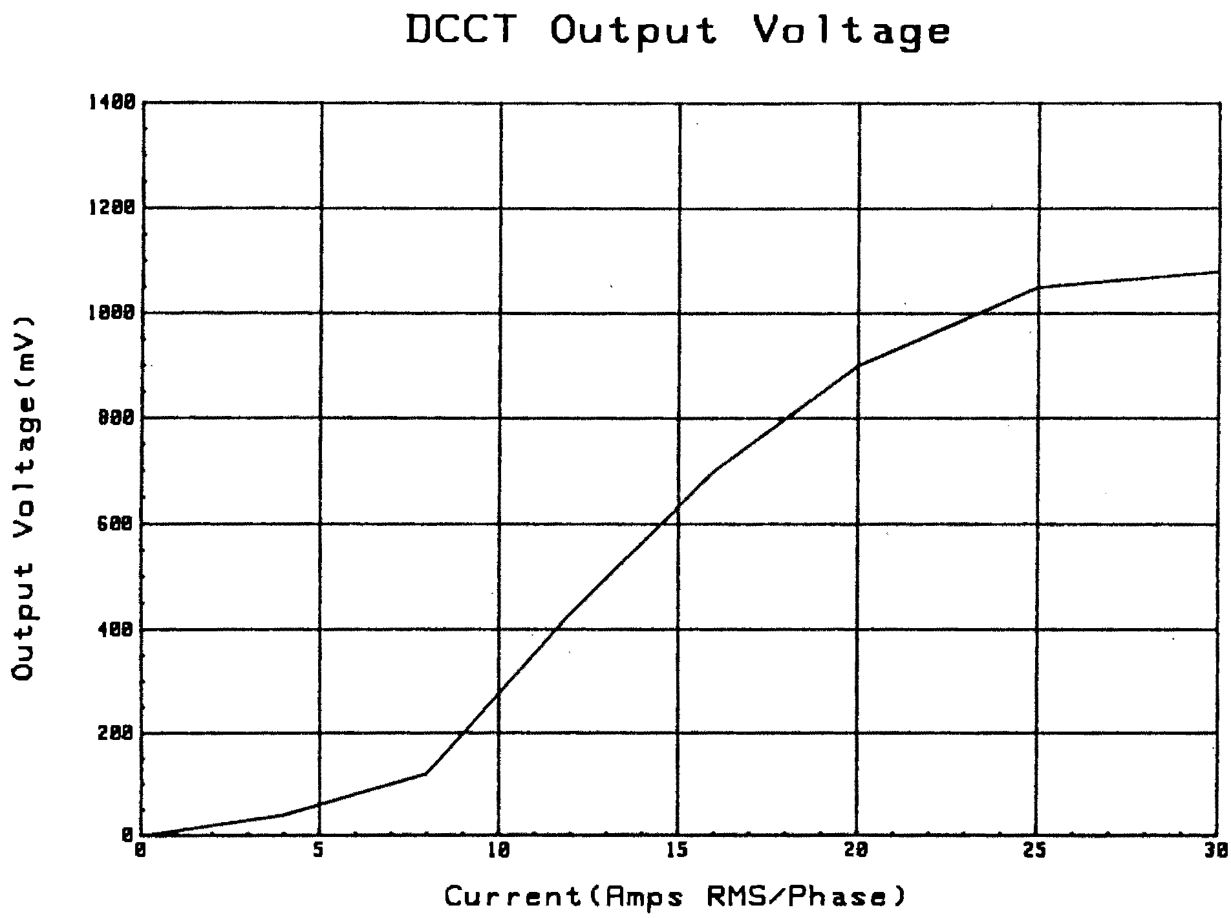

Figure 5.5(c) DCCT Output Voltage

It can be seen that the voltage relationship is nearly linear in the range 8 to 25 Amps RMS/phase. This is because the operation range of the DCCT does not include the kneepoint of the B/H curve outside these limits. Below 8 amps the operation is in the linear region and above 25 amps it is only in the saturation region of the B/H curve.

The operating range of the DCCT can be greatly extended if grade 3C8 toroids were used as they have higher values of B_{sat} and μ_r. These however, were not used as they were unobtainable in South Africa.

6. CONTROLLER

6.1 THE PHILIPS HEF4752 INTEGRATED CIRCUIT

6.1.1 Description of the HEF4752 I.C.

The Philips HEF4752 I.C. is PWM waveform generator. The I.C. is a standard 28 pin dual in line package and designed using single voltage supply LOCMOS technology. Fig. 6.1 shows the pin-out.

HEF4752 Pin_out.

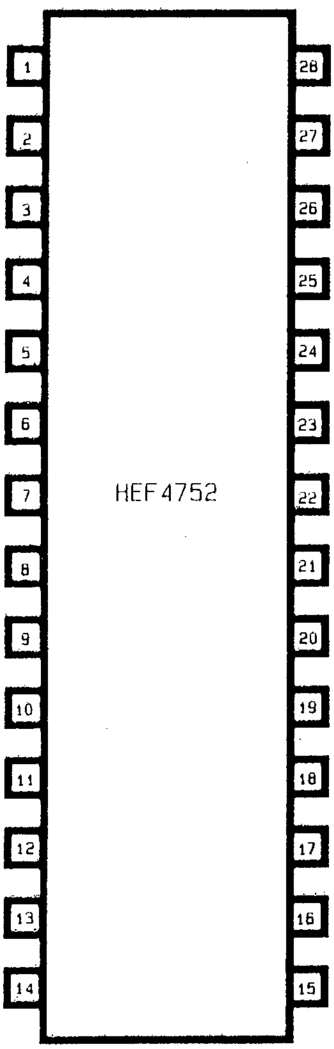

INVERTER DRIVE SIGNALS

8	ORM1	Red_phase main 1
9	ORM2	Red_phase main 2
10	ORC1	Red_phase commutation 1
11	ORC2	Red_phase commutation 2
22	OYM1	Yellow_phase main 1
23	OYM2	Yellow_phase main 2
20	OYC1	Yellow_phase commutation 1
19	OYC2	Yellow_phase commutation 2
3	OBM1	Blue_phase main 1
2	OBM2	Blue_phase main 2
1	OBC1	Blue_phase commutation 1
27	OBC2	Blue_phase commutation 2

DATA INPUTS

24	L	data
25	I	data
7	K	data
5	CW	data
13	A	data
15	B	data
16	C	data

CLOCK INPUTS

12	FCT	frequency clock
17	VCT	voltage clock
4	RCT	reference clock
6	OCT	output delay clock

CONTROL OUTPUTS

23	RSYN	R_phase synchronisation
26	VAV	average voltage
18	CSP	current sampling pulses

Figure 6.1(a) HEF4752 Pin-out

A block diagram showing the internal organisation of the HEF4752 is given in Fig. 6.1.1(b)

Block diagram of HEF4752

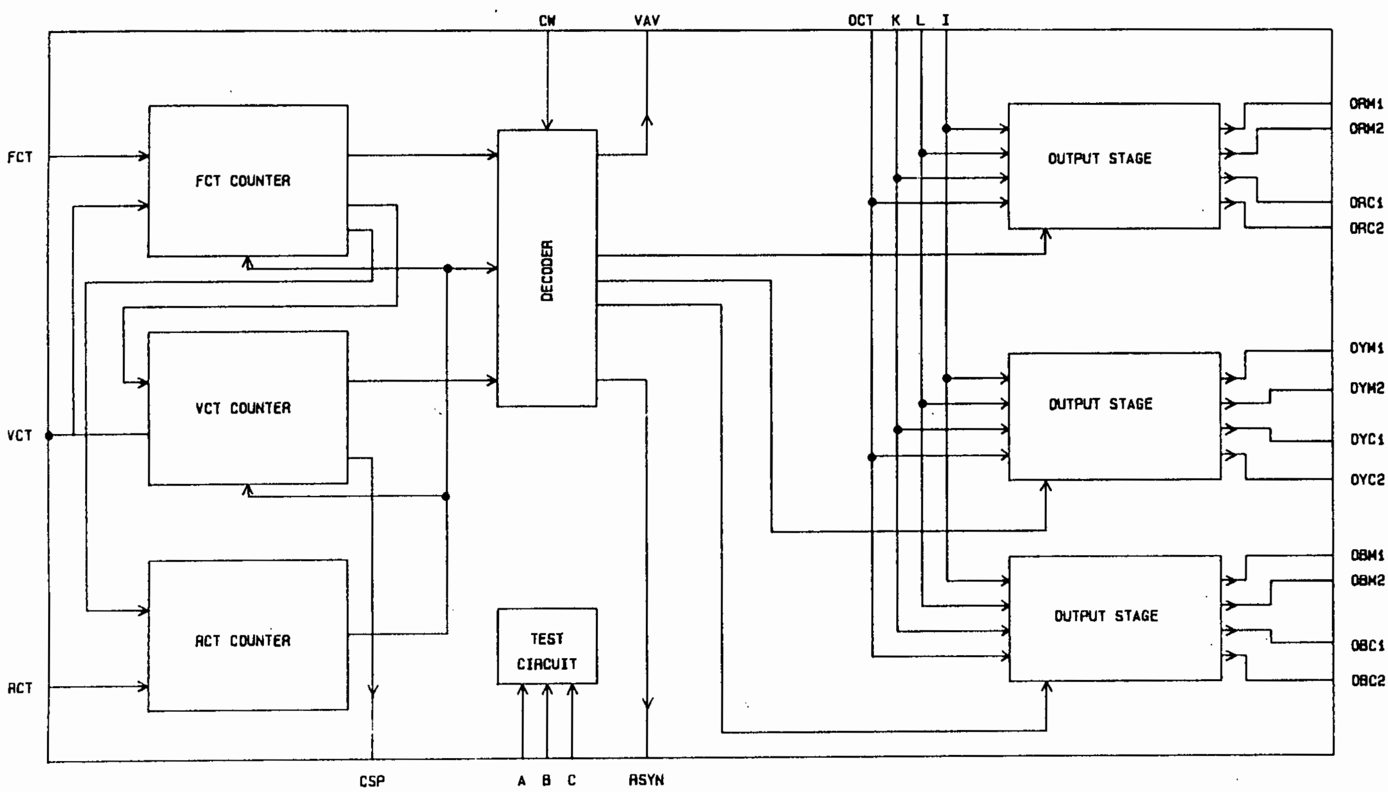

Figure 6.1.1(b) Block Diagram of HEF4752

The circuit comprises of 3 counters, 1 decoder, 3 output stages and a test circuit. The test circuit is used primarily for testing the I.C. during manufacture.

The output stages correspond to the R,Y and B phases of the inverter. Each output stage has four outputs, two main outputs and two which are used to trigger commutation thyristors, if required.

The essential function of the I.C. is to generate switching signals for the GTO's in the inverter. The switching sequence was explained in Chapter 4.

To ensure that the main outputs cannot be turned on simultaneously an interlock delay period is used to separate the On condition of the upper and lower outputs. This interlock delay period is determined by the inputs OCT and K[27].

Three input counters, FCT, VCT and RCT control the output frequency, voltage and PWM carrier frequency respectively.

There are also 4 data inputs : CW, K, L and I. The CW input controls the output phase sequence which provides forward and reverse direction control for induction motors. The data input I determines whether the drive signals to the inverter are for transistors or thyristors. It should be noted that the drive signals for GTO's are similar to those required by transistors. Input L provides a stop/start facility. Input K, in conjunction with the OCT input, is used to adjust the interlock delay period. Table 6.1 illustrates the conditions set up by the 4 data inputs.

Input CW	Low High	Reverse (R,B,Y) Forward (R,Y,B)
Input I	Low High	Transistor mode Thyristor mode
Input L	Low High	Stop (Signals inhibited) Start
Input K	Low High	Delay period (mSec)= $8/F_{OCT}$(kHz) Delay period (mSec)=$16/F_{OCT}$(kHz)

Table 6.1 Data Input Conditions

The HEF4752 has 3 control outputs: RSYN, VAV and CSP. RSYN is a pulse output which occurs before the first positive going zero transition of the R-phase voltage. It therefore provides a stable reference for triggering an oscilloscope.

The VAV output is a digital output which simulates the average of the expected Line-to-Line voltage of the inverter. It does however, exclude the effects of the interlock delay. VAV is useful in closed loop control applications.

CSP is a pulse train set at twice the inverter switching frequency.

6.1.2 <u>Range of Speed Control</u>

Variation in the motor speed is obtained by simply "stretching" (increasing the period) the PWM wave-form to make the motor run slower and "squeezing" (decreasing the period) it to run faster[28]. This is illustrated diagrammatically in Fig. 6.1.2(a)

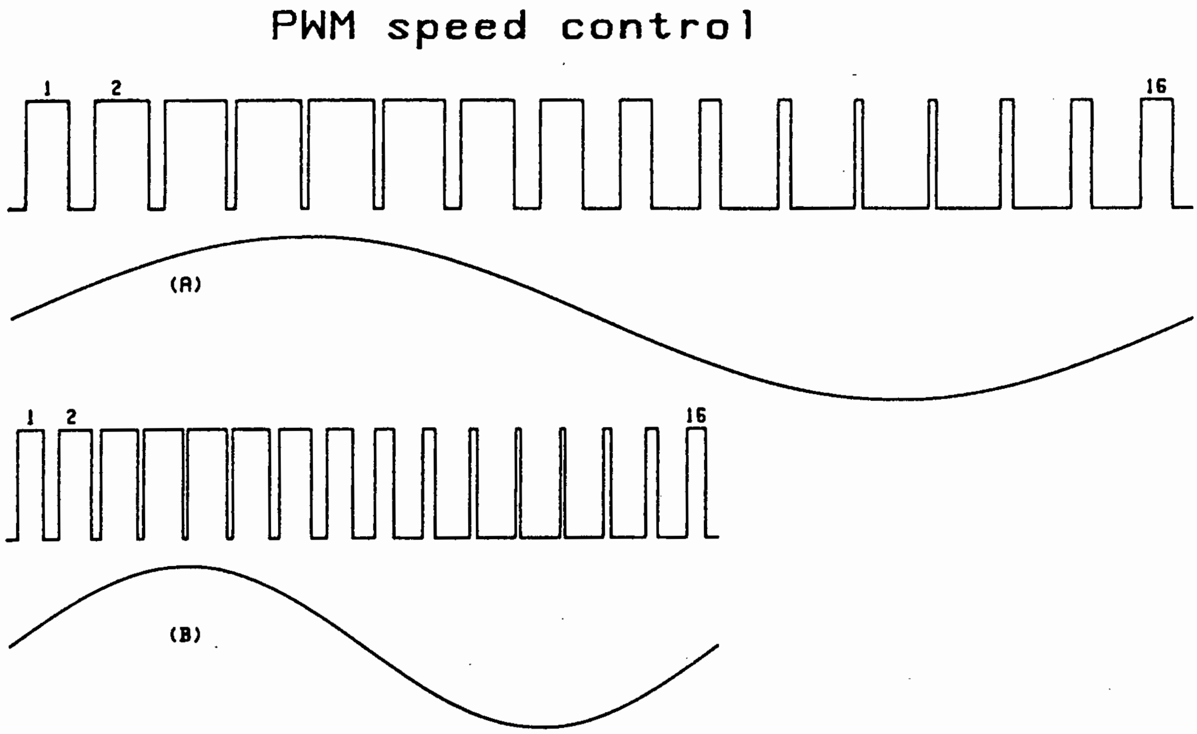

Figure 6.1.2(a) PWM Switching Sequence for
(A) Slow Output Frequency
(B) Faster Output Frequency

When excessively "stretched", the time spent switching to the positive or negative side of the D.C. Link becomes long compared to the electrical time constants which results in pulsating torques being developed by the motor. When excessively "squeezed" the switching frequency increases and power losses increase proportionally.

Because of these constraints the "stretch/squeeze" ratio is limited to 1:0,6 in the HEF4752. This could inflict a severe limitation on the range of speed control. This is demonstrated in Fig. 6.1.2(b) for a carrier frequency of a maximum of 1 kHz.

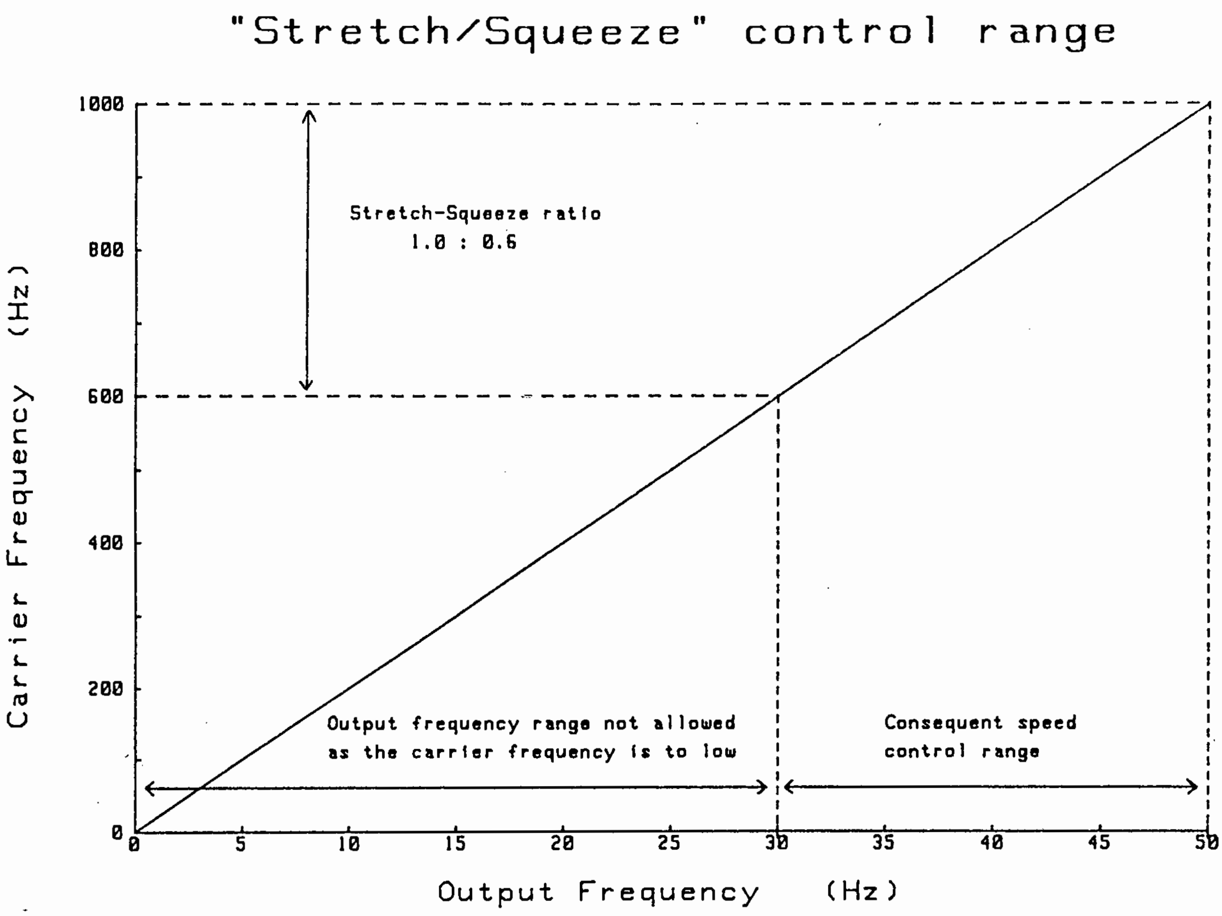

Figure 6.1.2(b) Speed Control for a "Stretch/ Squeeze" Ratio 1 : 0,6

To overcome this limitation the number of switching pulses per cycle is either decreased or increased accordingly. Thus the switching frequency (carrier frequency) is kept within a certain range while the output frequency can be varied over the complete range. This is often called "gear changing". This is shown clearly in Fig. 6.1.2(c). A small amount of hysteresis is included at the "gear change" points is to ensure that jitter is avoided when operating in these regions. The complete details of how this "gear changing" is implemented in the HEF4752 is given in reference [28].

The maximum switching frequency of the inverter is set by the value of the input frequency to RCT, F_{RCT}. The value of F_{RCT} is related to the maximum switching frequency, F_o, by:

$$F_{RCT} = 280 \times F_o \qquad (10)$$

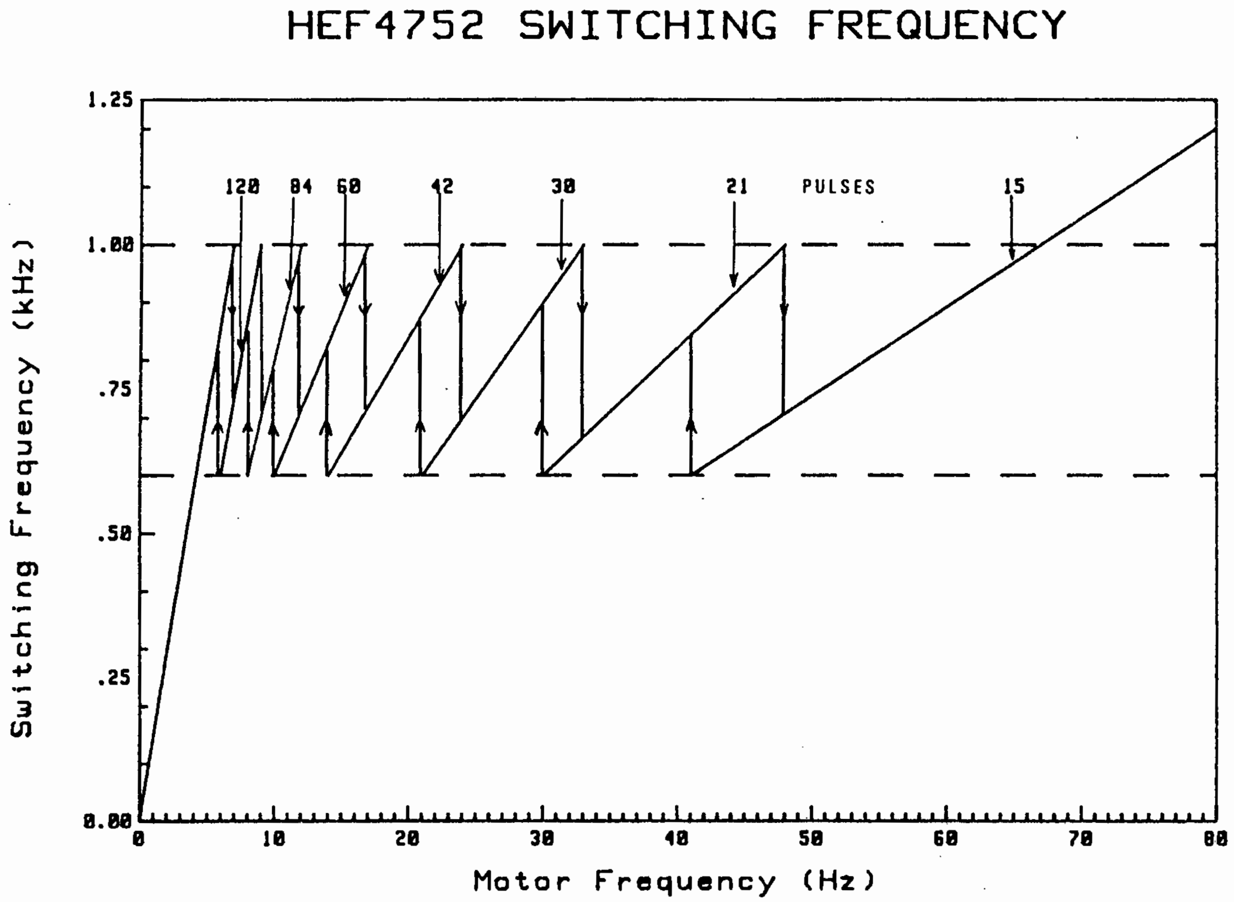

Figure 6.1.2(c) HEF4752 Switching Frequency

6.1.3 Output Voltage and Frequency Control

By controlling FCT (Frequency Control Trigger) and VCT (Voltage Control Trigger) the correct volts/hertz relationship for the induction motor is obtained [27],[28], [29].

The output of the inverter is related directly to FCT by the equation:

$$\text{Output Frequency} = \frac{F_{FCT}}{3360} \quad (11)$$

Speed control is therefore obtained by controlling the frequency input to FCT, F_{FCT}.

The frequency input to VCT, F_{VCT}, controls the depth of modulation of the PWM waveform and therefore controls the voltage output of the inverter. Increasing F_{VCT} reduces the depth of modulation and hence the output voltage, while decreasing F_{VCT} has the opposite effect.

The maximum undistorted sinusoidal output voltage which is obtainable in a system is determined by V_{DC}. The R.M.S. value of the fundamental component at 100% modulation is given by[27].

$$V_{RMS.} = 0.624 \times V_{DC} \quad (12)$$

The frequency at 100% modulation, $F_{m-100\%}$ can be determined by relating the R.M.S. output from the inverter to the motor rating as follows:

$$F_{m-100\%} = \frac{F_N \times 0.624\ V_{DC}}{V_N} \quad (13)$$

where F_N is the motor rated frequency and V_N is the rated R.M.S. voltage.

Once $F_{m-100\%}$ has been established, a value of F_{VCT} can be determined which will set the correct V/Hz relationship throughout the frequency range of the motor to be controlled. This nominal value of F_{VCT}, denoted $F_{VCT(Nom)}$, is related to $F_{m-100\%}$ by:

$$F_{VCT(Nom)} = 6720 \times F_{m-100\%} \qquad (14)$$

With F_{VCT} fixed at $F_{VCT(Nom)}$, the output voltage will be a linear function of the output frequency. Any required variation in this linear relationship is obtained by changing F_{VCT}. This enables the required Base-Boost to be used as described in Chapter 2. The implementation of this is shown later in section 6.4.

6.2 SPEED REFERENCE CIRCUIT

Speed control of the induction motor is achieved through control of the inverter output frequency. The frequency output from the inverter is in turn controlled by the frequency input to the FCT clock, F_{FCT}, of the HEF4752 I.C.. Using a voltage controlled oscillator, (VCO), as an interface between the controller and the FCT input, the problem of speed control becomes one of voltage control.

The rate at which the speed of a motor can be changed is limited by the inertia of the motor and load, and the available motor torque. As the stator frequency is altered, there is a lag in the response of the rotor, resulting in an increase in slip. Unless some limitation is placed on the rate at which the stator frequency can be changed, the increase in slip can result in the maximum torque being exceeded and the motor stalling. The speed reference circuit gives speed control together with control over the maximum rate of increase (acceleration), and decrease (braking control) in the stator frequency.

A simplified diagram of the speed reference circuit is illustrated in Figure 6.2(a) and a full circuit diagram, giving component values is given in Appendix 6.5.

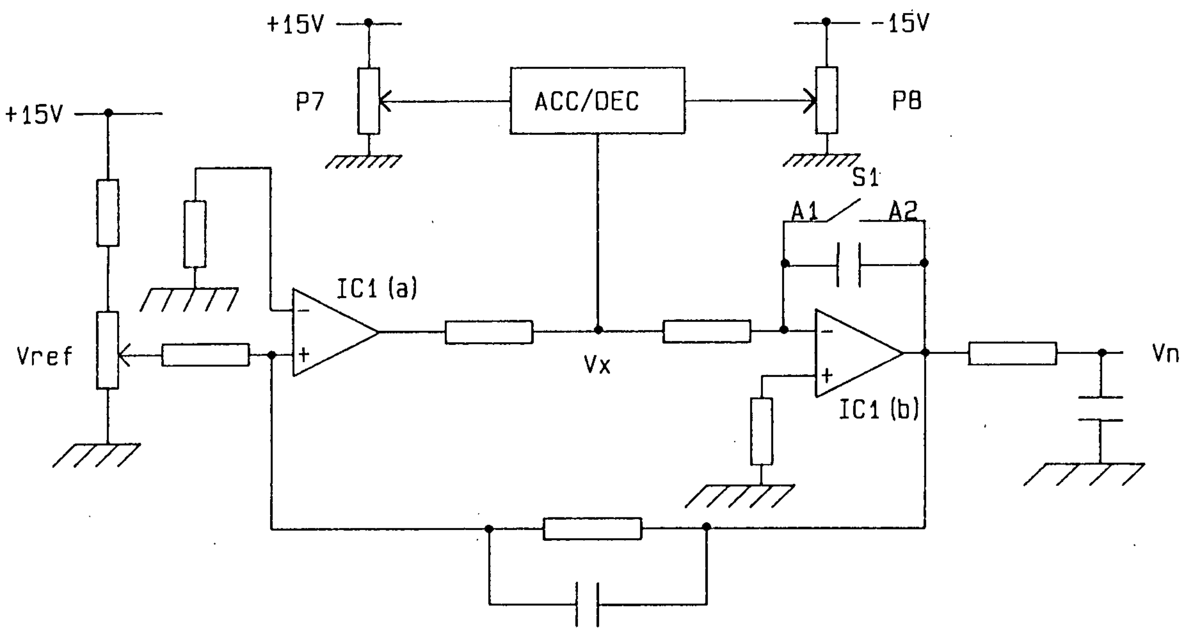

Figure 6.2(a) Speed Reference Circuit

The motor speed is determined by the potentiometer setting V_{REF}. The motor speed signal, V_N, is derived from V_{REF} via a comparator IC1(a) and integrator IC1(b) to give $V_N = -k\ V_{REF}$. A stepwise variation of V_{REF} results in a linear increase or decrease of the output signal V_N. The rate of variation of V_N can be adjusted via acceleration/deceleration potentiometers P7 and P8. As long as S1 is closed V_N is grounded. V_N is now used to control F_{FCT}. The operation of this circuit is shown in Fig. 6.2(b).

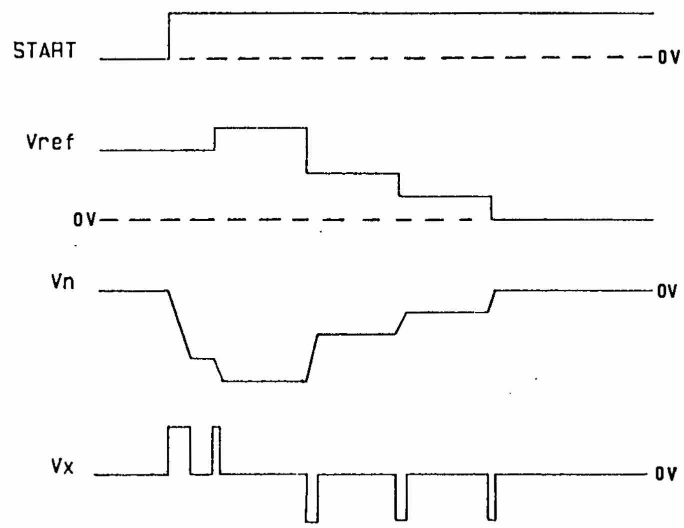

Figure 6.2(b) Speed Reference Circuit Signals

6.3 MOTOR CURRENT AND LINK VOLTAGE LIMITING CIRCUIT

The purpose of this circuit is to protect the Inverter against high motor currents and to prevent excessive D.C. Link voltages. It also provides a degree of stabilisation under large loads.

Excessive motor currents will result if the motor is allowed to operate outside a predefined slip window. This is shown in Fig. 6.3(a) below.

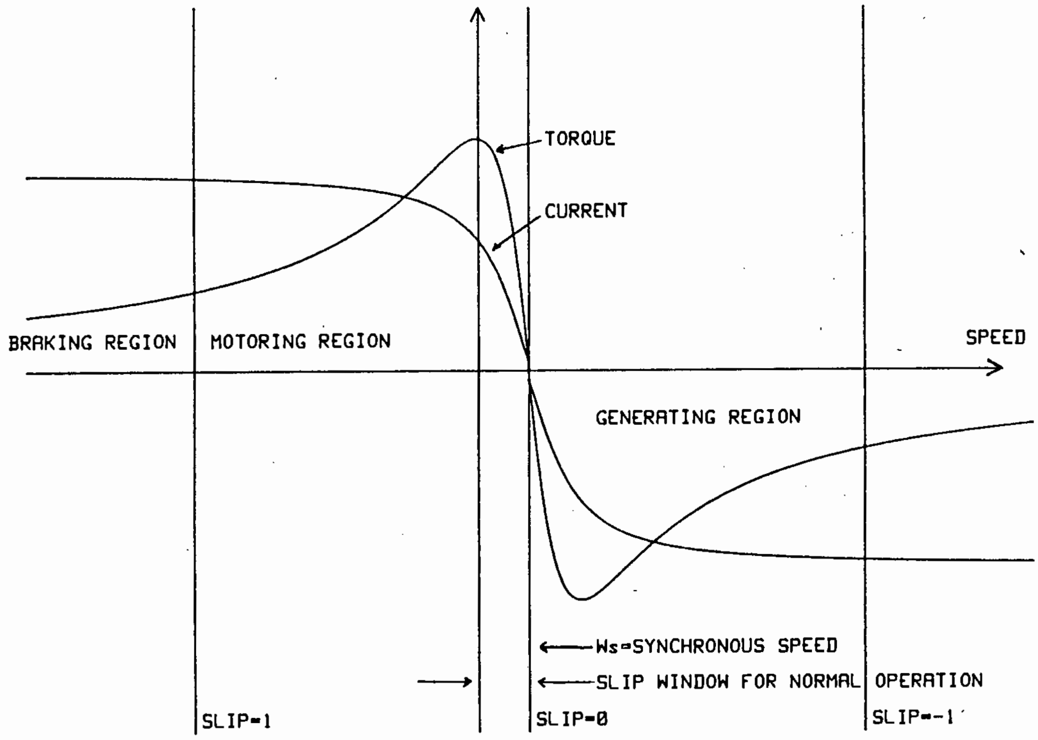

Figure 6.3(a) Torque and Current Characteristics for the Different Operating Regions of an Induction Motor.

In the motoring region high load torques or high acceleration rates will cause excessively high currents. If the inertia of the machine is large, the rate of change of frequency to obtain a new speed must be limited. This is illustrated below in Fig. 6.3(b). The sudden increase in the frequency applied to the motor causes the current to increase from point A to point B on the current curves.

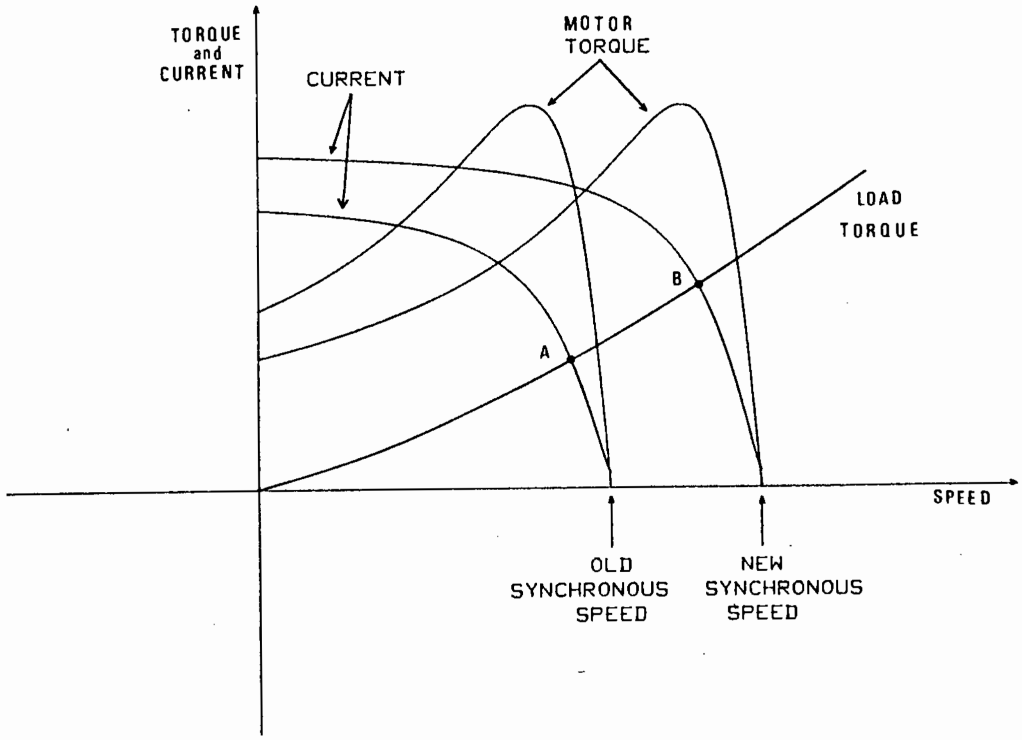

Figure 6.3(b) Current Increase due to Fast Change in Synchronous Speed

If a high current is detected while motoring it can be reduced by decreasing the synchronous speed.

If the motor speed were to rise above synchronous speed due to the load conditions or if the applied frequency was decreased to fast the motor would then operate in the generating region of Fig. 6.3(a). If control of the deceleration rate is not maintained high currents and a rising D.C. Link voltage will result due to regeneration.

Fig. 6.3(c) shows how the speed reference circuit can be adapted to incorporate feedback signals to limit the motor current and D.C. Link voltage.

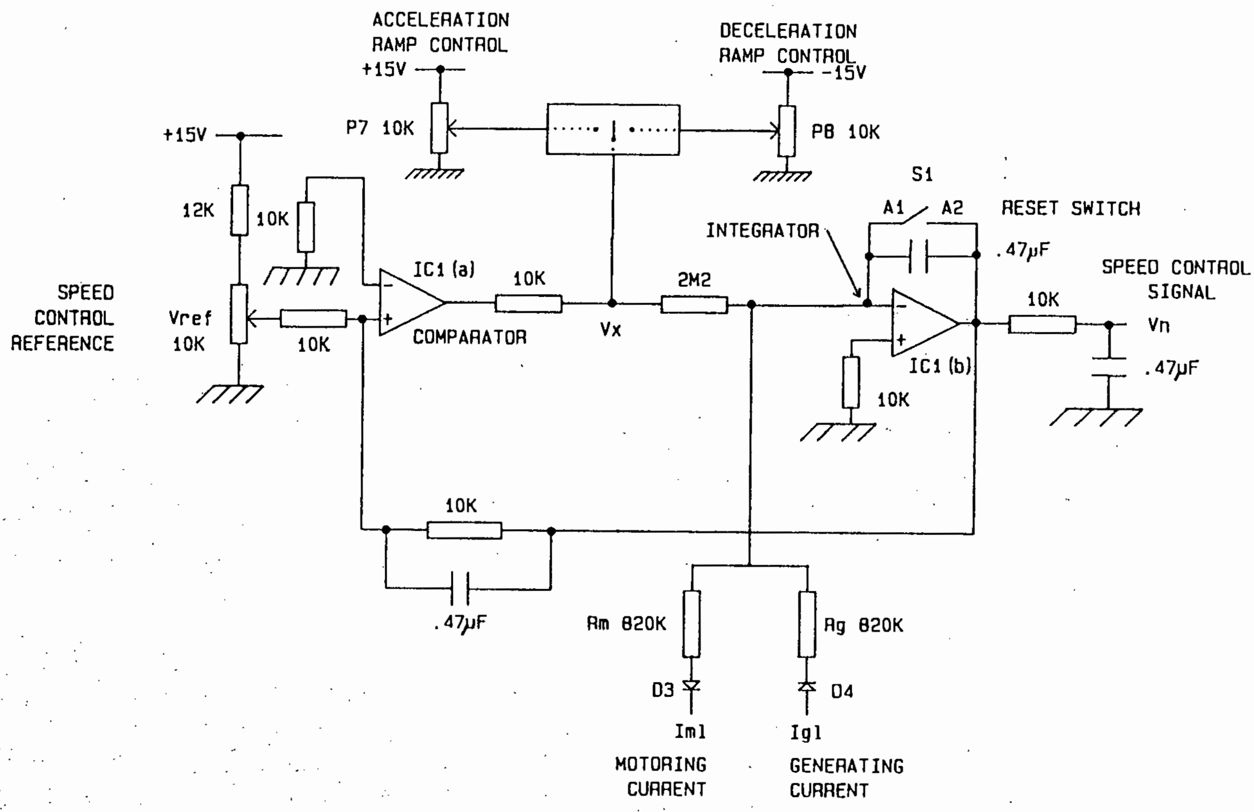

Figure 6.3(c) Adaptation of Speed Reference Circuit for Overcurrent and Overvoltage Protection

The signals I_{ML} and I_{GL} are derived from the motor current and voltage limiting circuit shown in Fig. 6.3(d). Signal I_{ML} is the current limiting signal in the motor mode, while I_{GL} is the current limiting signal in the generator mode.

To reduce motor currents in the motor mode, I_{ML} is driven negative. Diode D3 shown in Fig. 6.3(c) then conducts, so that the negative value of V_N is reduced, thus causing the synchronous speed to fall and the slip to be reduced.

For excessive motor currents in the generator mode, I_{GL} is driven positive. Diode D4 of Fig. 6.3(c) conducts and the negative value of V_N is increased. The synchronous speed rises, and the slip is again reduced.

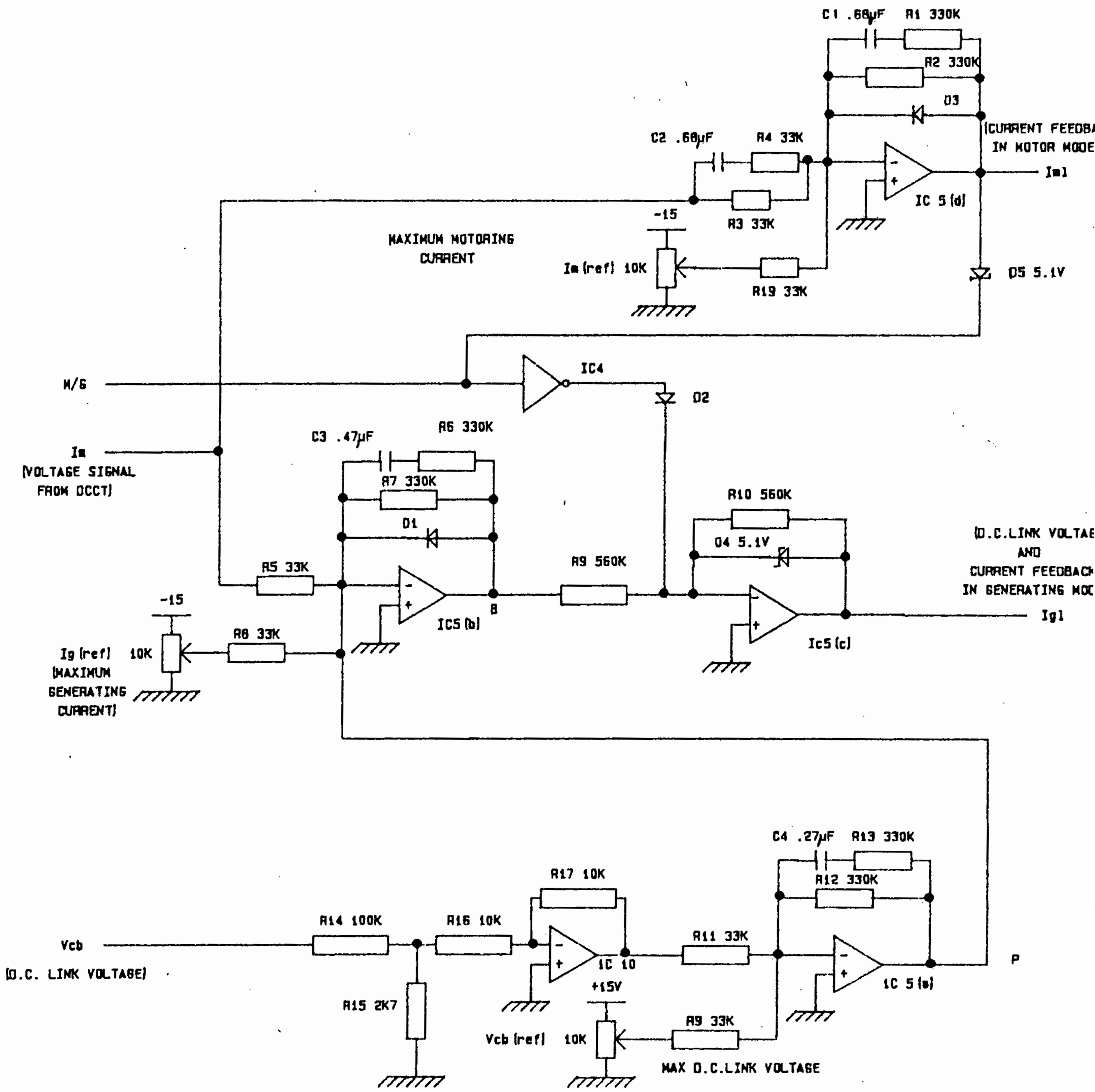

Figure 6.3(d) Current and Voltage Control Circuit

The current and voltage control circuit has three input signals I_M, M/G and Vcb.

The input signal I_M is a voltage proportional to the R.M.S. motor current and is derived from the DCCT's. For control of current in the motor mode the voltage I_M is supplied to the current limiting control amplifier IC5(d) where it is compared with the current reference signal for the motor mode, $I_{M(ref)}$. This circuit works as a three-term error amplifier with proportional-integral-derivative control action. The proportional gain of the circuit is given by R2/R3. The crossover frequencies for the differential action are determined by the value of R3, R4 and C2, while the crossover frequencies for the integral action are given by C1, R1 and R2[30].

The use of three-term controller gives an optimal response for the current limiting signal and prevents overshoot. In order to calculate the ideal integral and derivative time constants, the system response time must be known. Approximate theoretical values can be calculated, but the response time of the complete system should be measured to obtain the optimum values. For the component values shown the time constant was taken as 1 second.

By varying the setting of potentiometer $I_{M(ref)}$, the maximum motor current for the motor mode can be adjusted from 70% to 140% of the nominal motor current. Current limiting below 70% may cause instabilities if motor current is decreased below the required magnetising current.

Control of motor current in the generator mode is achieved by supplying I_M to the error amplifier IC5(b) of Fig. 6.3(d), where it is compared with the pre-adjusted reference signal $I_{e(ref)}$. As soon as I_M exceeds $I_{e(ref)}$, which sets the current limit level in the generating mode, the output of IC5(b) goes negative. This signal is fed to a unity-gain inverter whose output is I_{eL}.

To limit the DC link voltage in the generator mode, the signal, Vcb, which is proportional to the voltage across the smoothing capacitor, is supplied to a unity gain inverter IC10. The output from IC10 is Vcb*. From there it is fed to the error amplifier IC5(a) and compared with the maximum voltage reference value $Vcb_{(ref)}$. For Vcb* greater than $Vcb_{(ref)}$ the output signal P of IC5(a) goes positive. This signal is fed to the input of IC5(b) where it effectively reduces the current reference level for the generating mode.

The M/G signal is used to inhibit the I_{eL} signal whilst the motor is operating in the motor mode and inhibit I_{ML} when in the generating mode. The signal is derived by detecting the slope of the signal V_N as illustrated in Fig. 6.3(e). If the slope of V_N is negative the motor is accelerating. For the slope of V_N positive the motor is decelerating. When the slope of V_N is zero: i.e. the motor is running at a constant speed, the biasing of the differentiator causes the M/G signal to be LOW. The motor is therefore considered to be motoring. Signal M/G is LOW for the motor mode and HIGH for the generator mode.

Referring to Fig. 6.3(d) the inhibiting of the feedback signals is obtained as follows:

With M/G LOW diode D2 conducts, point B is held positive, the zener diode D4 is forward biased and the output I_{GL} is clamped at -0.6V, thus inhibiting the I_{GL} feedback signal.
With M/G HIGH the output I_{ML} is clamped at a maximum negative value of -0.1V by the reverse breakdown action of zener diode D5, inhibiting the I_{ML} feedback signal.

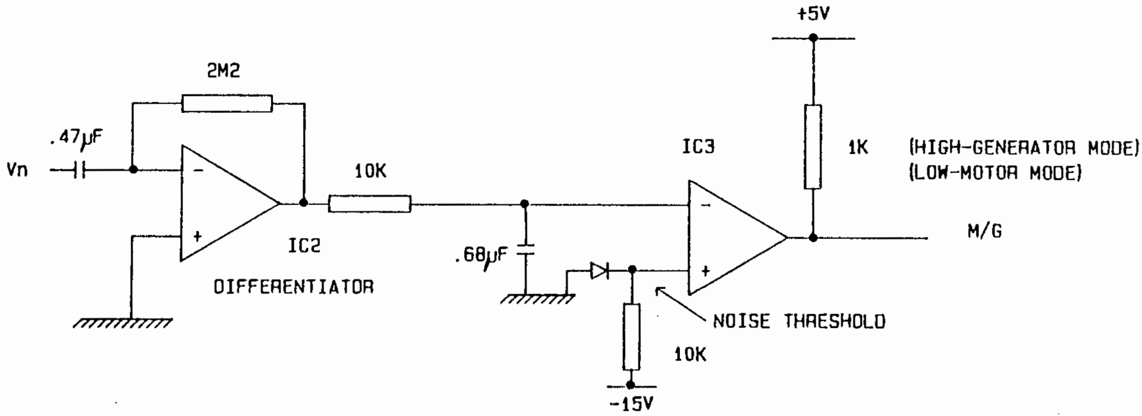

Figure 6.3(e) Circuit Diagram showing for the Derivation of the M/G Signal.

6.4 MOTOR VOLTAGE CONTROL AND BASE-BOOST

The RMS voltage from the Inverter is controlled directly by the VCT clock input of the PWM I.C. If the frequency of the input clock, F_{VCT}, is kept constant the PWM I.C. will ensure a linear Volts/Frequency relationship at the output of the Inverter. Thus by adjusting F_{VCT} correctly Base-Boost can be implemented. A Voltage Controlled Oscillator (VCO) is used to control F_{VCT}. Since the output voltage is inversely proportional to the frequency, the output voltage will be inversely proportional to the VCO control voltage.

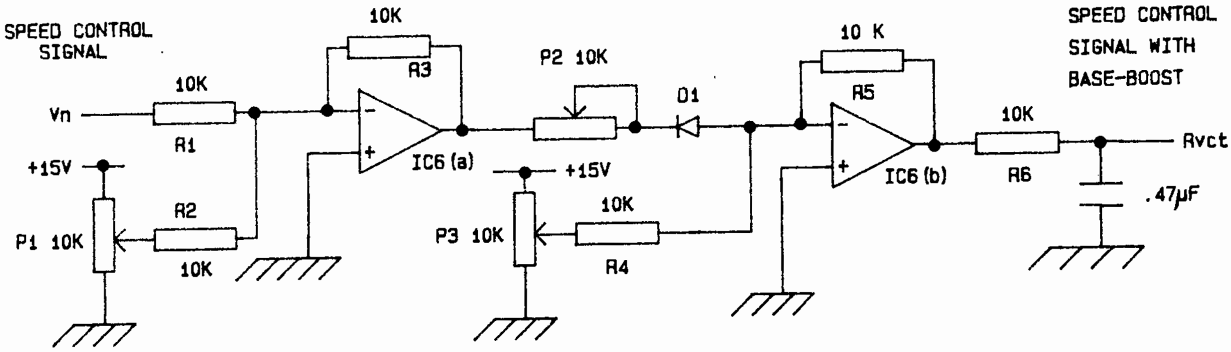

Figure 6.4(a) Base-Boost Circuit

A circuit which provides adjustable Base-Boost is illustrated in Fig. 6.4(a)

The circuit has a single input, the negative speed signal V_N derived from the speed reference circuit, and a single output R_{VCT}. For values of V_N more positive than the value given by:

$$V_N = V_{P1} \frac{R1}{R2} \qquad (14)$$

where V_{P1} is the voltage set by potentiometer P1, the circuit decreases the negative value of R_{VCT}. For values of V_N which are more negative than the value defined by equation 14, the output signal R_{VCT} is adjusted by potentiometer P_3 to obtain the normal rated motor voltage.

Equation 14 therefore defines the region of Base-Boost. For V_N as given by equation [14], the output of I.C.6(a) shown in Fig. 6.4(a) is zero. For more positive values the output of I.C.6(a) becomes increasingly negative, driving the output of I.C.6(b) and thus R_{VCT} more positive. For more negative values, the output of I.C.6(a) is blocked by diode D1. In the region of Base-Boost the degree of compensation may be adjusted by P2. Fig. 6.4(b) illustrates the effect of Base-Boost and the roles of P_1, P_2 and P_3.

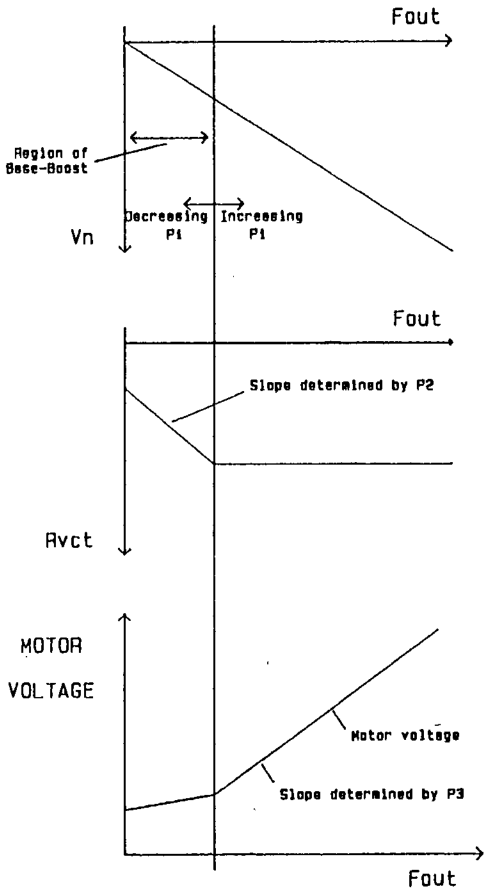

Figure 6.4(b) Base-Boost Signals

6.5 INPUT CONTROLS OF HEF4752 PWM INTEGRATED CIRCUIT

So far a number of independent circuits have been described. With the correct interconnections the required voltage and frequency signals, used to control the HEF4752 I.C., are obtained. The interconnections are shown in Fig. 6.5(a)

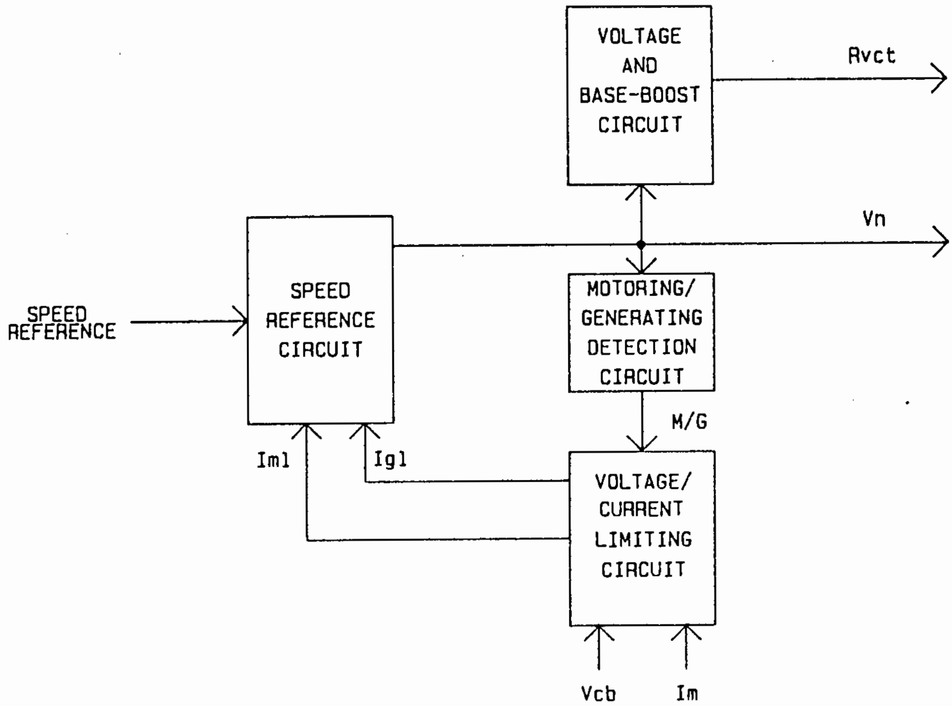

Figure 6.5(a) Interconnection Between Main Controlling Units

From the requirements of the HEF4752 discussed in Chapter 6.1, it is clear that these control signals can be interfaced using VCO's. Both R_{VCT} and V_N are negative control signals and must therefore be inverted before being supplied to the VCO's. The other two inputs, RCT and OCT, are controlled using VCO's with present potentiometers. The interconnection of the HEF4752 I.C. with the rest of the control circuitry, using VCO's as interfaces, is shown in Fig. 6.5(b).

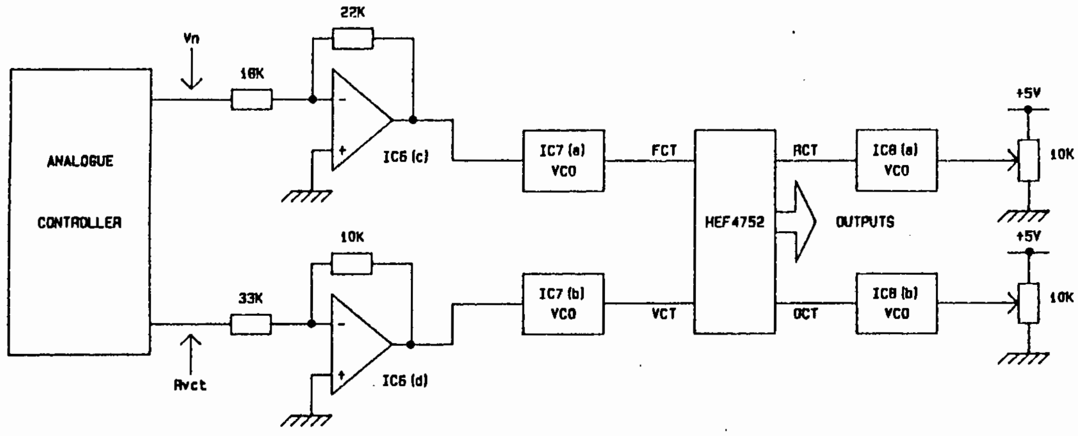

Figure 6.5(b) Interconnection of HEF4752 I.C.

A detailed circuit diagram, printed circuit board layout, component layout and component listing is given in Appendix 6.5.

6.6 MINIMUM PULSE WIDTH

As described earlier in Chapter 5.4.1 a minimum pulse width requirement must be realised by the controller to prevent damage to the GTO's when Firing.

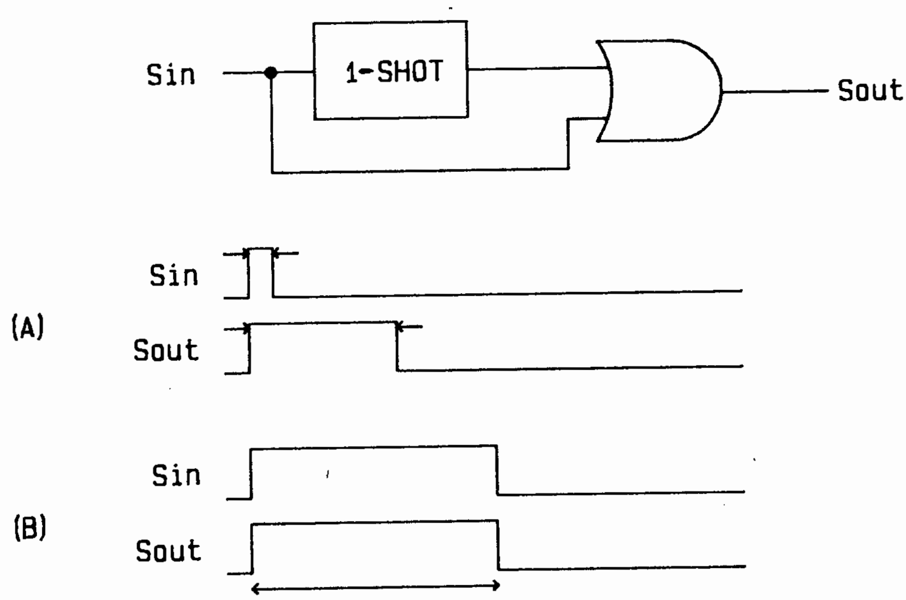

Figure 6.6 Minimum Pulse Width

Fig. 6.6 above shows a simple method of implementing the minimum pulse width requirement. A 1-Shot is configured to trigger on a positive edge and give an output pulse width of 30 μsec. By passing the resulting signal through an OR gate with the input signal, Sin, the output signal, S_{out}, has a guaranteed minimum pulse width of 30 μsec.

6.7 SHORT-CIRCUIT LATCHING AND PROTECTION

When a Short-Circuit occurs it is detected by monitoring the voltage across a shunt in the D.C. Link and two simultaneous functions must be implemented.

(1) The firing condition of the GTO's must be maintained until the Short-Circuit condition is cleared as discussed in Chapter 4.4.5.

(2) The crowbar thyristor must fire to clear the Short-Circuit current from the Inverter stage as discussed in Chapter 5.3.

Fig. 6.7 is a schematic diagram which shows how these conditions are met. When a Short-Circuit occurs the latch is disabled which causes the ON and OFF status of the GTO's to be maintained and simultaneously the Crowbar thyristor is fired. The signal, S_0, from the Short-Circuit detection circuit feeding the latch also causes the enable line to the HEF4752 to go low. This disables the outputs from the HEF4752. The "Enable circuit" is designed so that the output will remain low until the whole system is re-powered up. Once the Short-Circuit is cleared the latch enable signal goes high which results in all the GTO's being turned off. This is also shown in the timing diagram in Fig. 6.7. The Short-Circuit detection circuit is merely a comparator with an adjustable threshold.

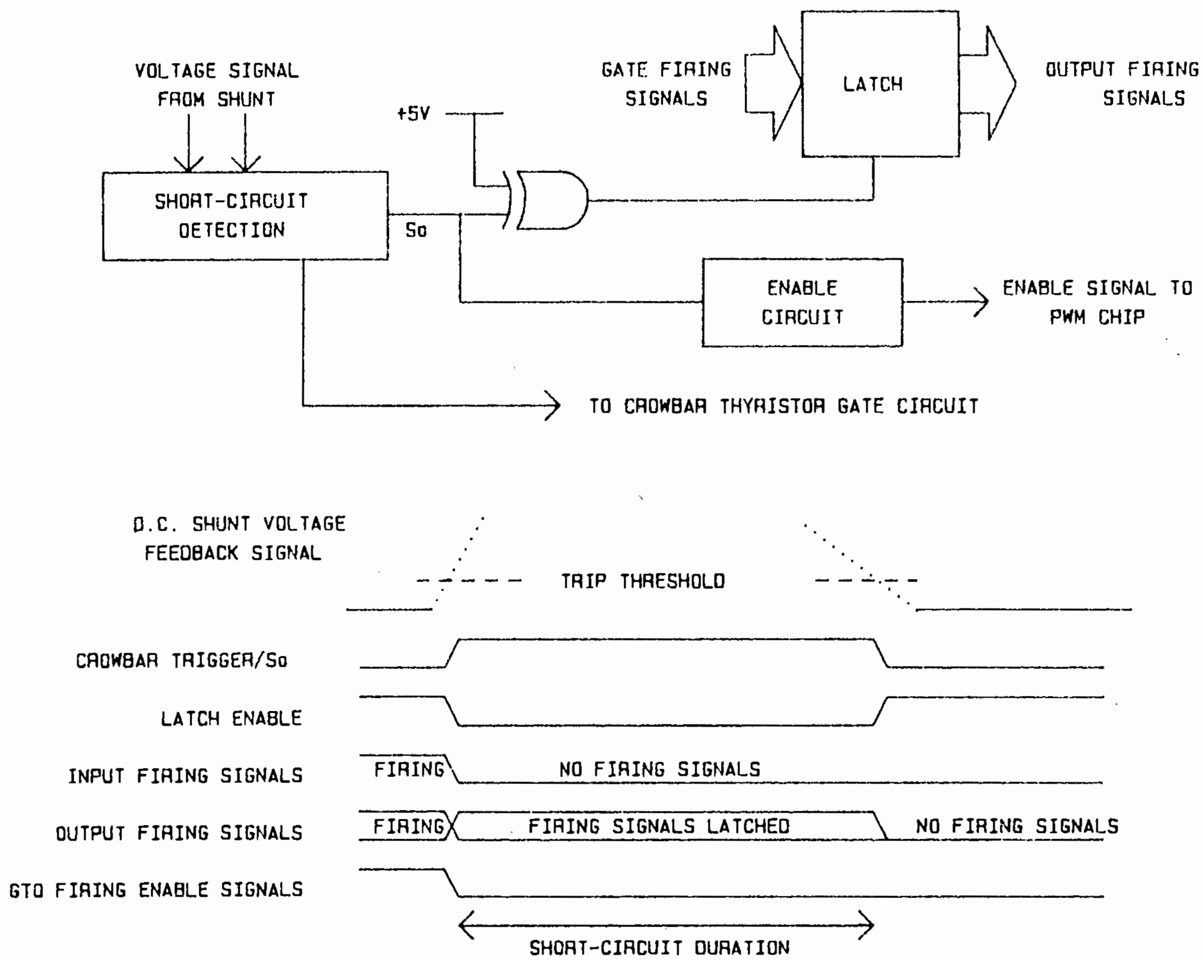

Figure 6.7 Short-Circuit Protection Circuit

6.8 BUFFERING FOR THE GATE DRIVE CIRCUITS

As discussed in Chapter 4.4.1 the output firing signals from the controller should be able to deliver 100 mA at 5 V to the Gate Drive circuits. This is far in excess of output current rating of TTL logic. Fig. 6.8 shows how these current requirements can be obtained using a TTL Buffer and driver transistor.

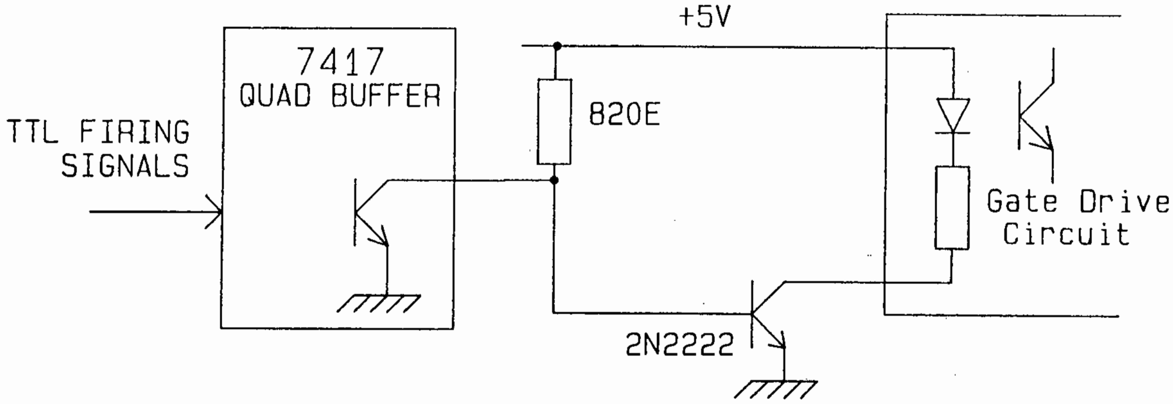

Figure 6.8 Buffer Circuit

6.9 INTER-CONNECTION OF HEF4752 OUTPUTS TO GATE DRIVERS AND PROTECTION CIRCUITRY

Fig. 6.9 shows how the firing outputs from the HEF4752 are connected to each stage of the control circuitry before it is applied to the GTO Gate Drivers. A detailed circuit diagram, printed circuit board layout, component layout and component listing is given in Appendix 6.9.

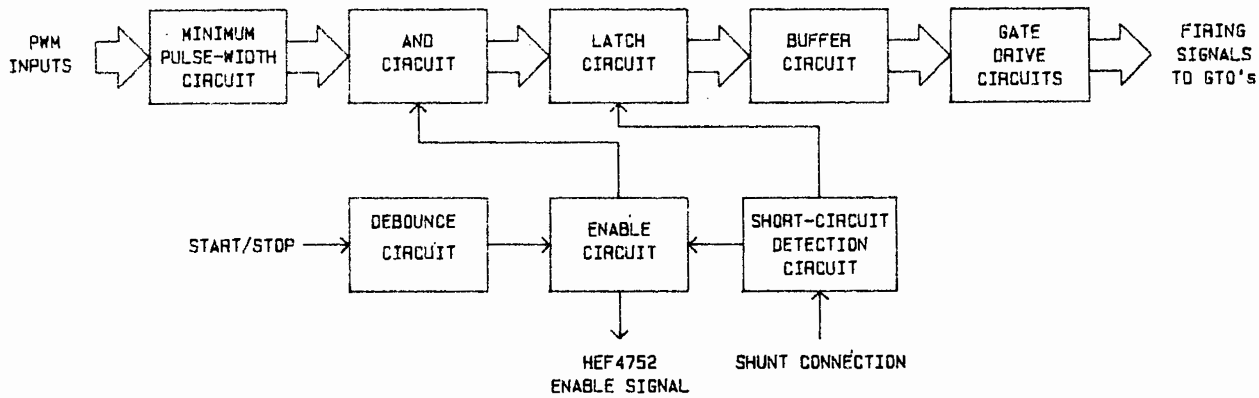

Figure 6.9(a) HEF4752 Firing Signal Interfacing Circuit

At the initial power-up of the VSD the output from the Short-Circuit flip-flop, S_A, in Fig. 6.9(b) goes High. This ensures that the Enable signal follows the Start/Stop signal.

The Start/Stop signal is obtained by switching S2 which is connected to a debounce circuit. When S2 is switched to position C the Enable signal will go High. When it is switched back to position A it will go Low. The operation of this switch is described in section 6.10. The debounce circuit in Fig. 6.9(b) is merely a "jam-type" RS flip-flop with pull up resistors at it's inputs[31].

At the occurrence of a Short-Circuit a pulse is applied to the Short-Circuit Flip-Flop. This signal comes from the Short-Circuit detection circuit. This resets to output, S_A, and it will not set again until the VSD is re-powered up. This ensures that the Enable signal is Low after the occurrence of a Short-Circuit.

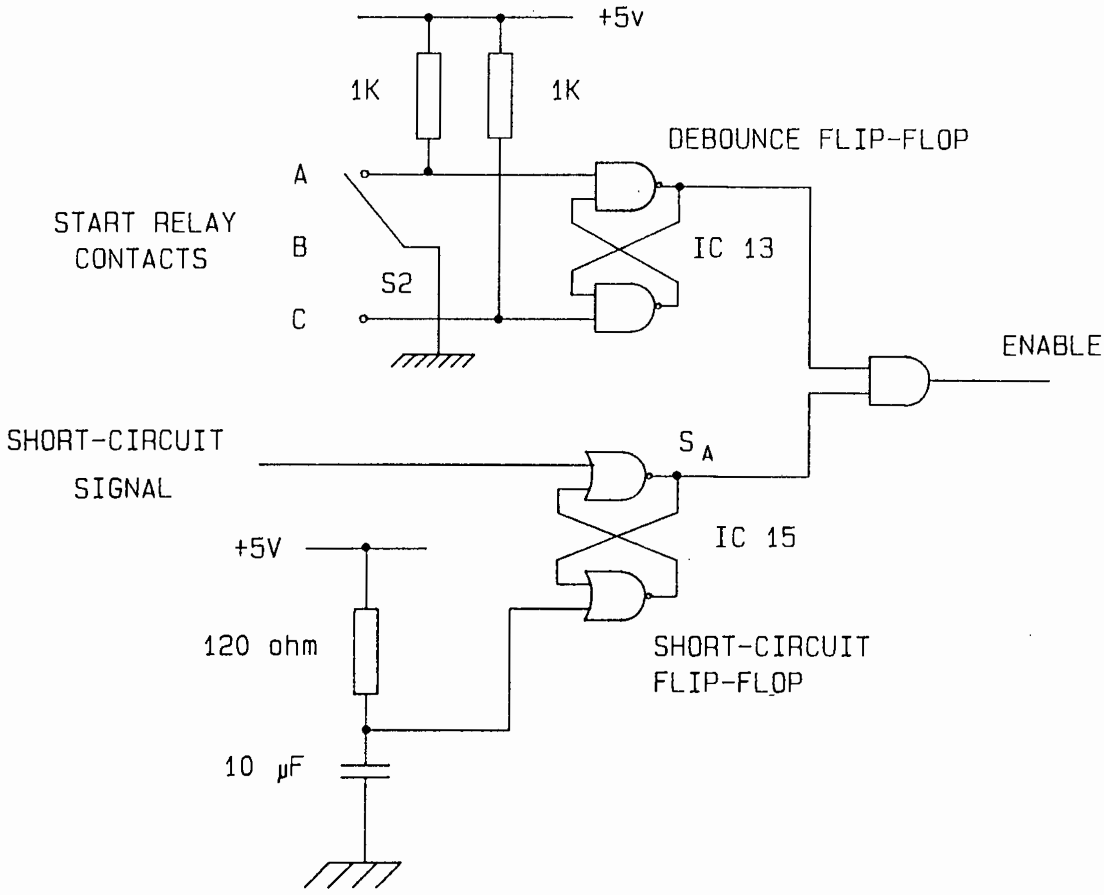

Figure 6.9(b) Enable Circuit

The AND block inserted between the Minimum Pulse-Width and Latch circuits of Fig. 6.9(a) is merely a safety condition. All firing signals are AND'ed with the HEF4752 enable signal. It ensures no spurious firing signals will be passed through to the Gate Drivers. The AND section is enabled when the Enable line is High.

6.10 CONTROLLER INTERLOCK AND CONTROL BOARD INTER-CONNECTION

The Controller Interlock is merely a relay which will give a High output when the START button is depressed and will maintain this condition until the STOP button is depressed. It also ensures that the Integrator capacitor in the speed reference circuit described in Chapter 6.2 is discharged when the system is turned off. This is shown in Fig. 6.10.

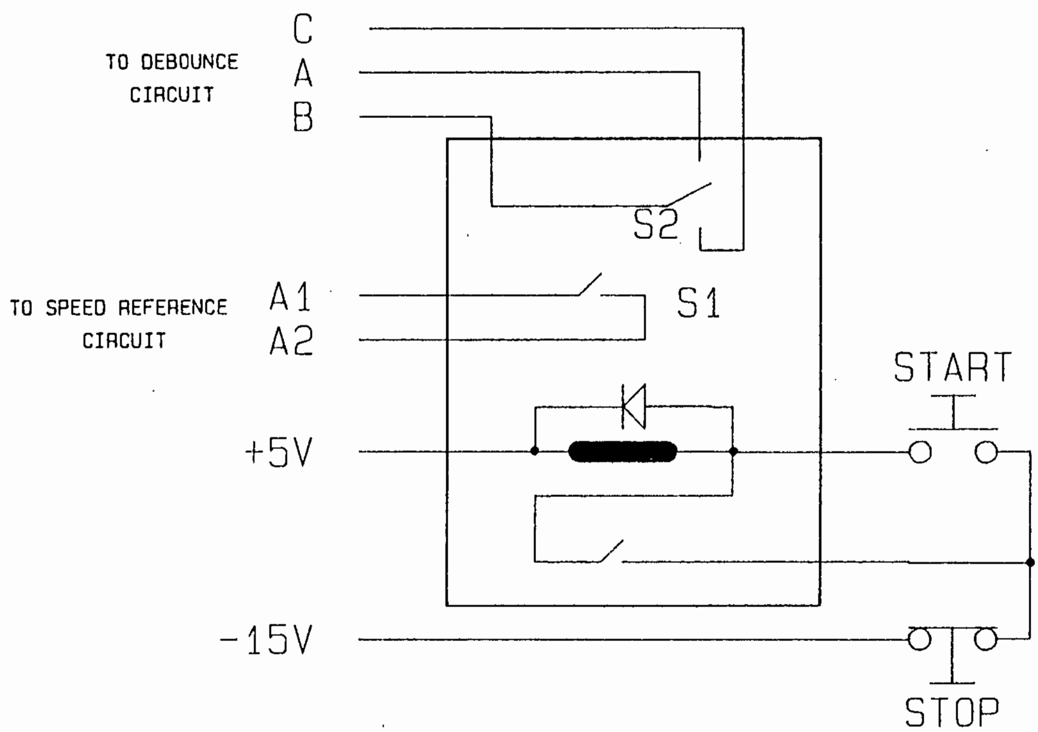

Figure 6.10(a) Controller Interlock

The inter-connection of the control boards and the Controller Interlock is shown in Fig. 6.10(b). The full detailed circuit inter-connection and component listing is given in Appendix 4.1.

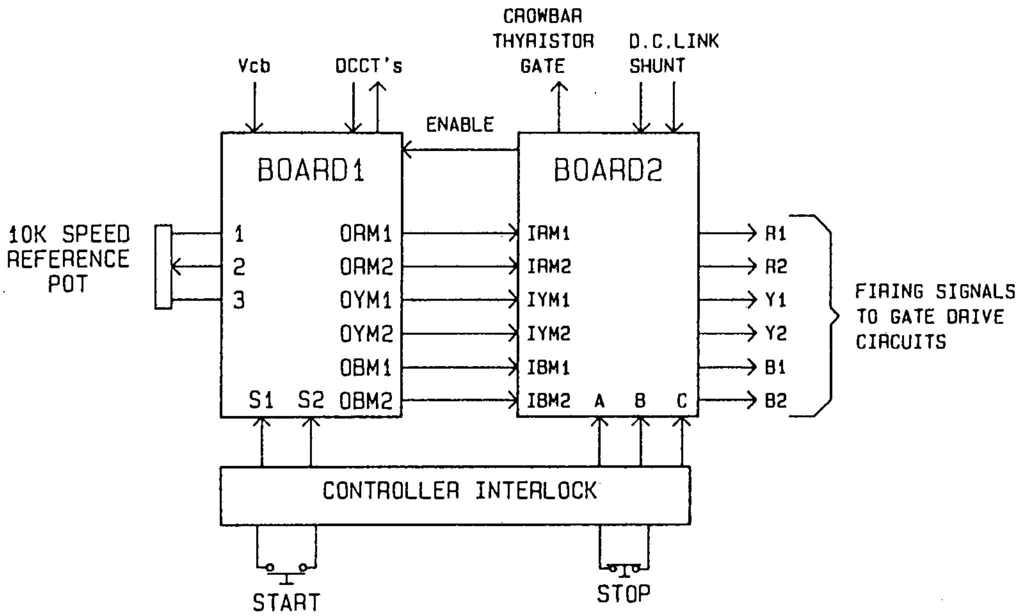

Figure 6.10(b) Control Board and Controller Interlock Connection

7. GATE DRIVE CIRCUITS

7.1 METHODS OF SWITCHING GTO'S ON AND OFF

The gate current requirements for switching a GTO can be met in essentially two manners. One is a dual power supply system where the ON and OFF gate currents flow from separate supplies. The other is the single power supply system where the ON and OFF gate current flow from one power supply[7]. Examples of these are shown in Table 7.1.

For the dual power supply system, closing S1 with S2 open turns the GTO on. Closing S2 and simultaneously opening S1 turns it off. Conceptually this is the most simple but it has the disadvantage of requiring a dual power supply.

For the single capacitor power supply system the GTO is switched on by opening S1. On closing S1 the capacitive discharge turns the GTO off by providing reverse gate current, Igq.

For a single reactor type power supply system the closing of S1 turns the GTO on. It is turned off when S1 is opened due to the energy stored in the reactor inducing Igq.

Both of these single power supply systems have the advantage of a physically smaller circuit and a less complicated power supply. They do however, have the major disadvantage that their maximum switching frequencies are limited by either an RL or RC time constant, which is not the case in a Dual Power supply system. Single power supply systems are also not very satisfactory in applications where the GTO is switching current through an inductive load. This is because Ig cannot flow continuously when the GTO is turned On. A dual power supply system can be configured to supply a continuous gate current, Ig, which is required in inductive load applications where the current lages the voltage.

Considering the above reasons it is obvious that a dual power supply switching system is the best option.

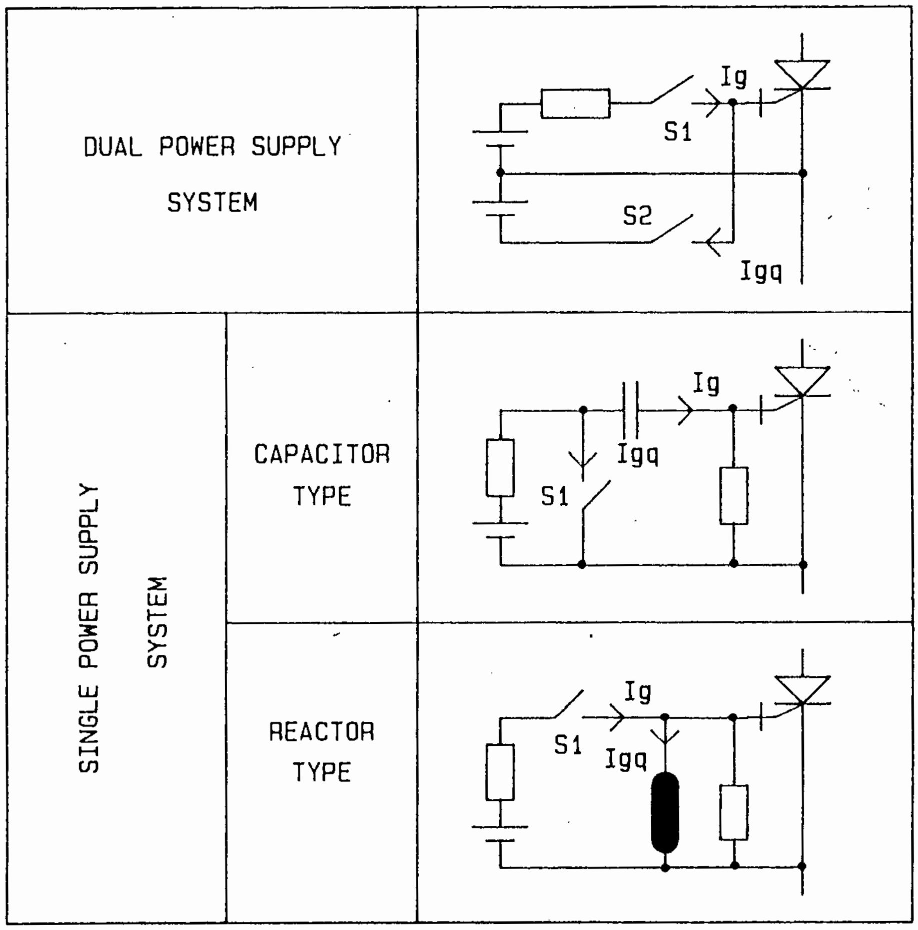

Figure 7.1 Examples of Basic Gate Drive Circuits

7.2 POWER SUPPLIES

An independent floating Dual Power Supply is required for the Gate Drive circuits of each GTO. To achieve this a transformer with 6 isolated, centre tapped, secondary windings is used.

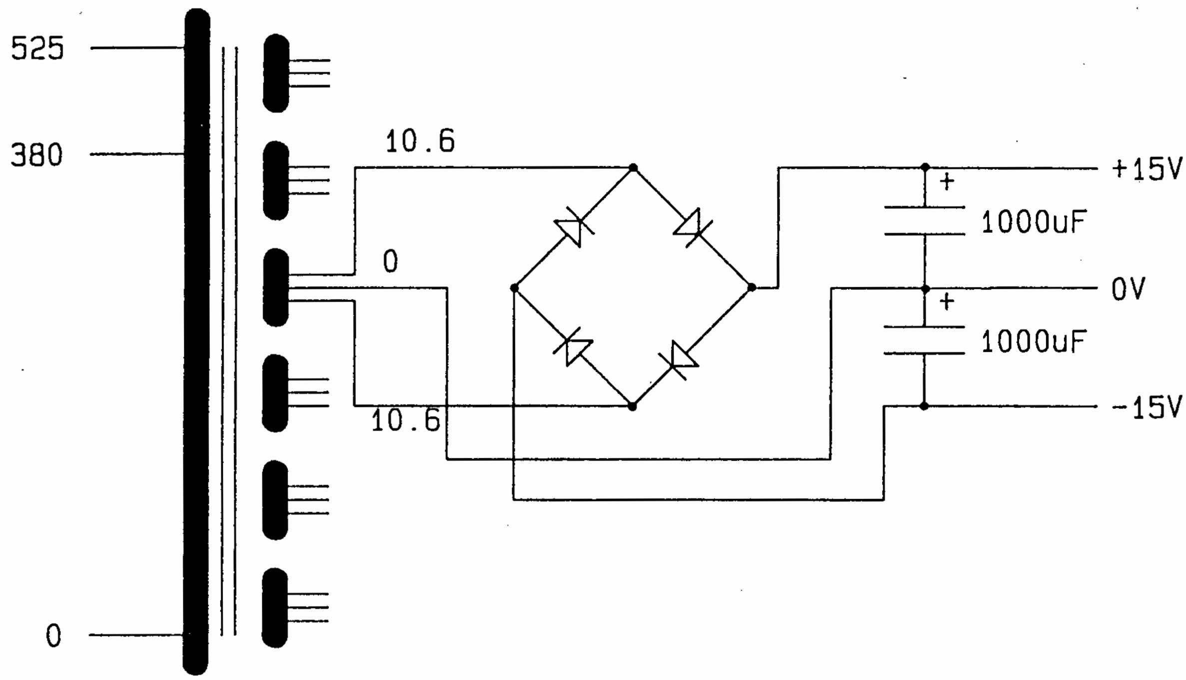

Figure 7.2 Gate Drive Circuit Power Supply

Fig. 7.2 shows how a simple isolated split rail power supply is achieved using a single phase bridge rectifier and two smoothing capacitors. The bridge rectifier and the smoothing capacitors are mounted on each Gate Drive circuit board.

7.3 OPTO-ISOLATION AND SIGNAL TRANSMITTING CIRCUIT

Signal Transmitting Circuit:

In order to make the gate circuit more compact and inexpensive a photo-coupler can be used as a means of isolating and transmitting control signals. In order to protect a GTO inverter against possible short circuit it is necessary to minimize the transmission delay time of the Turn-off signal. To do this the photo coupler can be used as a photo diode couple rather than a photo transistor coupler[10].

Fig. 7.3 shows the method that is used to amplify the signal transmitted by the photo coupler and the corresponding leakage current paths. The leakage currents are caused by the voltage variation between the input signal and the base of the corresponding amplifying transistor. These leakage currents flow via the stray capacitance C_o, which exists between the input terminal and photo transistor.

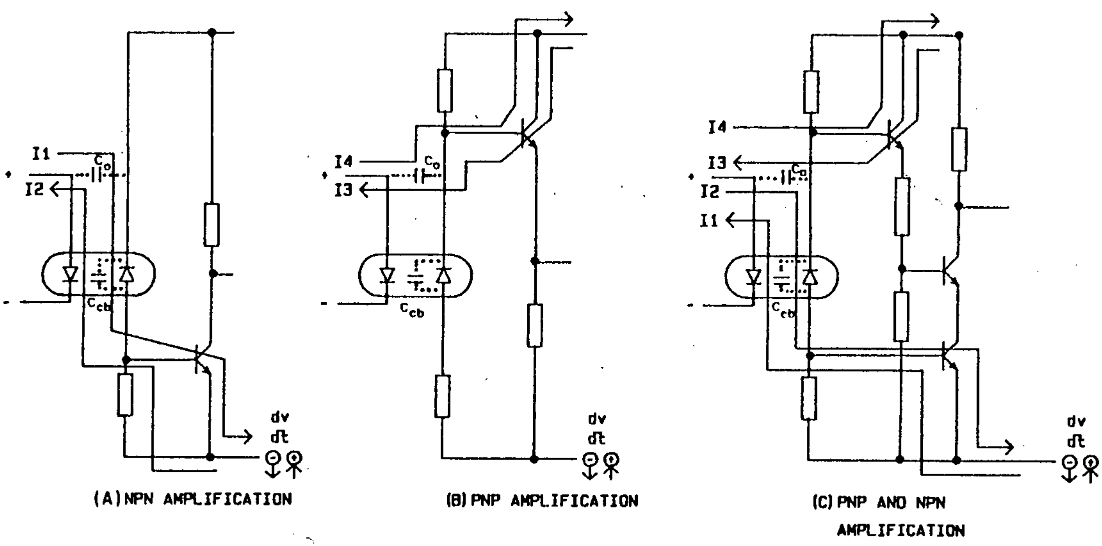

Figure 7.3 Operation of Photo-coupler and Amplifying Methods

If n-p-n transistor amplification is used, as in Fig. 7.3(a), the leakage current I1, flows when dv/dt is negative, thus resulting in erroneous firing of the GTO when it is switching off. The leakage current I2 flows when dv/dt is positive. This causes erroneous extinguishment of the GTO when it is turning on.

For p-n-p transistor amplification, as shown in Fig. 7.3(b) the leakage current I3 flows when dv/dt is positive which results in erroneous firing of the GTO when it is turning off. Leakage current I4 flows then dv/dt is negative causing erroneous extinguishment of the GTO when it is turning on.

In particular it is more difficult to avoid erroneous firing of the GTO due to leakage current I1 and I3 which resulted when dv/dt was negative and then positive respectively. Fig. 7.3(c) shows a method of avoiding this by using both n-p-n and p-n-p amplification in an AND configuration. this enables one to avoid erroneous firing of the GTO due to leakage current I1 and I3.

The problem of erroneous extinguishment of the GTO due to leakage current I2 and I4 still exists. This may be prevented by supplying a separate interlock for the n-p-n transistor, as shown in Fig. 7.3(d) and selecting the peripheral constants of the p-n-p transistor such that I4 is minimised. This results in stable operation of the signal transmitting circuit.

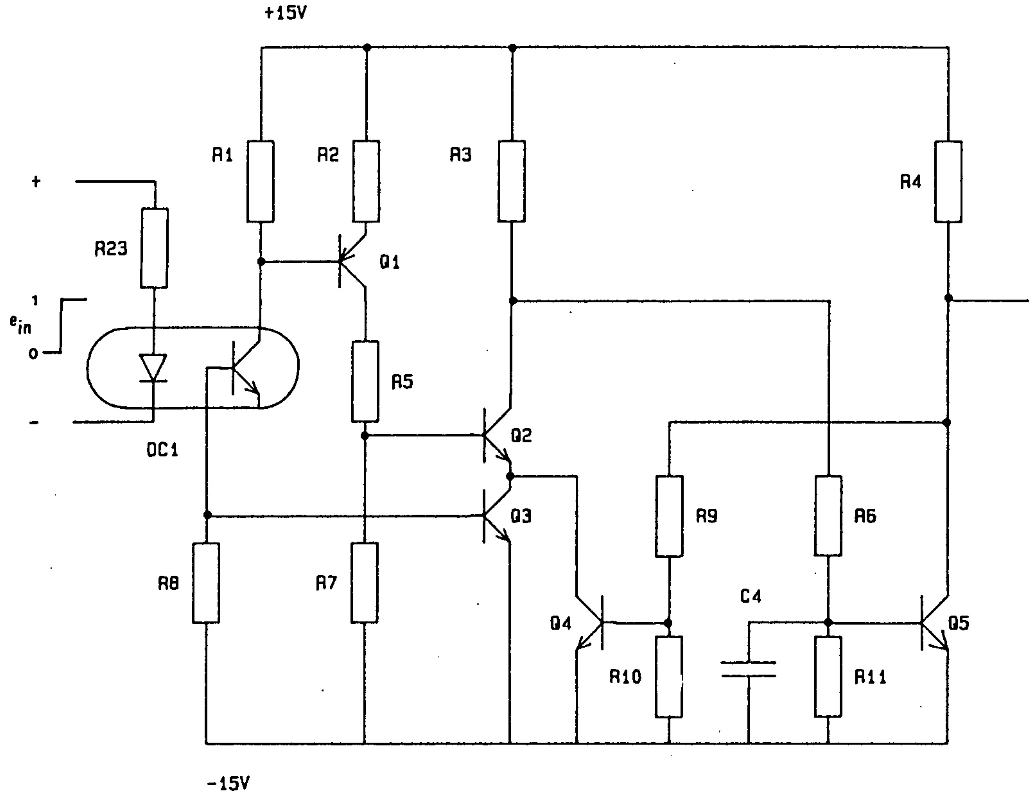

Figure 7.3(d) n-p-n Transistor Interlock

7.4 TURN-ON

Fig. 7.4(a) shows the principle of the output of a gate drive circuit which is designed to supply narrow pulse gate currents for GTO Turn-on. Usually the transformation of the gate current to a narrow pulse requires the insertion of a differential element into the base drive circuit of the Turn-on transistor Q6.

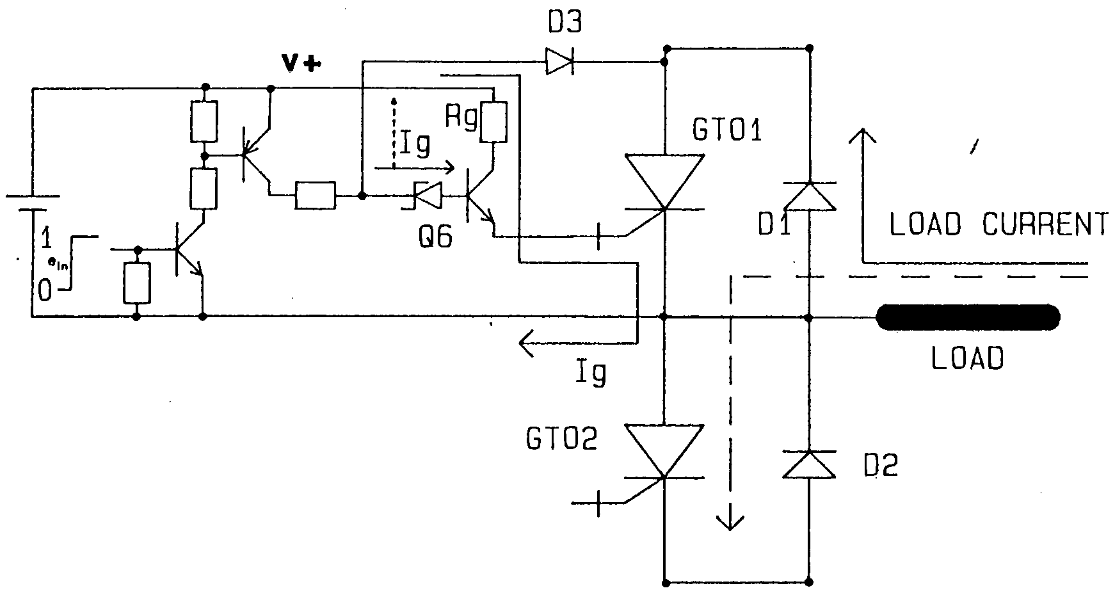

Figure 7.4(a) Principle of Supplying a Narrow Turn-on Current Pulse

In order to transform the Turn-on current to a narrow pulse and to ensure that normal Turn-on of the GTO results, the Turn-on pulse must be applied to the gate when the current through the freewheel diode D1 is zero and the GTO is thus forward biased. To implement this the anode voltage of the GTO is detected by D3. When the anode voltage is high with respect to the cathode D3 is reverse biased. This allows Q6 to be turned on by e_{in} and hence the GTO is turned on. As the GTO is turned on its anode voltage falls with respect to the cathode causing D3 to conduct, the base voltage of Q6 to reduce and Q6 to switch off. The Turn-on current is thus removed from the gate of the GTO. This gives the narrow Turn-on pulse as required.

This circuit is easily modified so that it can be used as a "Block Firing" circuit by removing D3 and replacing the gate Turn-on resistor with an R-C network as shown in Fig. 7.4(b)

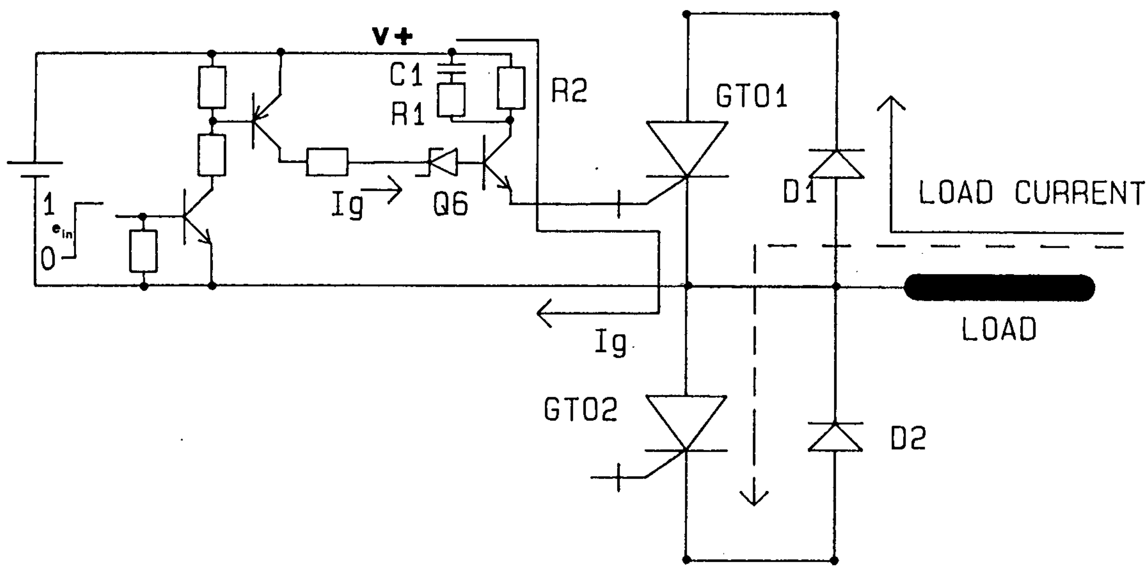

Figure 7.4(b) GTO Block Firing

This combination R-C inserted in the place of Rg allows a gate current to flow, such that

$$Ig = V+ \left[\frac{1}{R2} + \frac{1}{R1} e^{-t/R1C1}\right] \qquad (15)$$

The values of R1, R2 and C1 can be chosen to give the required Turn-on current waveform.

7.5 TURN-OFF AND THE COMPLETE GATE DRIVE CIRCUIT

Fig. 7.5 shows the overall configuration of a Gate Drive circuit for narrow pulse firing. This can be modified as described in Chapter 7.4 to implement "Block Firing".

Up to this stage the principles of the Turn-on circuit and the signal transmitting circuit have been explained. A feature which has not been explained yet is the production of a gate Turn-off pulse using an SCR. When the control signal e_{in} goes low the voltage at point A in Fig. 7.5 goes to approximately -15 volts which turns Q7 on and Q8 off. This in turn foward biases the gate of the SCR which then conducts and turns the GTO off. The SCR self-commutates once all the charge from the gate region of the GTO has been removed. It should be noted that an inductor, Lg, has been inserted in the Turn-off current path to provide a large voltage reversal at the gate over the brief Turn-off period of the GTO.

When the control signal e_{in} goes high the voltage at point A rises to approximately +15 volts which turns Q7 off and Q8 on and which prevents the SCR from firing. Thus stable operation of the GTO is realised.

A detailed circuit diagram and component listing is given in Appendix 7.5.

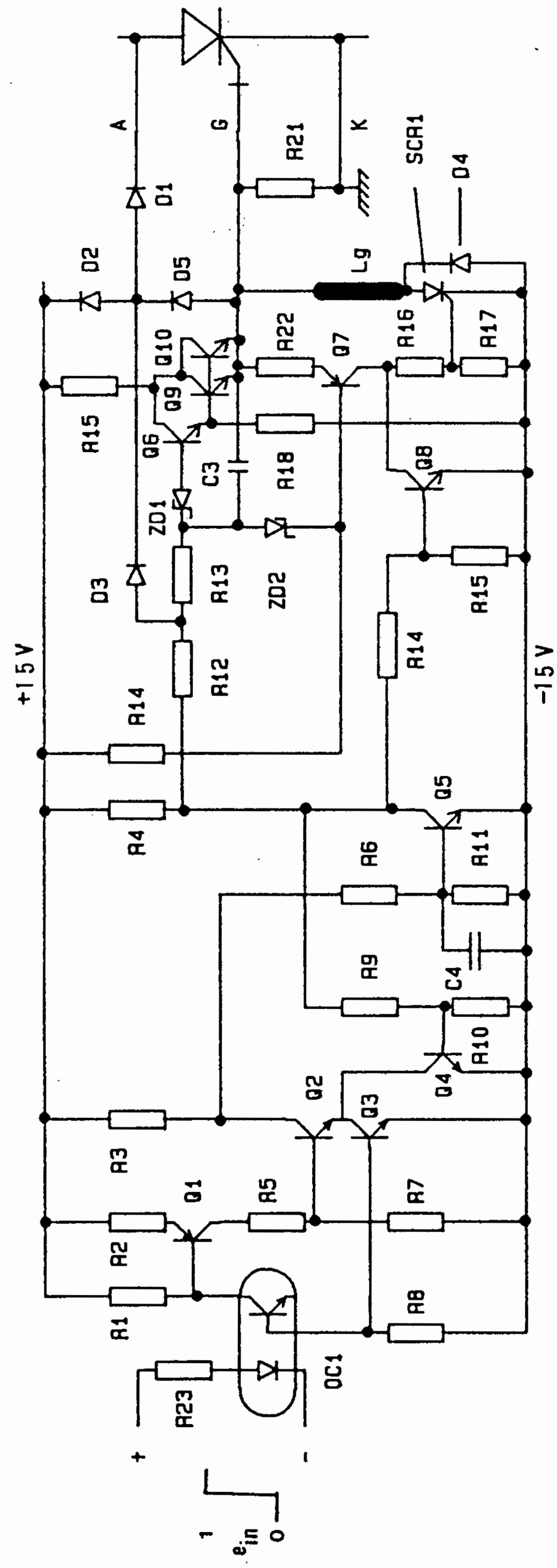

Figure 7.5 Complete "Narrow-Pulse" Gate Drive Circuit

8. TESTING, OPTIMISATION AND RESULTS

8.1 SINGLE GTO SWITCHINGS

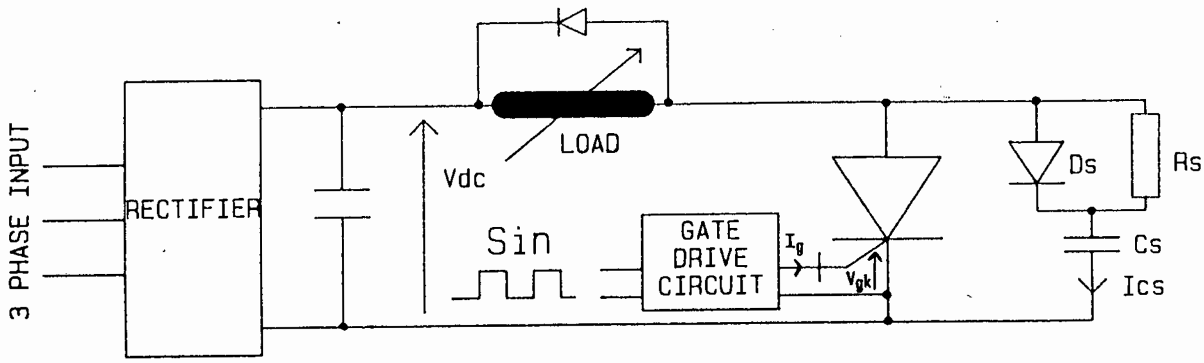

Figure 8.1(a) Single GTO Test Circuit

The performance of each switching element can now be evaluated. Fig. 8.1(a) shows a circuit which was used to test a single GTO under variable load conditions. Both AEG-TELEFUNKEN G200 and GG90R GTO's were tested.

Taking heed of the comments on snubber circuit design in Chapter 5.4.2 and using the theoretically calculated values of

$$R_s \leq 27\ \Omega$$
$$C_s \geq 0.22\ \mu F$$

the GTO was switched at 1 kHz with a unity On/Off ratio. Initially the applied voltage, $V_{D.C.}$, was limited to 200 volts and the gate drive circuit used was the "Narrow On-pulse" type.

When the primary current through the GTO, I_A, is less than the holding current the GTO tries to turn off. Due to the rise in voltage across the GTO at this instant the gate drive circuit supplies more gate current to prevent it doing this. This is shown clearly in Fig. 8.1(b). This can be advantageous over short periods, but can cause failure due to excessive power dissipation in the interdigitated gate region of the device.

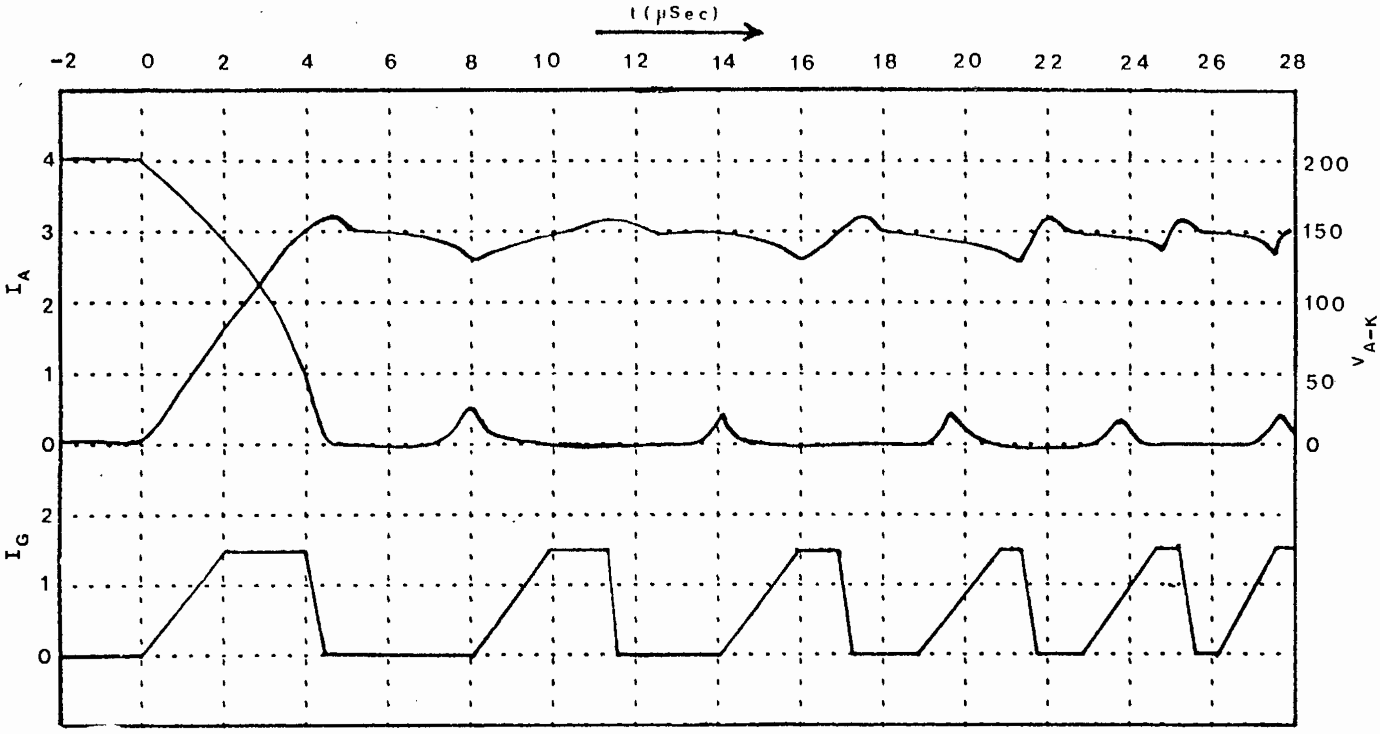

Figure 8.1(b) Repetitive Turn-on Firing

Further tests were then performed at higher currents and voltages and the snubber component values were optimised.

The optimised values values for the snubber components are

R_s = 5 Ω

C_s = 0.22 μF

DUBILIER high voltage, low inductance capacitors were used.

Fig. 8.1(c) to Fig. 8.1(f) show the relevant switching waveforms for both G200 and GG90R GTO's at different loads in the Chopper configuration of Fig. 8.1(a). Certain observations can be made from these waveforms

(1) The snubber discharge current of 7 amps at Turn-on remains constant irrespective of I_A.

(2) The snubber current at Turn-off increases as the load current increases.

(3) The tail current, I_{TQT}, increases as the load current increases.

(4) The gate current at Turn-off increases greatly as the load current increases. The Turn-off gain is approximately 2 at low currents, but it increases as the primary current through the GTO increases.

(5) I_A is greater than the holding current in all cases. Hence repetitive Turn-on firing does not occur.

(6) The reverse gate voltage is independent of the load.

(7) The transient current overshoot at Turn-on is not excessive.

(8) The dv/dt and di/dt ratings of the devices are not exceeded.

(9) The snubber capacitor is discharged within 7 μsec at Turn-on.

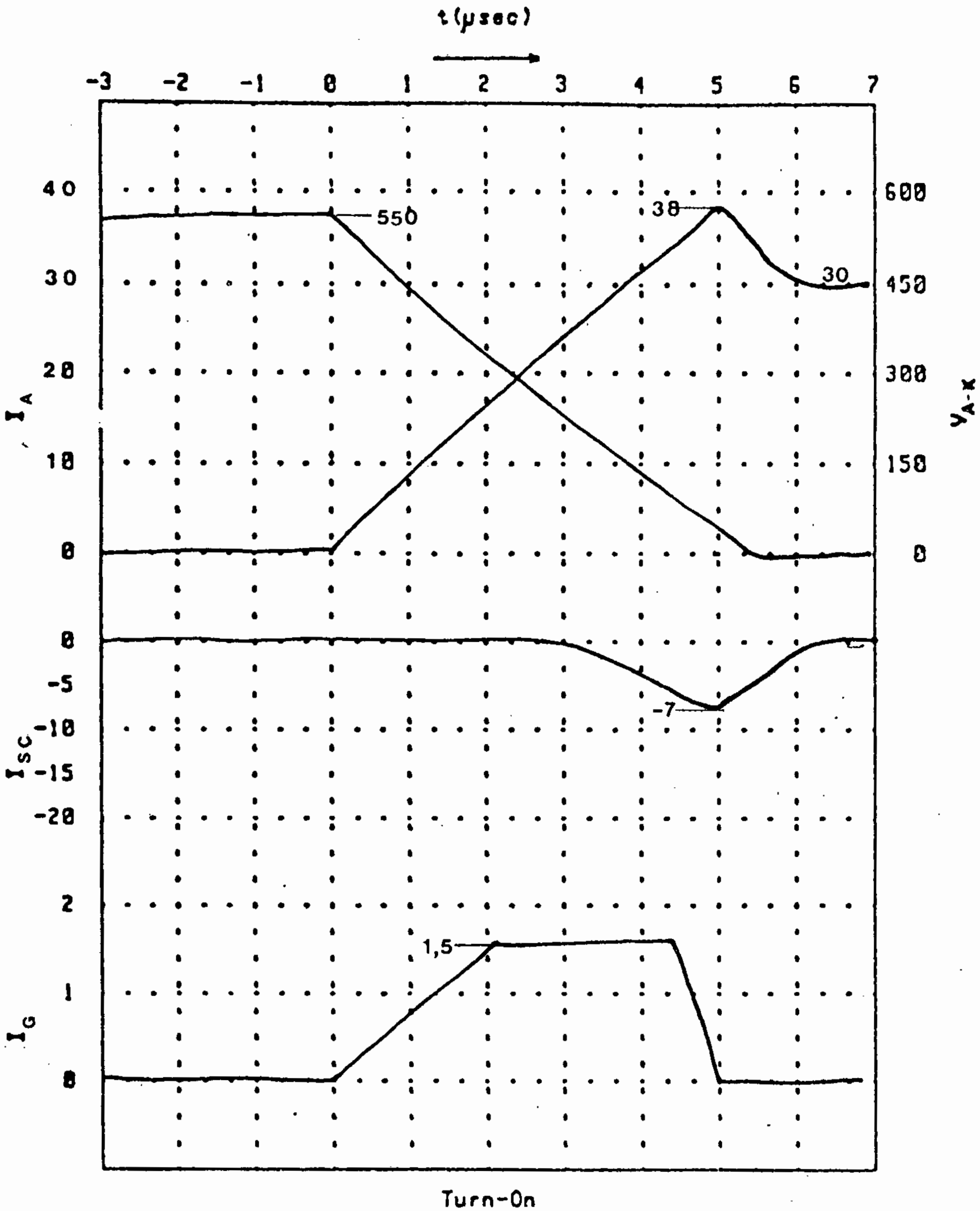

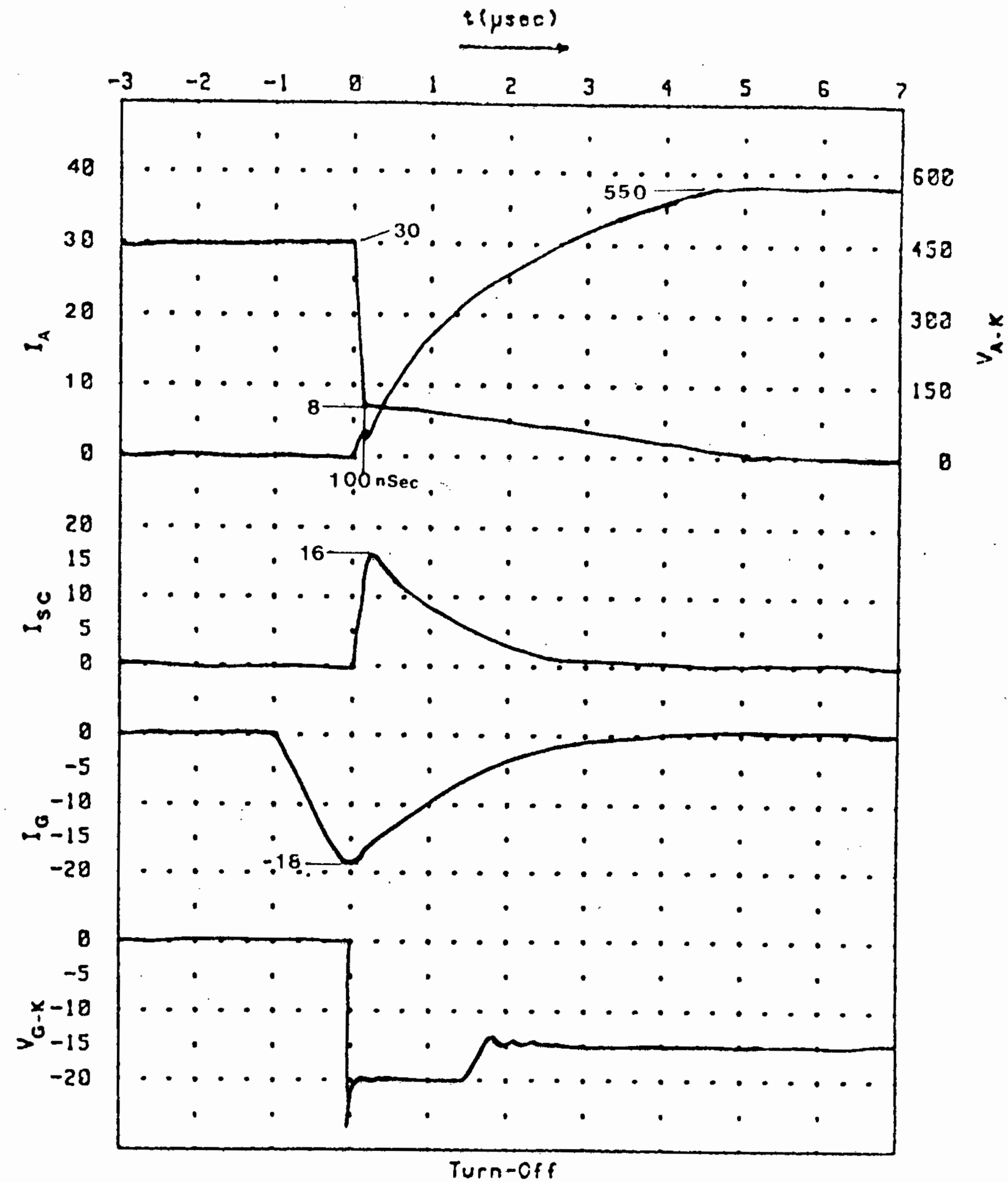

Figure 8.1(c) G200 Switching 30 Amps at 550 Volts

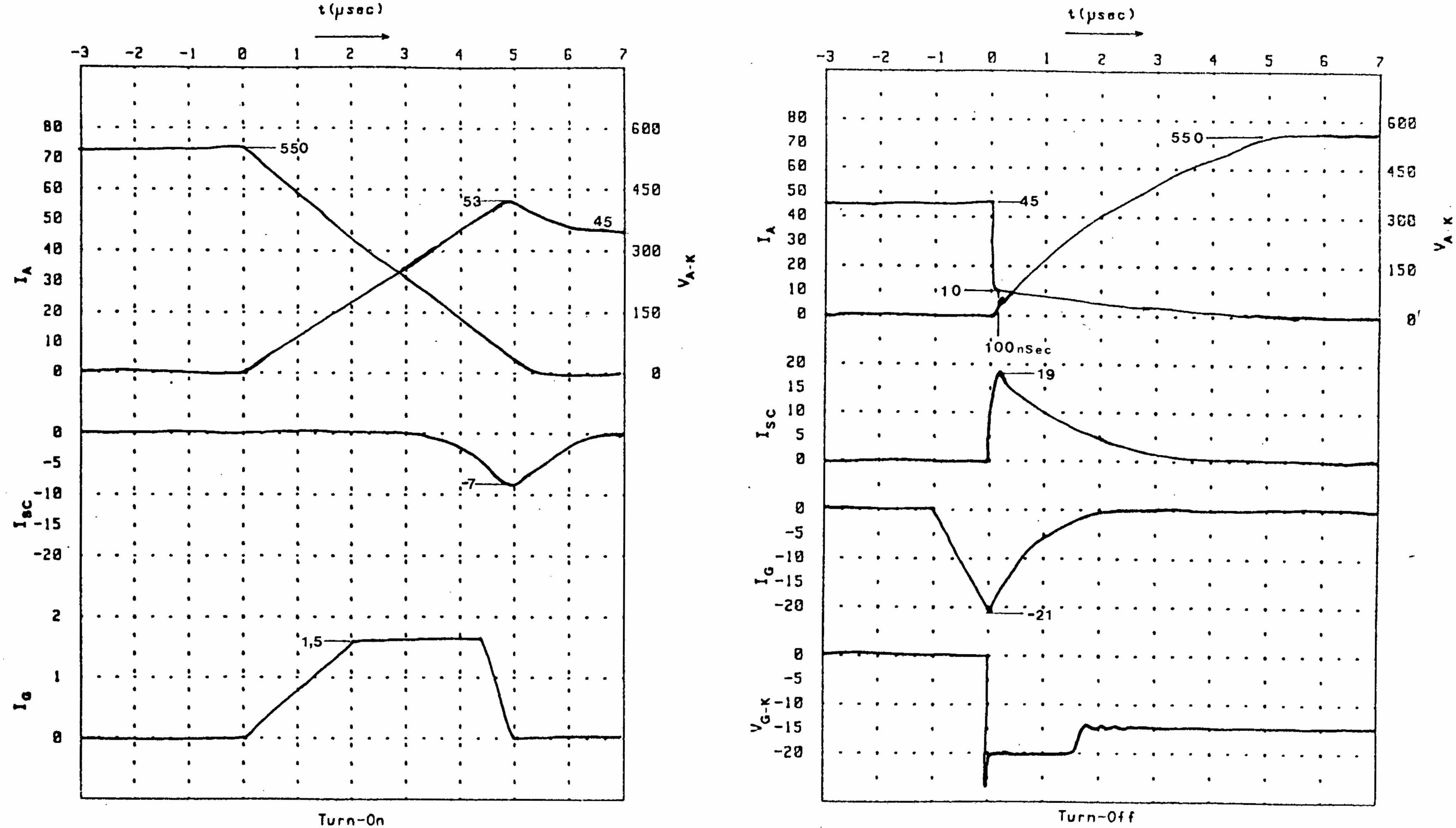

Figure 8.1(d) G200 Switching 45 Amps at 550 Volts

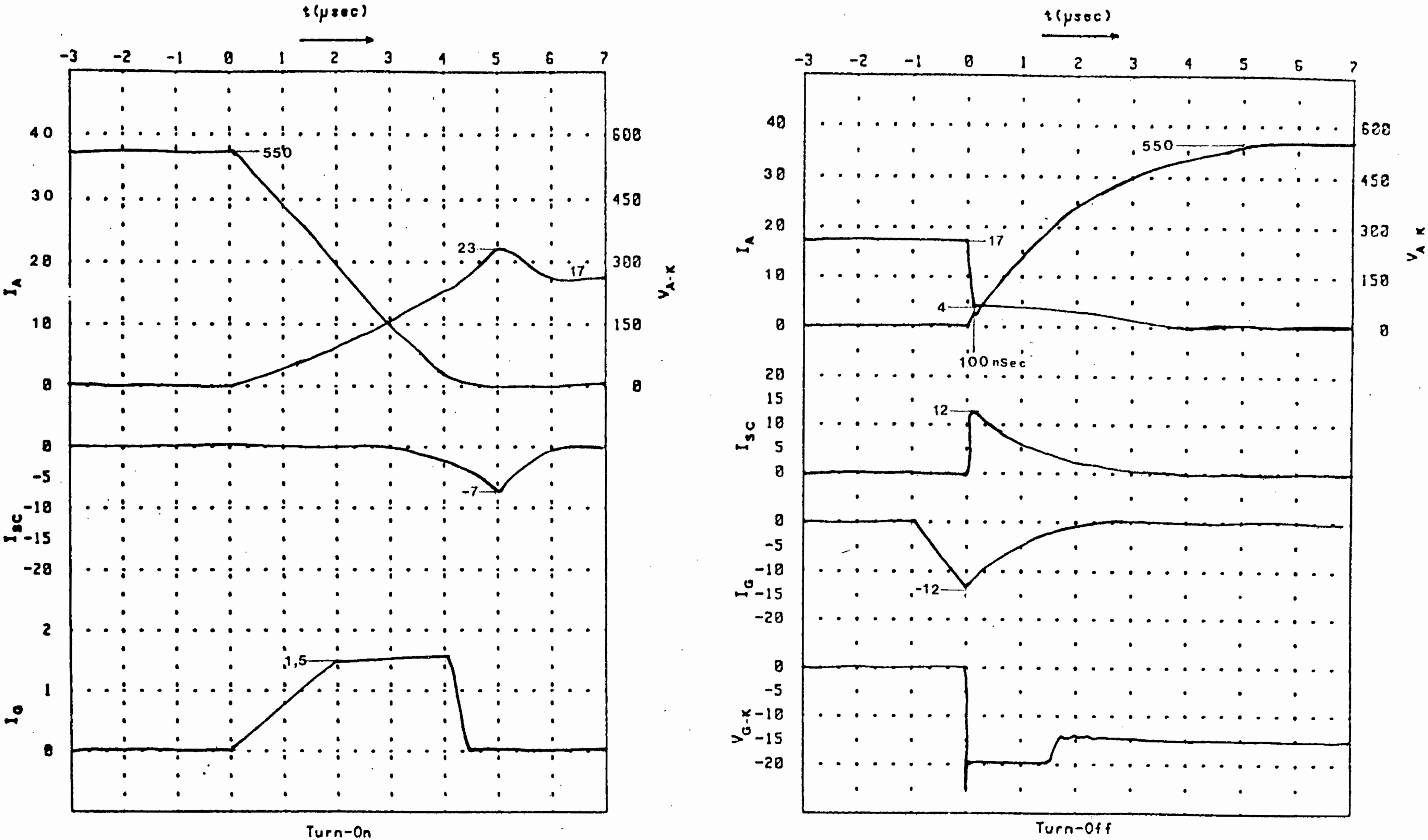

Figure 8.1(e) GG90R Switching 17 Amps at 550 Volts

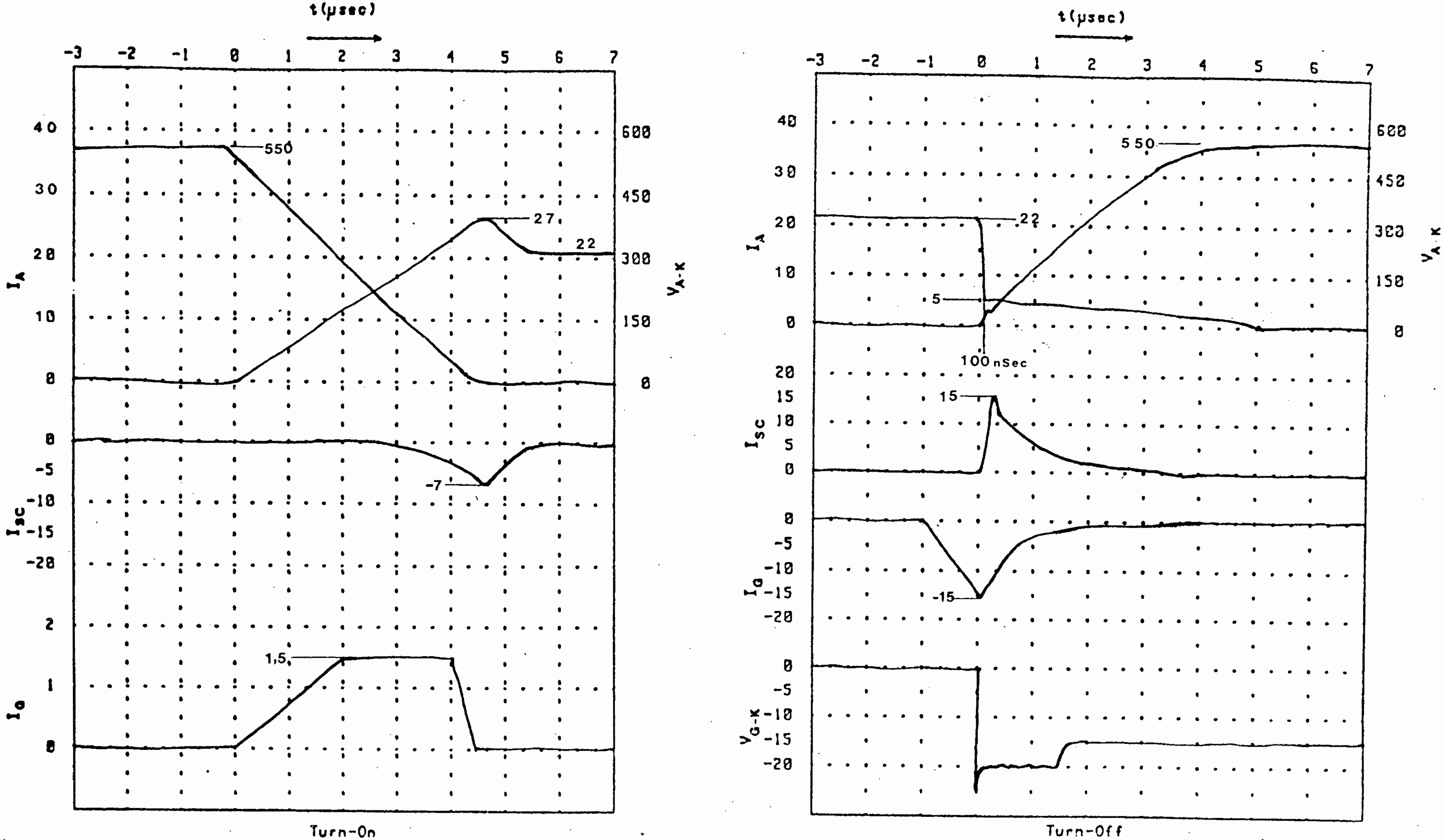

Figure 8.1(f) GG90R Switching 22 Amps at 550 Volts

8.2 PHASE ARM SWITCHING AND SNUBBER OPTIMIZATION

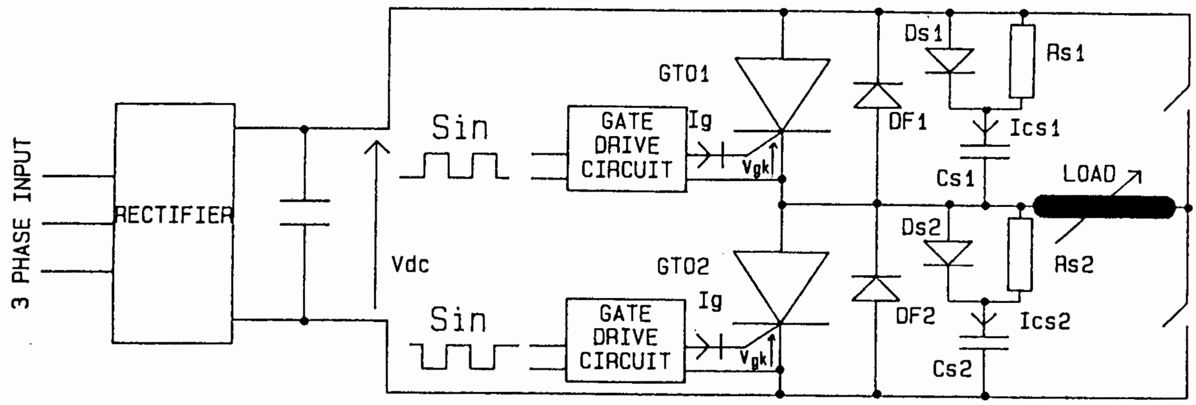

Figure 8.2(a) Phase-Arm Test Circuit

As discussed in Chapter 5.4.2 the values of the snubber components have to be altered when 2 GTO's are connected in a Phase-Arm configuration. Fig. 8.2(a) above shows a circuit which was used to test GTO's in this configuration. A single GTO is fired with the load across the opposing GTO. Fig. 8.2(b) and Fig. 8.2(c) show the switching waveforms for the load connected across GTO2, while GTO1 is fired at 1kHz. The values of R_s and C_s used are

$R_s = 5\ \Omega$

$C_s = 0.22\ \mu F$

These are the optimized values for a single GTO in a Chopper configuration. Fig. 8.2(b) and Fig. 8.2(c) show clearly how the transient overshoot of the Turn-on current is excessive when these snubber components are used. The magnitude the snubber current shoot-through is also shown. The magnitude of snubber discharge at Turn-on and snubber shoot-through can be limited by optimising the values of R_s and C_s. The optimized values of R_s and C_s are

G200: $R_s = 27\ \Omega$
$C_s = 0{,}044\ \mu F$

GG90R: $R_s = 27\ \Omega$
$C_s = 0{,}03\ \mu F$

The snubber capacitors of 0,044 μF and 0,03 μF were obtained by paralleling two 0,022 μF and three 0,01 μF capacitors respectively. This was done purposely so as to decrease the capacitor inductance. The snubber components were mounted as close as physically possible to the GTO's so as to limit the inductance in the connecting wires. Once again DUBILIER capacitors were used.

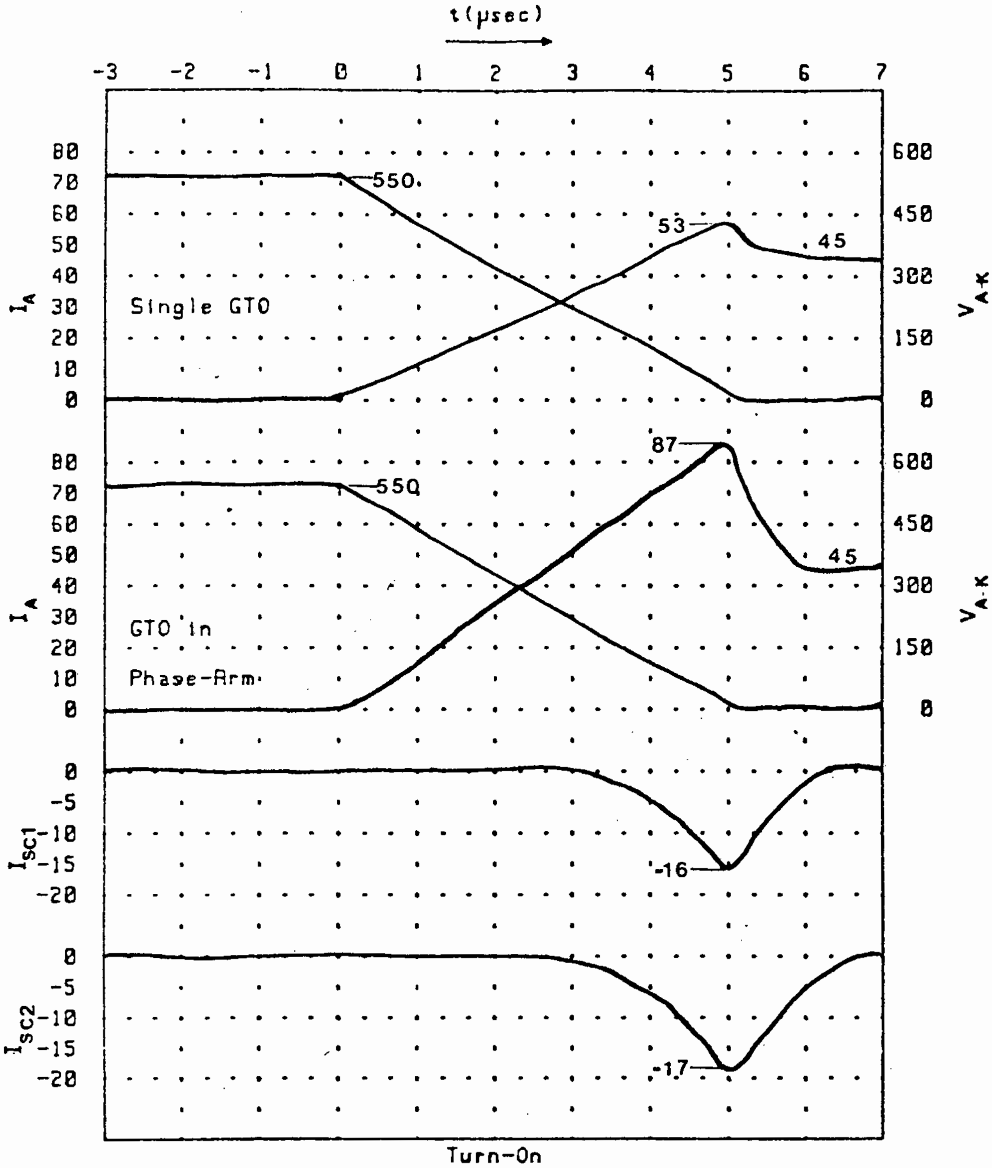

Figure 8.2(b) G200 Switching in a Phase-Arm

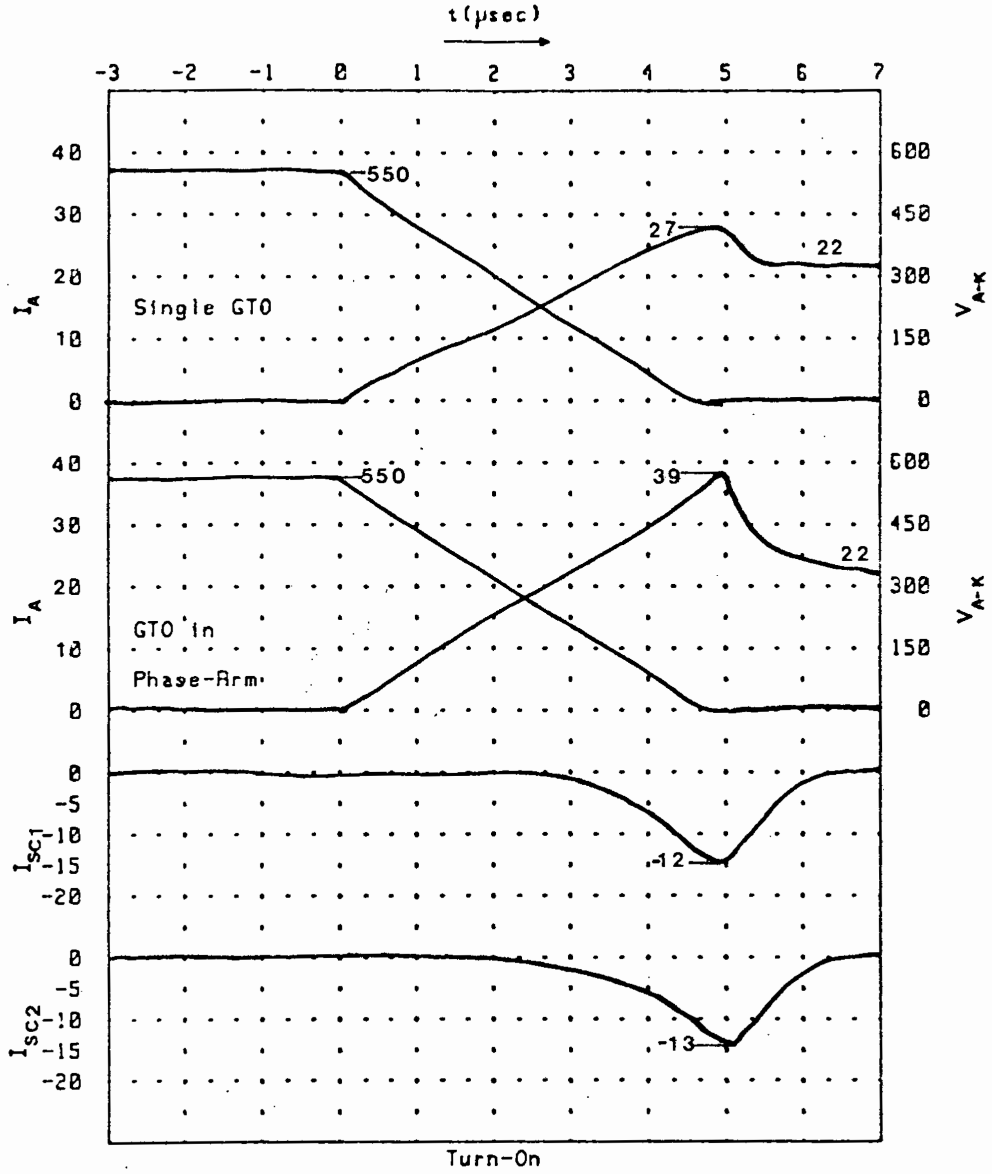

Figure 8.2(c) GG90R Switching in a Phase-Arm

These new snubber components and the GTO's connected in a Phase-Arm configuration produce different switching waveforms. These are shown for a G200 and GG90R in Fig. 8.2(d) and Fig. 8.2(e) respectively and are for the same load conditions shown in Figures 8.1(d) and 8.1(f) respectively.

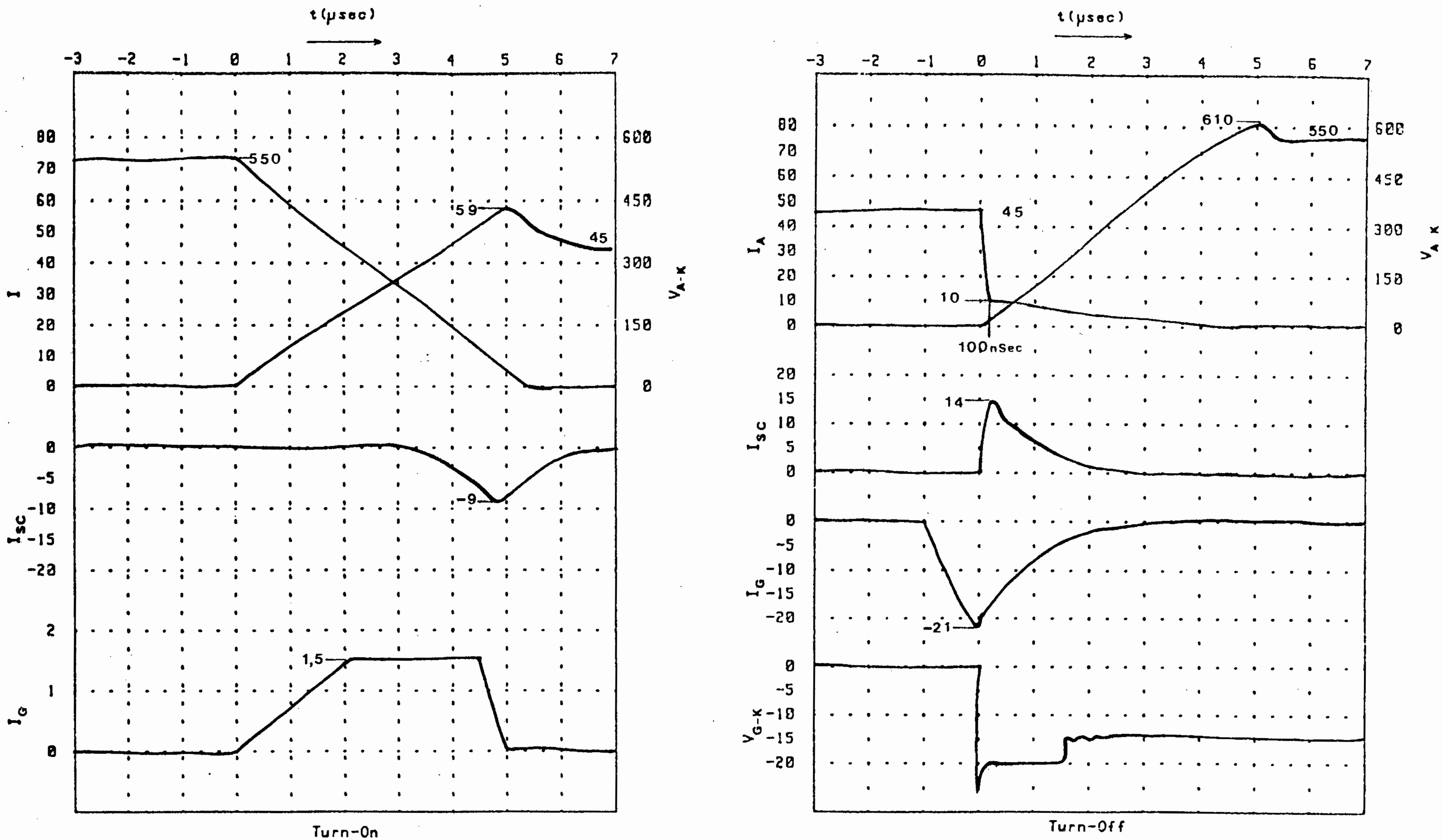

Figure 8.2(d) G200 Switching in a Phase-Arm

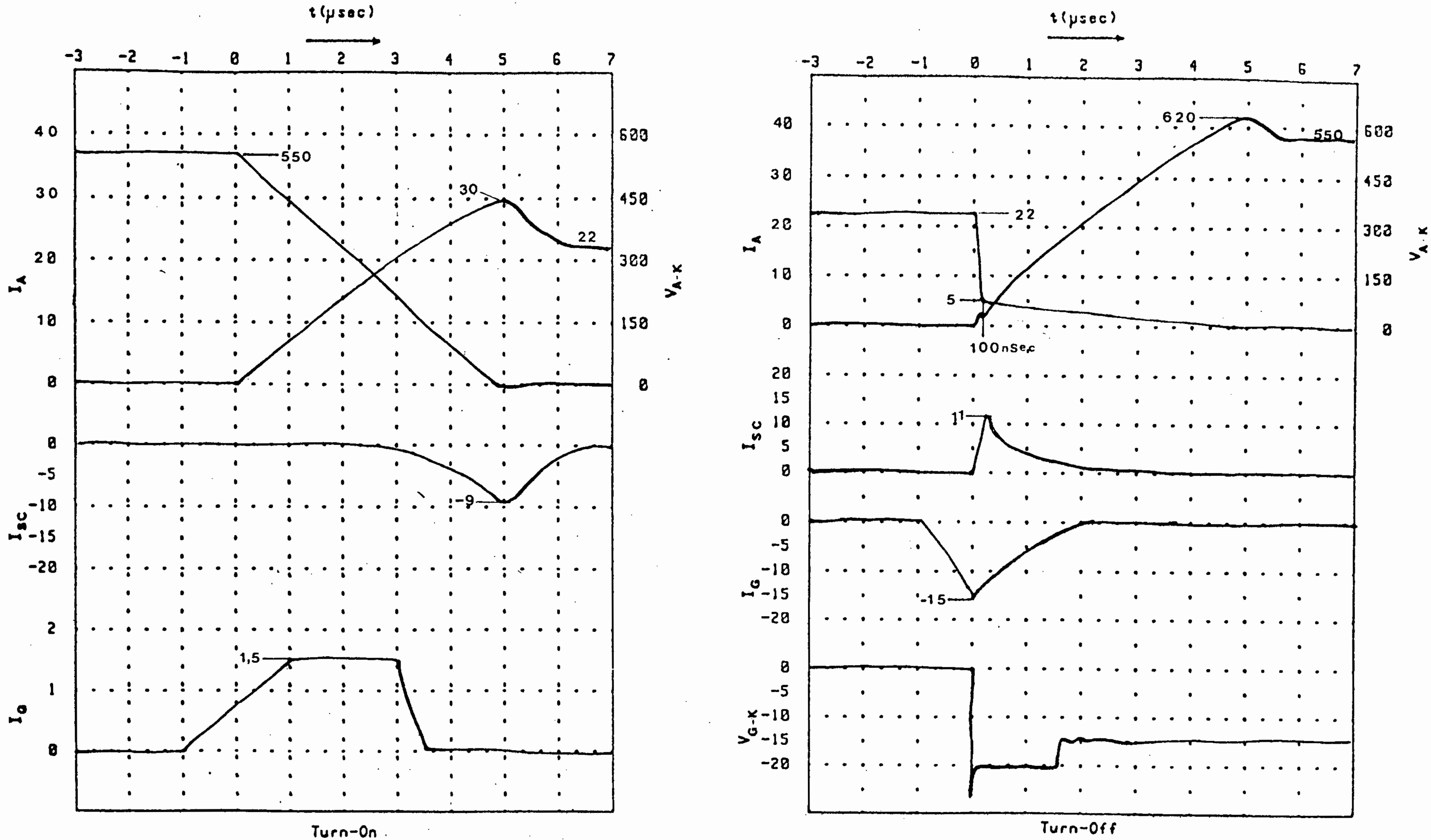

Figure 8.2(e) GG90R Switching in a Phase-Arm

Once again certain observations and comparisons can be made from these waveforms.

(1) The transient current overshoot due to snubber discharge and snubber shoot-through has been decreased from 42 to 14 amps for the G200's and from 17 to 8 amps for the GG90R's.
(2) The Turn-off voltage across the GTO displays a small transient of less than 70 volts.
(3) The Turn-off current into the snubber, I_{sc}, decreased due to the smaller snubber capacitor.
(4) The Turn-off time of the GTO is unaffected.
(5) The magnitude of the tail current is unaffected.
(6) The dv/dt across the GTO increases, but it is still within its specified rating.
(7) The gate current of the GTO is unaffected.

Further tests were performed on GG90R GTO's using Block firing. Some of the results are shown in Fig. 8.2(f). Comparing these results to those in Fig. 8.2(e) for a similar load condition it is seen that none of the physical switching conditions are altered. At low currents however, it did prevent self-extinguishment of the primary current through the GTO.

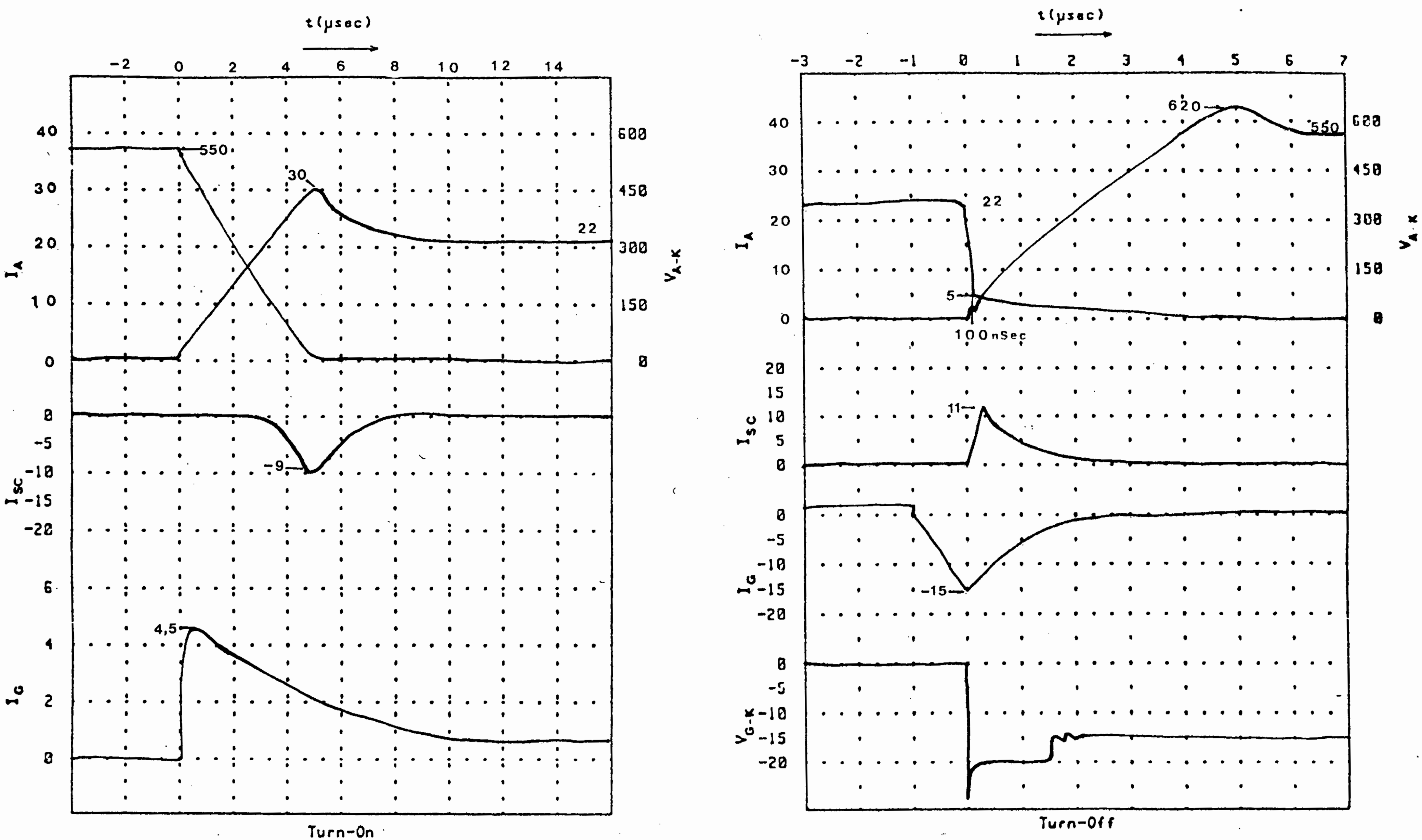

Figure 8.2(f) GG90R Switching in a Phase-Arm using Block Firing

8.3 CONTROLLER SETTINGS AND TESTING

The firing signals from the Controller were applied to the gate drive circuits of each GTO and the propagations delay of these signals from the output of the HEF4752 IC to the gate of each GTO was measured. This was done for Turn-on and Turn-off of all 6 GTO's.

The propagation delay at Turn-off was 4 μSec.

The propagation delay at Turn-on was

(1) 11 μSec minimum
(2) 14 μSec maximum

To calculate the interlock delay between the firing the GTO's in each Phase-Arm the following time periods have to be taken into account.

Interlock delay > (Maximum Turn-off propagation delay + Minimum pulse-width period + Turn-off time)

In Chapter 6.6 it was shown that the minimum pulse-width is 30 μSec.

From the switching results given in Chapters 8.1 and 8.2 it can be seen that a safe maximum Turn-off time would be 10 μSec.

Thus the Interlock delay > (14 + 30 + 10) μSec.
= 54 μSec

Interlock delay is demonstrated in Fig. 8.3

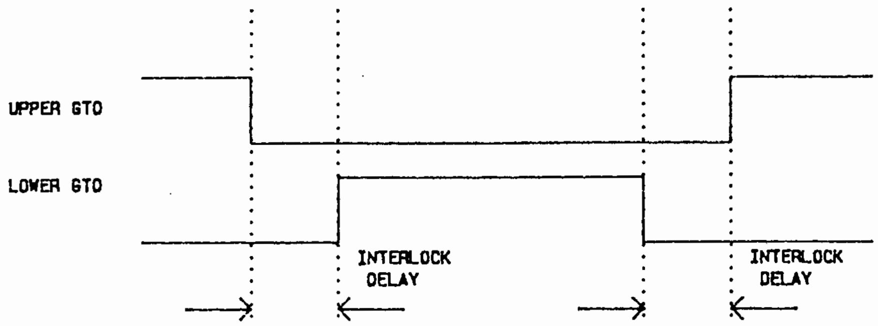

Figure 8.3 Interlock delay

From Table 6.1 the Interlock delay is given by

Interlock delay (mSec) = 16/ F_{OCT} (kHz)

Thus using a conservative Interlock delay of 60 μSec the input control frequency to the PWM chip, F_{OCT}, must be,

$$F_{OCT} = 266.7 \text{ kHz}$$

From Chapter 6.1.2, equation (10), the maximum switching frequency F_o, is determined by

$$F_{RCT} = 280 \times F_o$$

Thus for a maximum switching frequency of 1 kHz the input control frequency to the PWM chip, F_{RCT}, must be

$$F_{RCT} = 280 \text{ kHz}$$

From Chapter 6.1.3, equation (13), the frequency at 100% modulation is given by

$$F_{OUT(m)} = \frac{E_N \times 0{,}624 \times V_{DC}}{Vn}$$

Therefore for all initial tests which will be performed on a 380 volt Induction Motor.

$$F_{OUT(m)} = \frac{50 \times 0{,}624 \times 380 \times \sqrt{2}}{380}$$

$$= 44 \text{ Hz}$$

The 100% modulation potentiometer setting on the controller, according to equation (14) of Chapter 6.1.3, is

$$F_{VCT(Nom)} = F_{OUT(m)} \times 6720$$

$$= 295{,}7 \text{ kHz}$$

where $F_{OUT(m)}$ is 44 Hz

The maximum motoring and generating current was set to 20 Amps (RMS).
The over voltage protection was set to a maximum permissible value of 600 V_{DC}

No Base-Boost was applied to the motor.
The acceleration and deceleration rates of speed control were set to a minimum value for these initial tests.

Each Phase-Arm was then tested under no-load and load conditions to ensure that each GTO was switching correctly.

8.4 INITIAL MOTOR TEST RESULTS

The controller was set up as described in Chapter 8.3. and an Induction motor connected to the output of the inverter. The output frequency of the inverter was set for 30 Hertz and narrow on-pulse firing was used to trigger the GTO's. The complete firing sequence for the GTO's is shown below in Fig. 8.4(a).

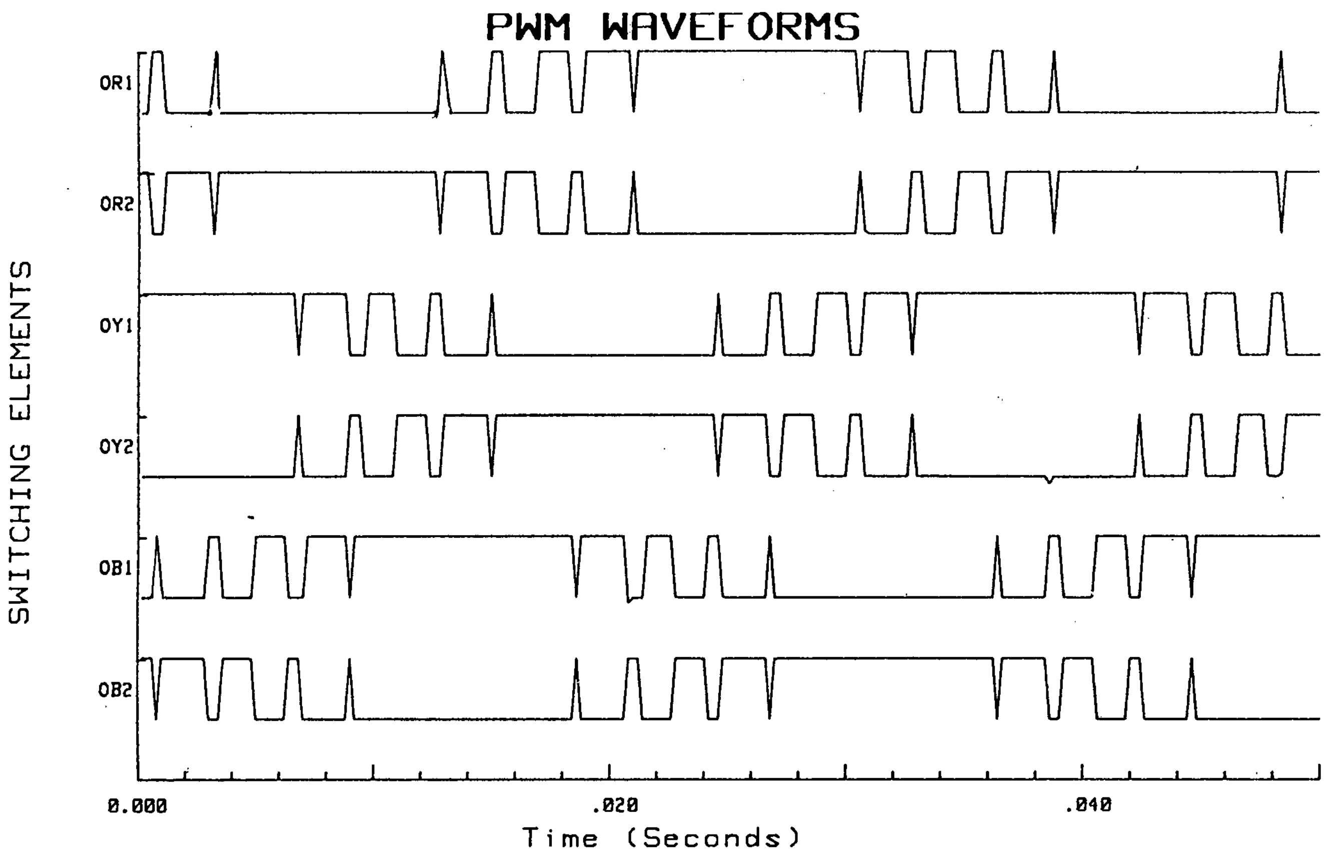

Figure 8.4(a) Firing Sequence for 30 Hz Output measured using a FET Scanner connected to an HP9836 computer

The D.C. Link voltage was 550 Volts and the resultant RMS line voltage from the inverter was 232 volts. The Induction motor was loaded until the peak value of the Fundamental was approximately 8 amps.

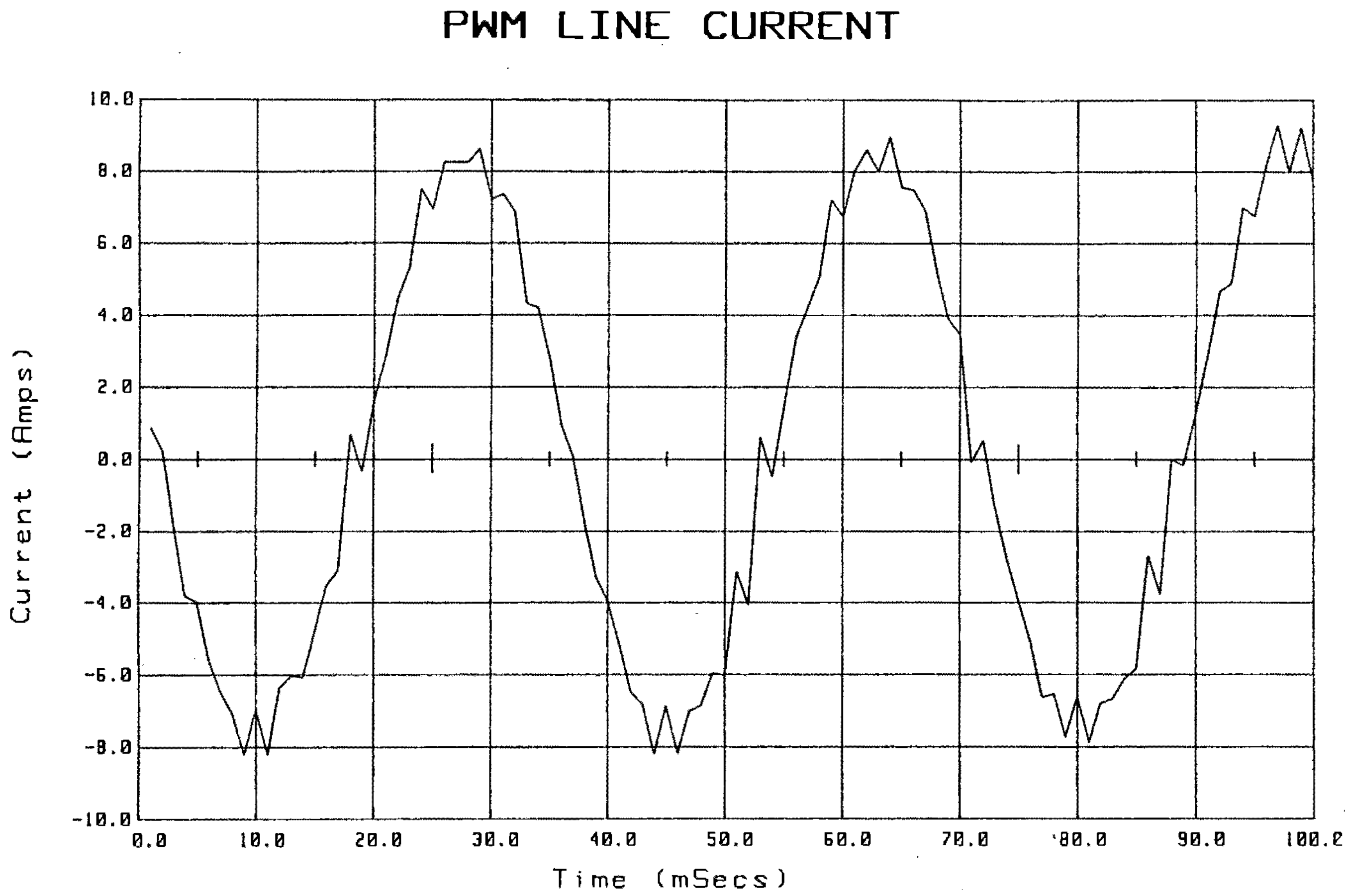

Figure 8.4(b) Line Current at 30 Hz

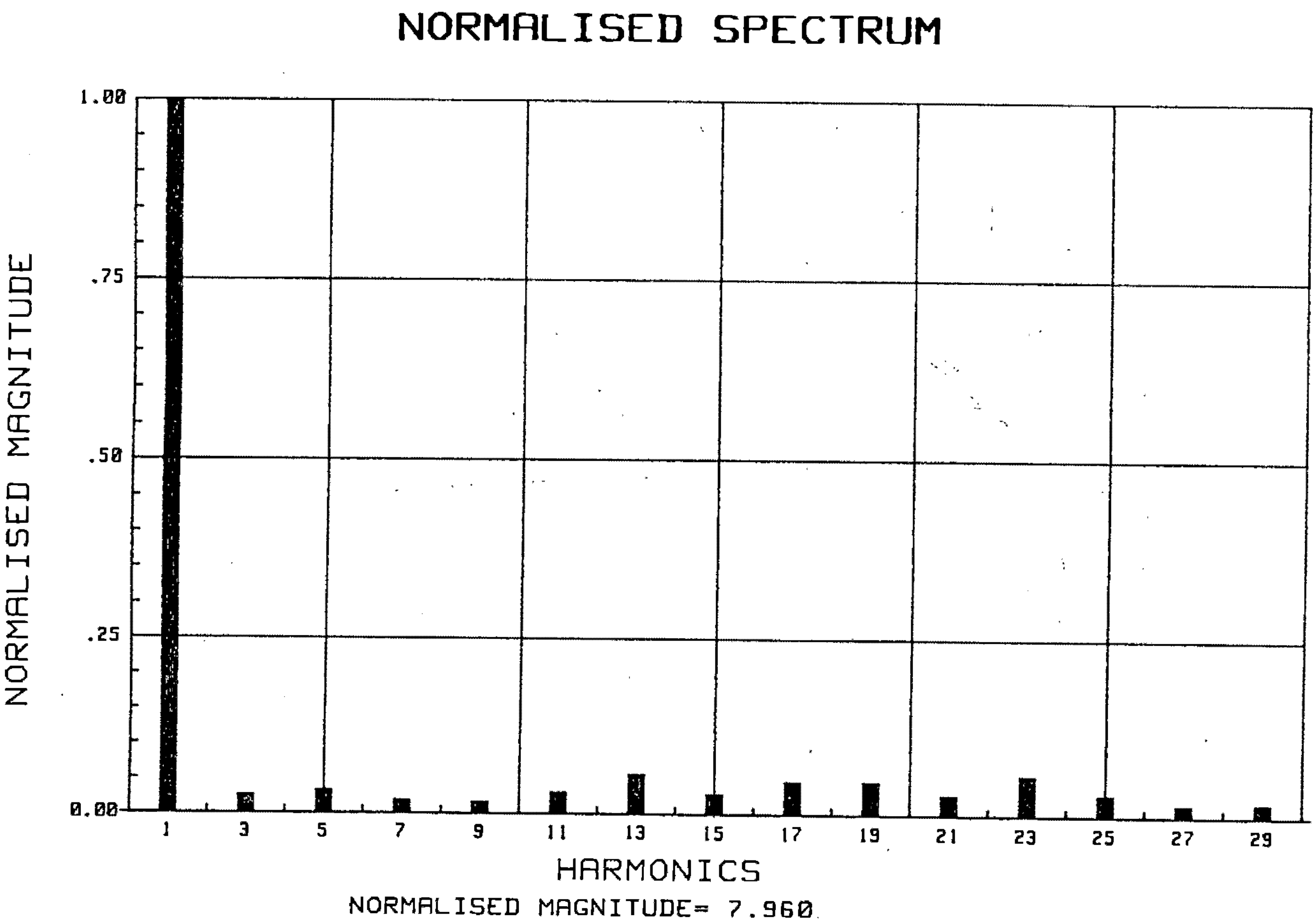

Figure 8.4(c) Current Spectrum at 30 Hz

Figures 8.4(b) and 8.4(c) are the line current and it's associated spectrum respectively. The spectral analysis of the current waveform was performed using both the Discrete Fourier Transform and Slonim methods described in Chapter 3, giving results which correlated with discrepancy of less than 1%. The peak value of the fundamental current is 7,96 amps.

The total power input to the VSD was 2100 watts and the outpower was 1780 watts. This gives an efficiency of approximately 85%.

Table 8.4(a) lists the percentage values of the harmonic currents for a fundamental output of 30Hz.

Harmonic Number	% of Fundamental
1	100
3	2,9
5	3,3
7	1,9
9	1,5
11	3,3
13	5,6
15	3,3
17	4,1
19	4,2
21	3,3
23	5,9
25	1,5

Table 8.4(a) Current Harmonics at 30Hz

Using the same procedure and conditions as before the output frequency from the inverter was increased to 50 Hz. The firing sequence is shown in Fig. 8.4(d). The Induction motor was once again loaded until the peak value of the fundamental was approximately 8 amps. The associated line current and it's spectrum are shown in Figures 8.4(e) and 8.4(f) respectively. The peak value of the fundamental is 8.2 amps. The input power to the VSD was 3700 watts and the output power was 3190 watts. This gives an efficiency of approximately 86%.

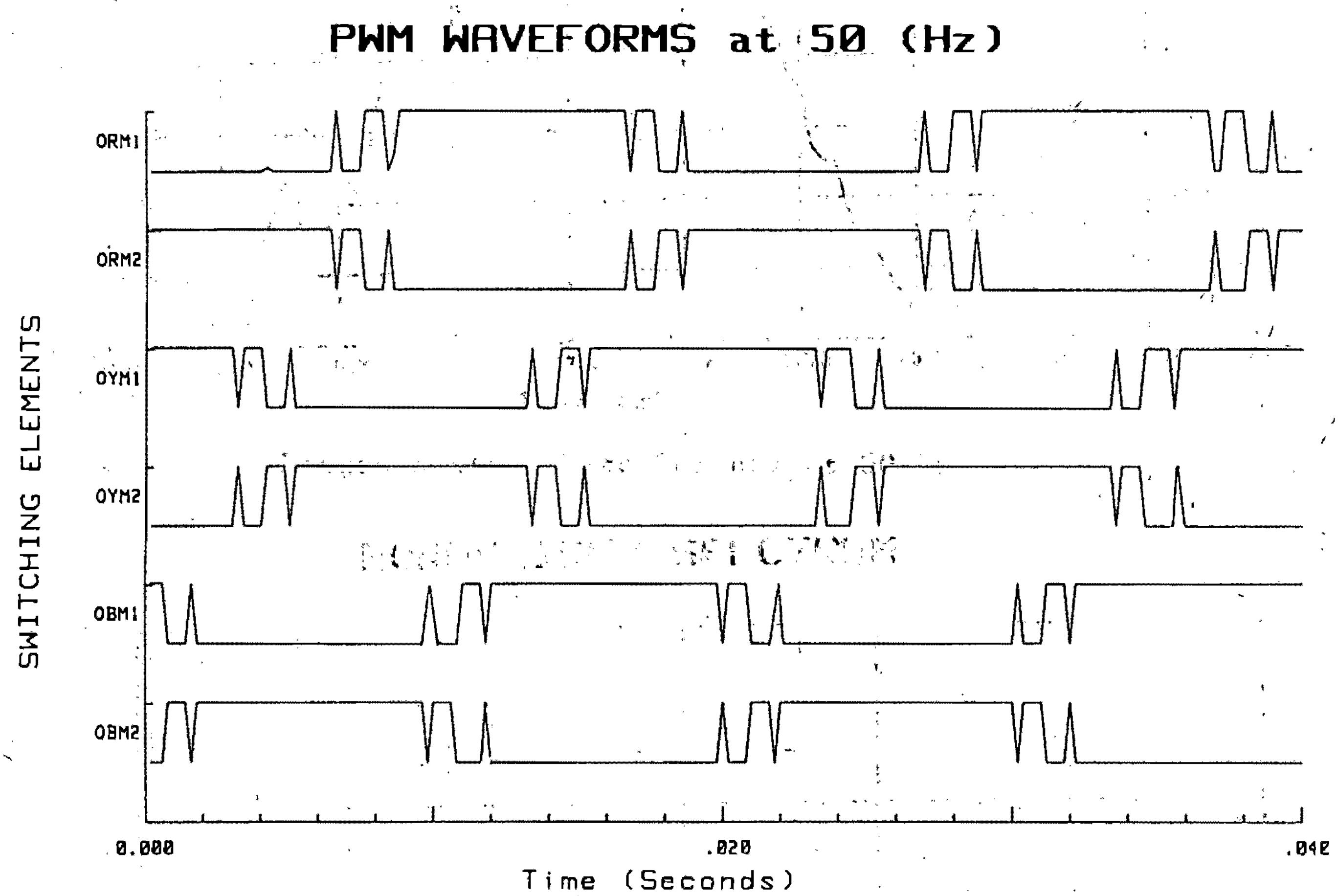

Figure 8.4(d) Firing Sequence for 50 Hz Output

Table 8.4(b) gives the percentage values of the harmonic currents for a fundamental output of 50 Hz.

Harmonic Number	% of Fundamental
1	100
3	1,0
5	4,8
7	2,2
9	0,5
11	3,0
13	3,7
15	1,0
17	4,1
19	2,2
21	1,5
23	3,0
25	1,5

Table 8.4(b) Current Harmonics at 50 Hz

The major advantage associated with using PWM techniques, i.e. the low harmonic content of the line current, can be seen in Figures 8.4(c) and 8.4(f).

Figure 8.4(g) shows an output current waveform and it's associate voltage waveform at 30 Hz. This shows the current lagging on the voltage, as is expected with an induction motor. This corresponds with the discussion in Chapter 4.3.

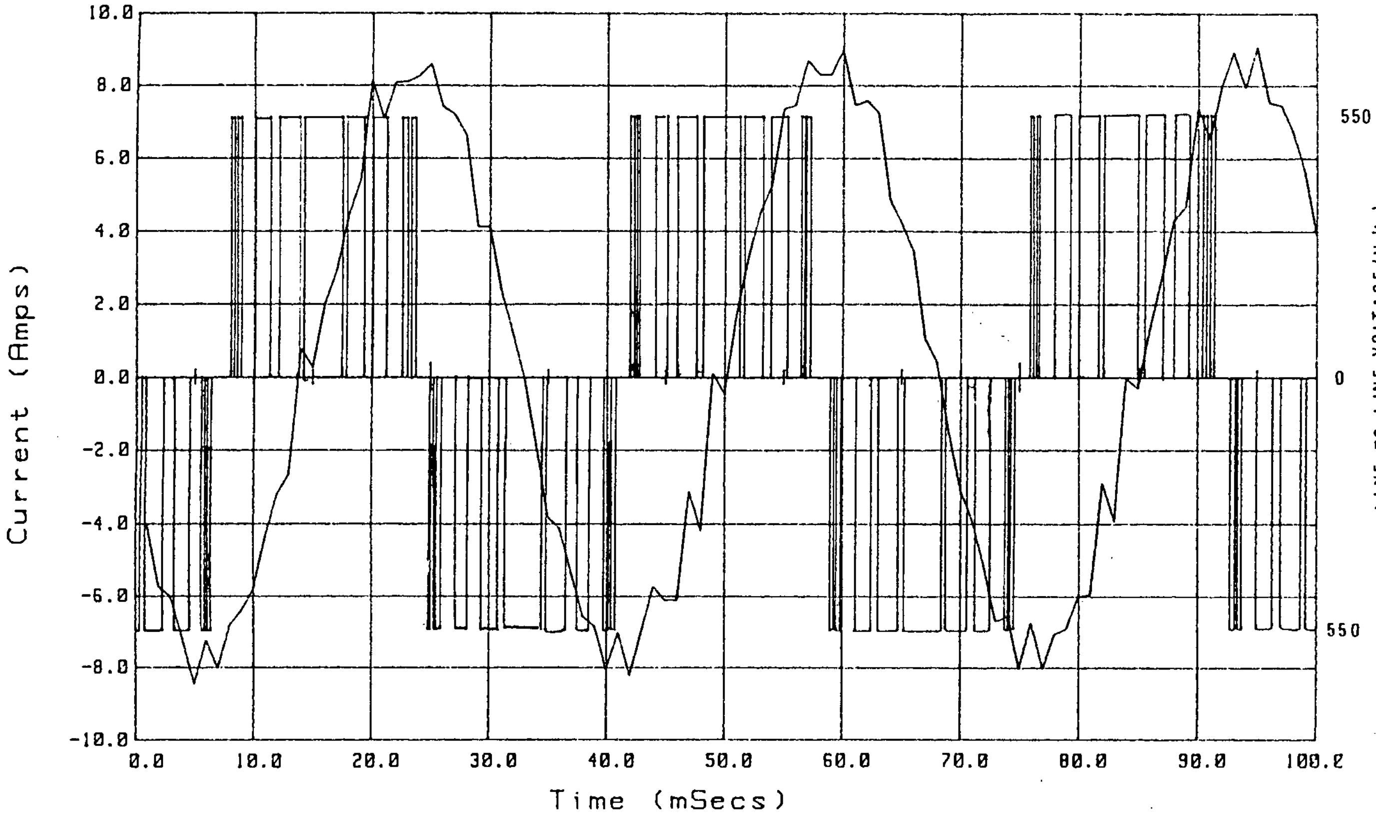

Figure 8.4(g) Output Current and Voltage Waveforms at 30 Hz

If the firing sequences for these switching waveforms are examined closely it will be seen that a conduction path always exists between each of the upper GTO's and it's 2 opposing GTO's in the other phases. If this condition is not met the GTO will attempt to extinguish but it will be prevented from doing so if repetitive on-pulse firing is used, as described in Chapter 8.1.

When the output frequency was decreased to 12 Hz this was found to be the case. Fig. 8.4(h) shows the voltage across a single GTO in a Phase-Arm configuration attempting to Turn-off. From this it can be seen that excessive power dissipation will occur in the interdigitated gate region of the device, which destroys it.

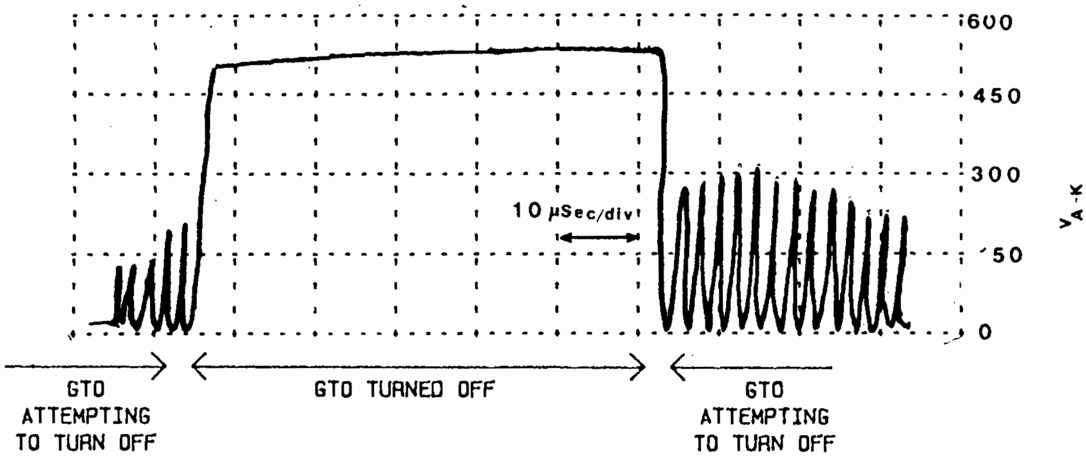

Figure 8.4(h) GTO Attempting to Turn-off

Up to this stage the results of the Induction motor being driven by the Inverter are using G200 GTO's as the main switching elements.

In an attempt to limit expenditure and due to a kind donation from AEG-TELEFUNKEN a limited number of GG90R GTO's were made available and they were used for further testing. Block Firing gate drive circuits were used to prevent the GTO's from turning off as described earlier.

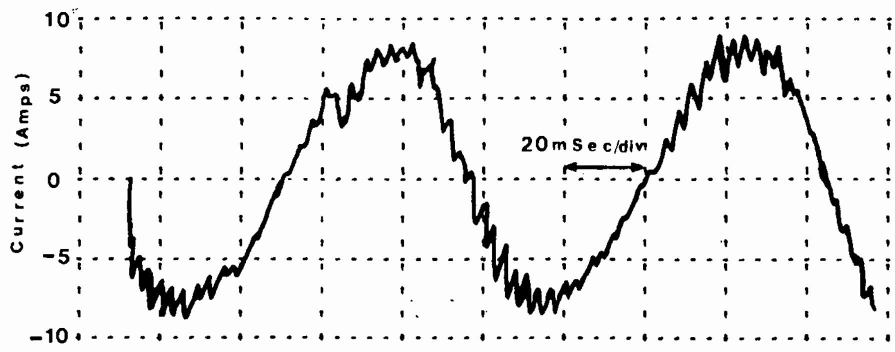

Figure 8.4(i) Line Current for an output frequency of 12 Hz

Fig. 8.4(i) shows the line current to the motor at 12 Hz, which has a very close sinusoidal approximation.

8.5 THE HARMONIC OUTPUT FROM THE VARIABLE SPEED DRIVE

Numerous so called PMW USD's are available commercially. Table 8.5 lists the harmonic content of two of these at an output frequency of 30Hz. The results from the GTO drive under development are also tabulated.

Harmonic	Prototype GTO Drive	Fenner/Mitsubishi Drive	Siliconics Drive
2	-	14,5	-
3	-	-	-
4	-	10,3	-
5	-	-	16
7	-	-	17
9	-	-	-
11	-	-	10
13	5,6	-	5
15	-	-	-
17	4,1	-	-
19	4,2	-	-
21	-	9,3	-
23	5,9	-	-
24	-	15,5	-
25	-	-	-

Table 8.5 The Percentage Output Current Harmonics of Three Different VSD's. The Fundamental Output Frequency is 30 Hz.

From the results in Table 8.5 it is clear that the magnitude of the harmonic components from the GTO Drive are less than those for the Fenner/Mitsubishi and Siliconics Drives. This will lead to very little heat build-up in the motor.

Further analysis of the switching waveforms for other output frequencies was done. Fig. 8.5(a) shows the harmonic content of the output voltage from the GTO Drive when the number of pulses per cycle is 21 and Fig. 8.5(b) is for 30 pulses per cycle. From these graphs it can be seen that the magnitude of the fundamental and the harmonics are not affected by the number pulses per cycle. The harmonic number increases as the number of pulses per cycle increase. The four harmonics shown in each figure are the major ones and they are situated as two sidebands on either side of twice the chopping frequency per cycle.

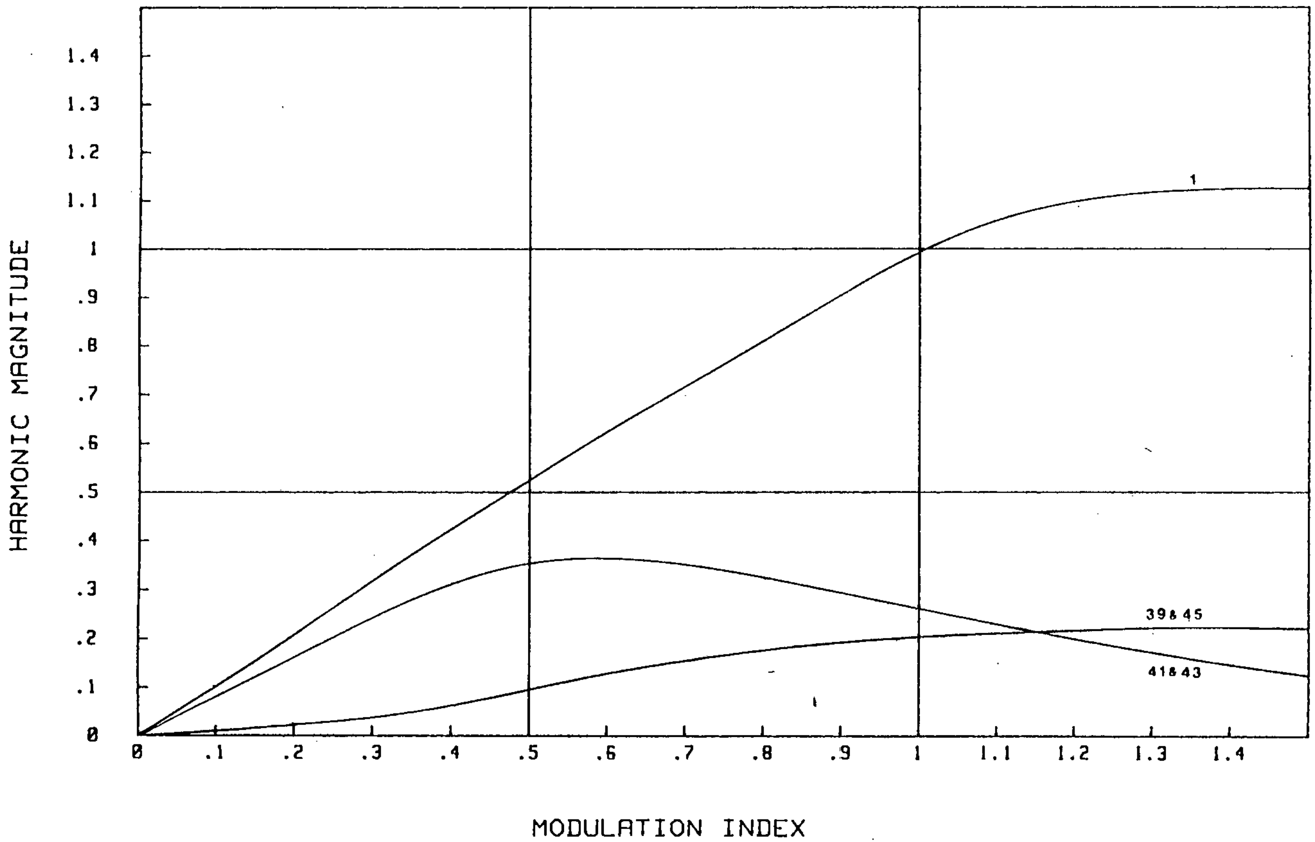

Figure 8.5(a) PWM Voltage Harmonics for 21 Pulses per Cycle

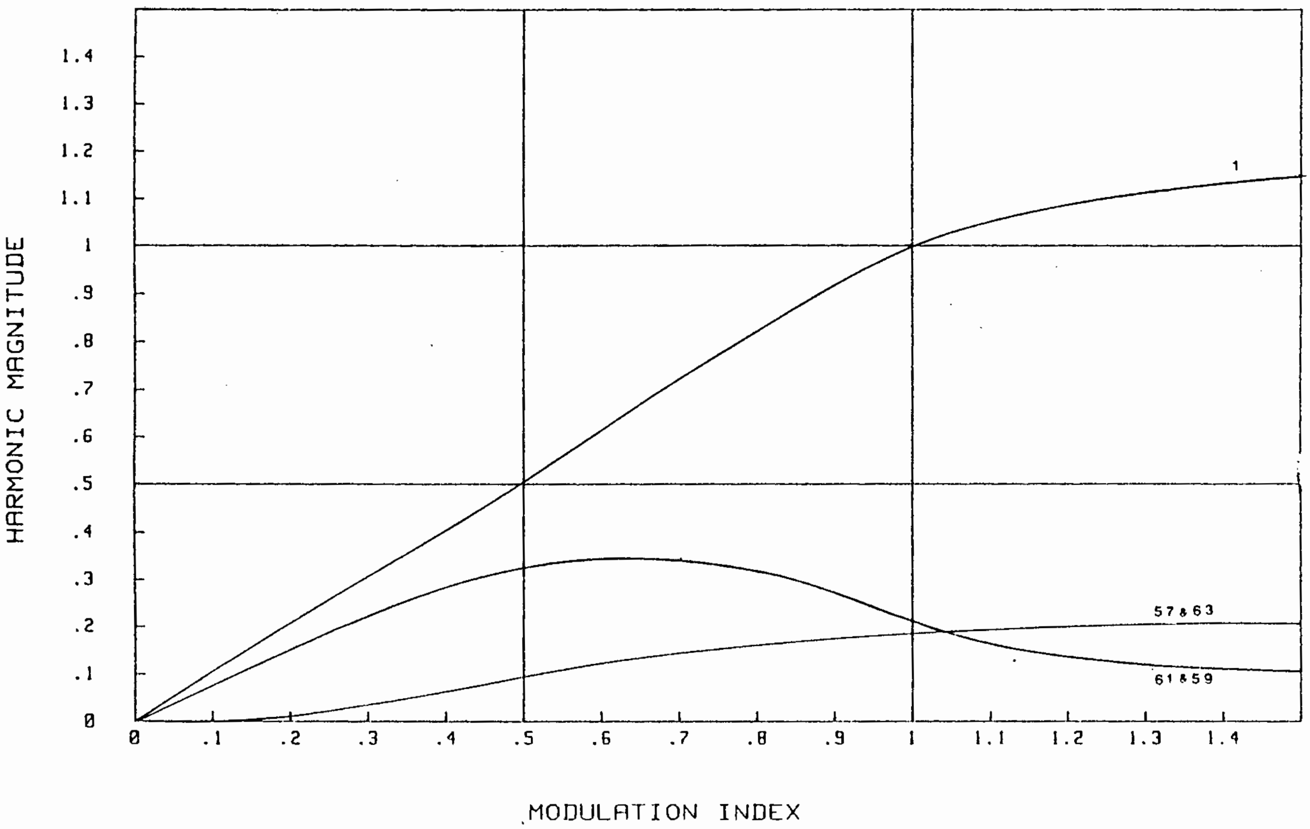

Figure 8.5(b) PWM Voltage Harmonics for 30 Pulses per Cycle

This shows that the modulation strategy which is used is very effective. These results agree with those obtained by G.B. Kliman in reference [20] and R.H. Lee in reference [31].

8.6 SHORT-CIRCUIT PROTECTION

Short-Circuit tests were performed by applying a short to the Inverter. The current in the D.C. Link prior to the Short-Circuit was 30 amps. Initially tests were performed using a high speed, 50 Amp, SIEMENS Silized fuse. Fig. 8.6(a) shows the current in the D.C. Link under Short-Circuit conditions when using a SIEMENS furse. The current has a peak value of 380 amps after 0,75 mSec. The Short-Circuit is completely cleared after 1mSec.

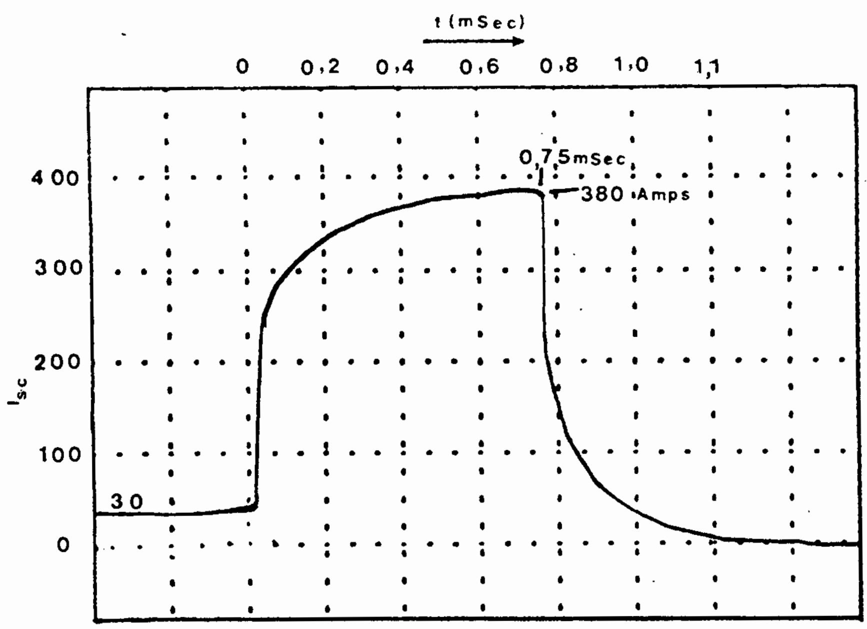

Figure 8.6(a) D.C. Link Current during Short-Circuit Conditions using a SIEMENS Silized Fuse

To limit expenditure "water" fuses were used. Details of their theoretical design and operation are contained in reference [32]. Fig. 8.6(b) shows the current the D.C. Link at the occurrence of a Short-Circuit when using a water fuse. The maximum Short-Circuit current was cleared after 6 μSec. This is much faster than using a SIEMENS Silized fuse, but because of their physical construction and the corrosive nature of water they are not suitable for use in an industrial unit.

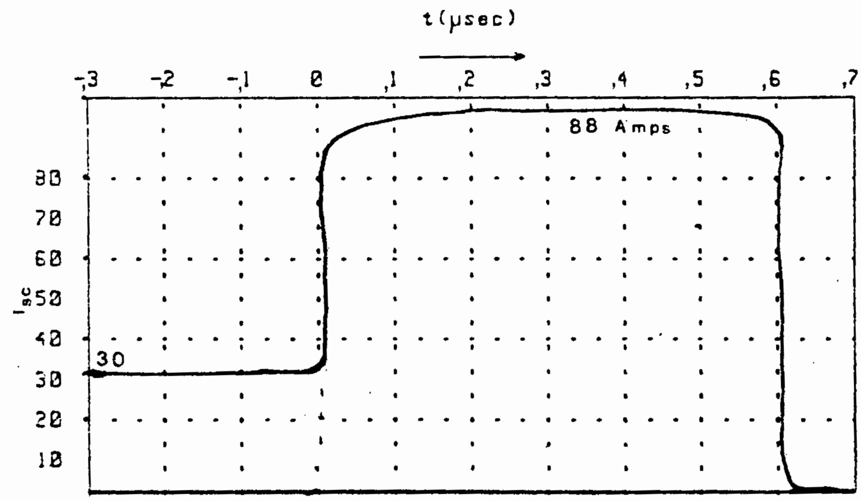

Figure 8.6(b) D.C. Link Current during Short-Circuit Conditions using a "Water" Fuse.

8.7 INDUCTION MOTOR CHARACTERISTICS AT VARIABLE FREQUENCIES

Variable frequency tests were performed on the GEC 525 volt Induction motor. Fig.8.7(a) shows the torque/speed characteristics of the motor for a number of frequencies, showing measured and predicted curves.

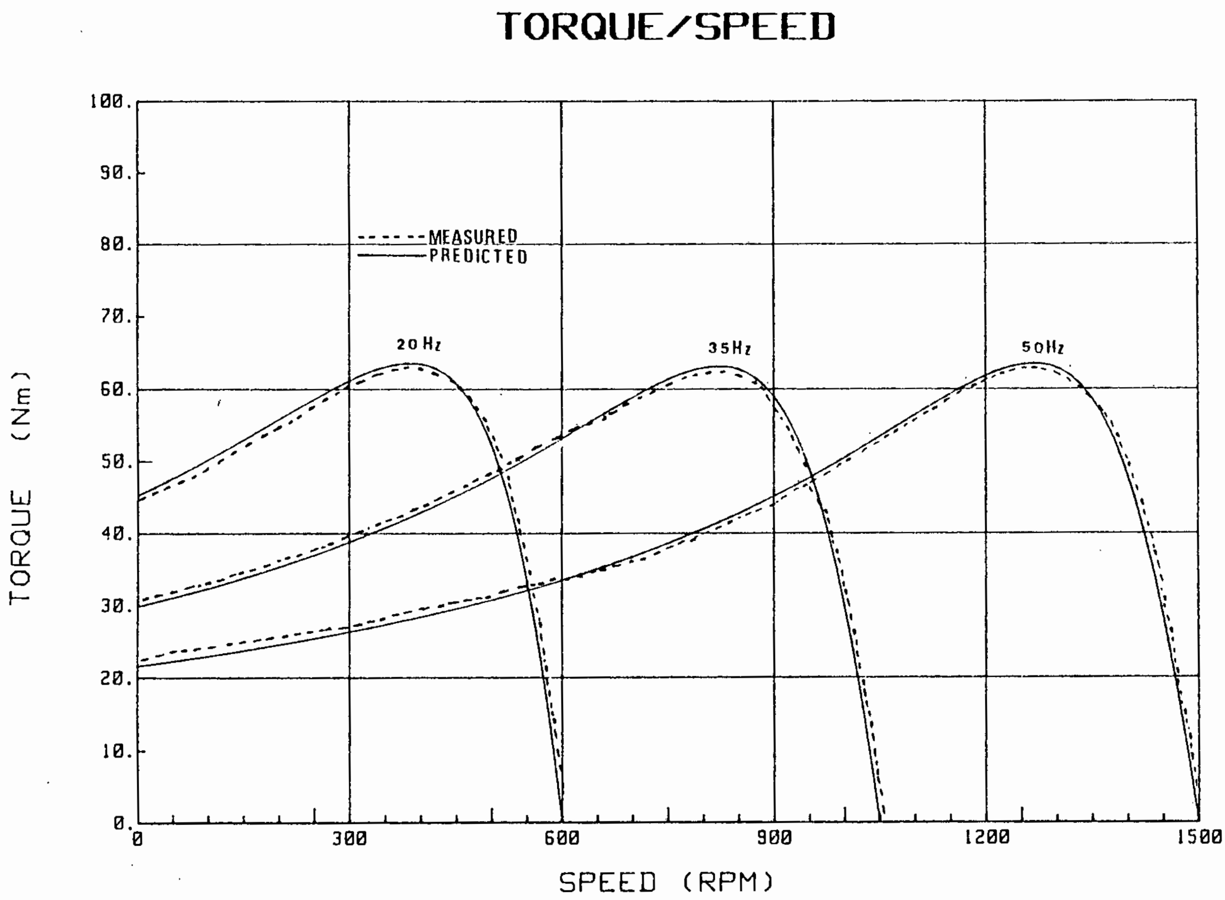

Figure 8.7(a) **Measured and Predicted Torque/Speed Characteristics for 3 Frequencies**

Table 8.7(a) compares the measured and predicted values of Pull-Out torque for the frequencies used in Fig. 8.7(a). The values given in Table 8.7(a) clearly show the correlation between the measured and predicted values, with a discrepancy of 3.5% in the worst case.

Frequency (Hz)	T_{max} (Predicted) (Nm)	T_{max} (Measured) (Nm)
50	63.5	62.5
35	63.7	61.5
20	63.7	61.9

Table 8.7(a) Measured and Predicted Values of Pull-out Torque at Different Frequencies

From these results it is clear that the method used for obtaining the amount of Base-Boost required, as described in chapter 2.4, is very effective. The variation of Rotor Resistance with frequency also ensures that the predicted slip window for normal operation corresponds with the measured one.

Table 8.7(b) gives the measured and predicted values of voltage required by the Induction motor to have the correct value of Pull-Out torque over it's complete operating frequency range. These values are plotted in Fig. 8.6(b).

Frequency (Hz)	Predicted Voltage (Volts)	Measured Voltage (Volts)
50	525	525
45	482	484
40	431	435
35	382	387
30	336	341
25	290	294
20	240	244
15	204	210
10	146	152

Table 8.7(b) Measured and Predicted Values of Voltage to Obtain Required Pull-Out Torque.

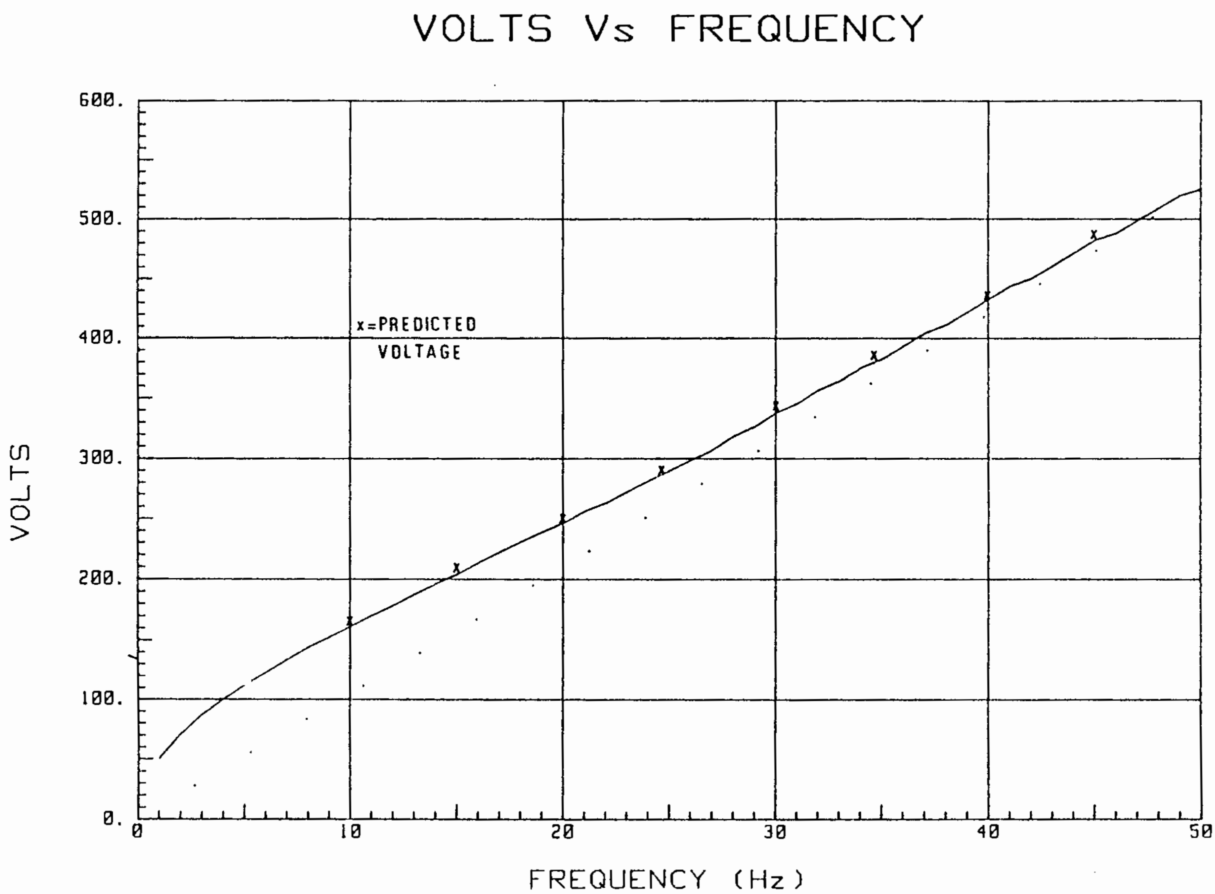

Figure 8.7(b) Graph Showing Measured and Predicted Values of Voltage to Obtain the Required Pull-Out Torque.

8.8 FURTHER DEVELOPMENT WORK

So far from the results obtained it is clear that using GTO's in a PWM Inverter is very effective. Further work should still be done to develop the system into a complete industrial unit. However, this was not done as the necessary financial support was not made available. Certain other options should also be investigated and attention should be given to the final packaging of the unit before it will be suitable for industrial applications.

Further attention should be focused on the power stage of the gate drive circuits. Transistors 9 and 10 of the Gate Drive circuits which supply the Turn-on gate current to the GTO's, should be replaced with Field Effect Transistors, FET's. This will increase the rate of rise of the Gate Turn-on current di_g/dt, and the GTO's will turn on faster. The power dissipation in the GTO's will be decreased by doing this. By using FET's in place of Bipolar Junction Transistors, BJT's, for transistors 9 and 10, the time taken for the Gate Drive Circuit to swop from the "On" condition to the "Off" condition will be decreased. This will enable the interlock delay setting to be reduced and the performance of the inverter will be improved.

Block Firing must be used to hold the GTO's on. This will cause a small increase in the power required by each Gate Drive circuit, but it will not cause any significant decrease in the overall efficiency of the VSD.

The present analogue controller should be modified to incorporate Tacho Feedback. This can be done by inserting an option selection switch in the feedback loop between IC1(a) and IC1(b) of the speed reference circuit. A plug in socket should also be included in the controller to allow the drive to be operated from an optional remote control centre if required.

If a really sophisticated and industrially competitive Drive is to be developed a separate project should be started solely to develop a digital controller. This controller should be designed so that it incorporates the Philips HEF4752 PWM IC as the modulation strategy which is uses, is particularly effective for use with GTO's. Vector control should be used as the overall control method of the complete Drive as this would make it superior to most present D.C. Drives. Full digital control will also make it easy to interface it into a modern process control system without using complicated additional equipment. It would also allow pre-programmed EPROM's to be used to customise the Drive for very specific industrial applications.

Dynamic Braking or Regeneration facilities are two areas that must be investigated fully so that the Drive will have a faster response time when it is in the decelerating mode. This is essential so that the Drive can be incorporated in precision, high performance applications.

Reference [33] describes a high voltage switch mode power supply which operates off the D.C. Link of a VSD. A similar power supply should be designed and tested and the results of which should be compared to the present power supply which operates off the 3 phase input. If its operation is successful, it will eliminate the use of Transformer 1 which drives the present power supply for the control logic.

By inserting a saturable reactor transformer in the D.C. Link fault currents through the Inverter will be limited. This will obviate the need for a Crow-bar Thyristor across the D.C. Link. It will also mean that expensive fuses will not have to be re-placed after a short-circuit. Also by limiting the current in the D.C. Link the destruction of the GTO's in the Inverter will be minimised. The design and construction of a saturable reactor transformer requires a large amount of theoretical design and experimental work.

For further testing of the Inverter discrete compo-nents should be used, and not Power Block modules. This ensures that only a single component, either a GTO or a Freewheel Diode, needs to be replaced when it is damaged and not a whole Power Block module. This also enables the current to be measured in each individual component. In the final unit Power Block modules should be used as they are more com-pact and they can be mounted easily on heatsinks without isolation problems.

Work on final industrial packaging should be done and where possible the components mounted in posi-tion before further testing. This will enable the problems of noise and stray coupling to be elimin-ated. Compactness also reduces inductance and resistance found in unnecessarily long leads. The VSD should be mounted in a cabinet which is drip proof and preferably dust proof.

Since the VSD is intended to be suitable for use in the South African mining industry, the final design must comply with the necessary legislation and specifications. A summary of these is given below.

(i)	Regulation C58 of the Occupational Safety Act, 1983 - Electrical Installations in Hazardous Areas	
(ii)	The Mines and Works Act	
(iii)	SABS0108 -	Code of Practice for the classification of hazardous locations and the selection of electrical apparatus for use in such locations.
(iv)	SABS0119 -	Reduction of explosion hazards by segregation, ventilation and pressurisation of electrical equipment.
(v)	SABS3141971 -	Flameproof enclosures for electrical apparatus
(vi)	SABS5491977 -	Intrinsically safe electrical apparatus
(vii)	SABS9691970 -	Enclosures for electrical apparatus (dust ignition proof, hose proof or both)
(viii)	SABS9701971 -	Non-sparking electrical equipment for use in Class 1, Division 2 locations.

9. CONCLUSION

A large number of papers have been published describing methods obtaining an analytic solution of the harmonic content of PWM waveforms, most of which are for very specific idealised and theoretical cases. Simplifying assumptions are made which do not take factors such as Interlock Delay and Over-Modulation into account. They do however, give a reasonable idea of the expected spectral content of these waveforms. The Discrete Fourier Transform and Slonim methods are both accurate methods of obtaining the actual harmonic content of the output from an Inverter. The results in Chapter 8.4 clearly show the advantages of using PWM methods over other modulation methods. There is a very small harmonic content in the line current of the test motor, especially the 3rd, 5th and 7th harmonics. The higher order harmonics have a negligible effect on the output torque of the motor.

By maintaining the same Pull-Out torque for an Induction motor over it's complete range of operating frequencies, the required Volts/Frequency relationship can be predicted very accurately. For this method to be accurate the Rotor resistance should vary linearly with frequency as it does approximately in practice. This is shown in Chapter 2.2.

The use of GTO's as a "Power Switch" is very effective. When switching resistive or inductive loads using a single GTO they are relatively easy to use. The complications of self-extinguishment arise when switching inductive loads in a full bridge. "Block Firing" in this situation is essential. The latching of GTO's at their current switching condition under short-circuit is also a relatively new concept which is encountered when using GTO's.

The analogue control system developed in Chapter 6 must be converted into a digital controller for the Variable Speed Drive to become commercially competitive. The scale of such a controller is so large that a separate project should be started for this sole purpose.

The question of upgrading the system from 380 Volts to 525 Volts has not been broached yet. After communicating with Dr. J. Witens of Brown Boveri Corporation, Power Semi-Conductor Development Division, in Switzerland he stated that:

> "For a 525 Volt application, Semi conductors with a maximum blocking voltage of 1500 Volts are required".

This statement refers to use of GTO's in a bridge configuration. For single GTO's in a Chopper configuration it is possible to use 1200 Volt devices which are being used at present.

1500 Volt devices have been advertised since the end of 1984, but have not yet been made available on a commercial basis by any of the major manufacturers. At present a 380 Volt system is viable and a 525 Volt system will be viable if 1500 Volt GTO's are made commercially available in the near future.

If 1500 Volt GTO's are available on a commercial basis a full development team and a large amount of capital will be required to produce a commercially competitive PWM Variable Speed Drive for use in a 525 Volt reticulation system.

These recommendations should however, be taken in the light that no other Power Semi-conductor Switching Element will be developed to supersede this range of GTO's. On reply to a question to this effect Dr. J. Witens replied:

> "We must agree to the statement that GTO's in the range of up to 200 Amps and 1600 Volts could be replaced by BJT's in the near future".

It therefore remains for developments in this field to be monitored closely before further work is done in developing a 525 PWM Inverter, using GTO's.

If 1600 Volt BJT's are commercially available they should be used in preference to GTO's as their Base Drive Circuit is simpler to implement than Gate Drive Circuits for GTO's. They can also be switched at higher frequencies and do not self-extinguish when the collector current is small, as is the case with GTO's.

REFERENCES

(1) GENERAL ELECTRIC COMPANY
Gate Turn-Off Switch, Publication 150.60, March 1962

(2) STORM, H.F.
Introduction to Turn-Off Silicon-Controlled Rectifiers. IEEE Winter General Meeting January 1963, pp 375-382.

(3) APPLICATION NOTE AN6457
Characteristics and Applications of RCA Gate Turn-Off Silicon-Controlled Rectifiers.

(4) GENERAL ELECTRIC COMPANY
NPN Latching Power Transistor, General Electric Technical Publication 50.88, March 1979.

(5) IKEDA, Y and SAKURADA, S
Gate Turn-Off Thyristor and Drive Circuits, Hitachi Review, Vol. 29, No. 3. (1980) pp 127-130

(6) AEG,
Proper Triggering of Gate Turn-Off Thyristors, Technical Information 14.

(7) MARCONI ELECTRONIC DEVICES
Gate Turn-Off Thyristor Application Notes.

(8) AEG-TELEFUNKEN
Gate Turn-Off Thyristors, Technical data 1984/1985.

(9) HALL, J.K. and MANNING, C.D.,
Switching Properties of Gate Turn-Off Thyristors. Loughborough University of Technology, United Kingdom.

(10) MATSUDA, Y and FUKUI, H.
Application Engineering of Gate Turn-Off Thyristors. Hitachi Review, Vol. 31, No. 4, (1982), pp 173-176.

(11) ENSLIN, N.C.
How Accurate is the Induction Motor Model when Applied to Modern Squirrel Cage Machines. University of Cape Town, Department of Electrical Engineering, Research Review, Vol. 8, No. 1, Feb. 1984, pp 7-10.

(12) HINDMARSH, J.
An Integrated Lecture and Laboratory Course in Electrical Machines. Department of Electrical Engineering and Electronics, UMIST, England.

(13) HINDMARSH, J.
Electric Machines and Drives, Pergamon, p.77

(14) SAY, M.G.
Alternating Current Machines, Pitman, p.264.

(15) CONNORS, D.P. and ARC, D.A.,
Application considerations for A.C. Drives, IEEE Trans. on Industrial Applications, Vol.IA-19, No. 3,1 May/June 1983, pp 455-460.

(16) WILLIAMS, I.J.
Induction Motors for Inverter Drives up to 200 kW. GEC Journal for Industry, Vol. 6, NO. 1, Feb. 1983, pp 28-35.

(17) ABBOTT, W.
Practical Geometry and Engineering Graphics, Blackie and Son. p. 150.

(18) BIRINGER, P. and SLONIM, M.,
Determination of Harmonics of Converter Current and/or Voltage Waveforms. (New method for Fourier Coefficient Calculations), Part 1 : Fourier Coefficients of Homogenous Functions. IEEE Trans on Industrial Applications. Vol IA-16 No. 2, March/April 1980, pp 242-247.

(19) SLONIM, M., RAPOPORT, I. and BIRINGER, P.,
Calculation of Fourier Coefficients of Experimentally Obtained Waveforms. IEEE Trans on Industrial Electronics and Control Instrumentation, Vol. IECI-28, No. 4, November 1981, pp 330-335.

(20) KLIMAN, B. and PLUNKETT, A.,
Development of a Modulation Strategy for a PWM Inverter Drive. IEEE Trans on Industry Applications; Vol. IA-15, No. 1, Jan/Feb 1979, pp 72-79.

(21) VAN WYK, J.D.,
Oor Skakelaargedrag in Wisselrigtertakke met Pulswydtemodulalie. Randse Afrikaanse Universiteit, Fakulteit Ingenieurswese Interne Verslag. Nr. END-10-EI-74-2, Sept. 1984.

(22) LANDER, C.W.,
Power Electronics, McGraw-Hill, p. 343.

(23) THOMPSON, C.S.F.,
Power Transistors in the Switching Mode.
Sescosem, p28.

(24) VAN WYK, J.D.,
Kritieke Skakelversynsels in Wisselrigters met Bipolere Transistors vir Spannings bo 200V en Pulsfrekwensie bo 5 kHz. Randse Afrikaanse Universiteit, Fakulteit Ingenieurswese, Interne Verslag, NR.RAU-END-2-EI-74-2.

(25) UDELAND, T., JENSET, F. and STEINBAKK, A.,
A Snubber Configuration for both Power Transistor and GTO PWM Inverters. IEEE Power Electronic Specialist Conference Record. 1984, pp 42-53.

(26) HOULDSWORTH, J.A.,
Purpose-Designed Ferrite Toroids for Isolated Current Measurement in power Electronic Equipment. Electronic Components and Applications, Vol. 3, NO. 2, February 1981, pp 101-109.

(27) STARR, B.G. and VAN LOON, J.C.F.,
LSI Circuit for AC Motor Speed Control, Electronic Components and Applications, Vol. 2, No. 4, August 1980, pp 219 - 229.

(28) GILLIAM, J.E.,
Understanding and Using the Philips A.C. Motor Speed Control I.C. HEF4752, Mullard Technical Report MP08201, December 1982.

(29) HOULDSWORTH, J.A. and ROSINK, W.B.,
Introduction to PWM Speed control System for 3-Phase A.C. Motors. Electronic Components and Applications, Vol. 2, No. 2, February 1980, pp 66-79.

(30) ROSINK, W.B.,
Analogue Control System for A.C. Motor with PWM Variable Speed Drive. Electronic Components and Applications, Vol. 3, NO. 1, November 1980, pp 6-16.

(31) LEE, R.H.
Simplifying the Analysis of Harmonic Content in Complex Inverter Switching Waveforms. Proceedings of Powercon 8, GI-2, 1981.

(32) HOFFMAN, K.P.
Power Transistor Inverter. University of Cape Town, Electrical Engineering, B.Sc. Thesis, 1979. pp 57-62.

(33) BURGUM, F. and JANSSON, L.E.
Auxiliary Power Supply for AC Motor Speed Control System, Electronic Components and Applications, Vol.3, No.4, August 1981, pp. 245-250.

BIBLIOGRAPHY

ADAMS, R.D. and FOX, R.S.
Several Modulation Techniques PWM Inverter, IEEE Conference Record of Fifth Annual Meeting of Industry and General Applications Group, 1970, pp. 687-693

AMATO, C.J.
A Simple and Speedy Method for Determining the Fourier Coefficients of Power Converter Waveforms, IEEE Conference Record of Fourth Annual Meeting of Industry and General Applications Group, 1969, pp. 477-483.

ANDRESEN, E.C. and BIENIEK, K,
On the Torques and Losses of Voltage- and Current-Source Inverter Drives, IEEE Transactions on Industry Applications, Vol. IA-20, No. 2, March/April, 1984, pp. 321-327.

BROWN BOVERI REVIEW
Static Frequency Changers with "Subharmonic" Control in Conjunction with Reversible Variable-Speed A.C. Drives. August/September 1964, pp. 555-577.

BURGUM, F.J. and NIJHOF, E.B.G.
Inverter Circuit for a PWM Motor Speed Control System. Electronic Components and Applications, Vol. 2, No. 3, May 1980, pp. 130-143.

BURGUM, F, NIJHOF, E.B.G. and WOODWORTH, A.
Gate Turn-Off Switch, Electronic Components and Applications, Vol. 2, No. 4, August 1980, pp. 194-202.

DE BUCK, F.G.G.
Losses and Parasitic Torques in Electric Motors Subjected to PWM Waveforms, IEEE Transactions on Industry Applications, Vol. IA-15, No. 1, January/February 1979, pp. 47-53.

FUKAZAWA, K and NOVOTNY, D.W.
The Influence of Volts/Herz Control on Filter Impedance Effects in VSI-Fed Induction Machines, IEEE Transactions on Industry Applications, Vol. IA-18, No. 3, May/June 1982, pp. 230-239.

GIBSON, H. and HEARD, J.S.
Fast Over-Current Protection with G.T.O. Thyristors, Stafford Laboratory, G.E.C. Power Engineering Ltd., Stafford, U.K.

GOLDBRUNNER, W. and VETTER, H.
Capacitors for GTO Thyristors, Siemens Components XIX No. 6 1984, pp. 264-268.

GRANT, D. and HONDA, A.
Applying International Rectifiers Gate Turn-Off Thyristors, International Rectifier AN-315A.

GRANT, T.L. and BARTON, T.H.
Control Strategies for PWM Drives, IEEE Transactions on Industry Applications, Vol.IA-16, No. 2, March/April 1980, pp. 211-215.

HONBU, M., MATSUDA, Y., MIYAZAKI, K. and JIFUKU, Y.
Parallel Operation Techniques of GTO Inverter Sets for Large A.C. Motor Drives, IEEE Transactions on Industry Applications, Vol. IA-19, No. 2, March/April 1983. pp. 198-205.

HONDA, A and PELLY, B.
Applying International Rectifier's 160PFT Type Gate Turn-Off Thyristors, International Rectifier AN-315.

IKEDA, Y.
Gate Turn-Off Thyristors, Hitachi Review, Vol. 31, No. 4, 1982. pp. 169-172

JIMBO, Y., UEDA, A. and ITAHANA, H.
GTO Applications to Traction Motor Drives, Hitachi Review, Vol. 31, No. 4. (1982), pp. 189-194

KANZAKI, T. and MORIYA, F.
Three-Phase GTO Inverter for Auxiliary Power Source on Rolling Stock. Toshiba Review, No. 139, May/June 1982, pp. 30-35.

KLIMAN, G.B.
Harmonic Effects in Pulse Width Modulated Inverter Induction Motor Drives, IEEE/IAS 1972 Annual Meeting, 1972, pp. 783-790

MATSUDA, Y., FUKUI, H., AMANO, H., OKUDA, H., WATANABE, S. and ISHIBASHI, A.,
Development of PWM Inverter Employing GTO. IEEE Transactions on Industry Applications, Vol. IA-19, No. 3, May/June 1983, pp. 335-342.

McMURRAY, W.

Optimum Snubbers for Power Semiconductors, IEEE Conference Record of Sixth Annual Meeting of Industry and Application Group, 1971, pp. 885-893.

OHASHI, H.

Snubber Circuit for High-Power Gate Turn-Off Thyristors, IEEE Transactions on Industry Applications, Vol. IA-19, No. 4, July/August 1983, pp. 655-664.

PAICE, D.A. and MATTERN, K.E.,

Application of Gate Turn-Off Thyristors in 460-V 7.5-250-hp AC Motor Drives, IEEE Transactions on Industry Applications, Vol. IA-19, No. 4, July/August 1983, pp. 554-560.

PAICE, D.A. and MATTERN, K.E.,

Gate-Turn-Off Thyristors and Their Application. Westinghouse Electric Corporation, USA.

PASSERINI, B., TENCONI, S. and ZAMBELLI, M.

High Power Gate Turn-Off Thyristors : Characteristics and Ratings, Ansaldo Elettronica Industriale S.p.A., Italy.

PENKOWSKI, L.J. and PRUZINSKY, K.E.,

Fundamentals of a Pulsewidth Modulated Power Circuit. IEEE Transactions on Industry Applications, Vol. IA-8, No. 5, September/October 1972. pp. 584-592.

PHILIPS

The BTV60 - First in a New Generation of GTOs. Technical Publication 132.

PHILIPS

The Gate Turn-Off Switch in PWM A.C. Motor Control, Technical Publication 031

PHILIPS

GTOs for PWM Control of A.C. Motors. Technical Publication 124.

RICE, J.B.

Design of Snubber Circuits for Thyristor Converters, IEEE Conference Record of Fourth Annual Meeting of Industry and General Applications Group. 1969, pp. 485-489.

SCHOLEY, D.

Induction motors for Variable Frequency Power Supplies, IEEE Transactions on Industrial Applications, Vol. IA-18, No. 4, July/August 1982, pp 368-372.

SLONIM, M.A. and BIRINGER, P.P.,

Determination of Harmonics of Converter Current and/or Voltage Waveforms (New Method for Fourier Coefficient Calculations), Part II: Fourier Coefficients of Nonhomogeneous Functions.
IEEE Transactions on Industry Applications, Vol. IA-16, No. 2. March/April 1980. pp 248-253.

SONE, S. and IRINATSU, H.
Very Precise Turn-Off Timing Control of Gate Turn-Off Thyristors, University of Tokyo, Japan

SUEYOSHI, O., UASUOKA, I. and KAWAI, I.,
GTO Inverter for Electric Multiple Unit Induction Motor. Toshiba Review, No. 143, Spring 1983, pp. 21-26.

TAYLOR, P.D.
A Comparison of GTO Thyristor Device Designs, Marconi Electronic Devices Ltd.

TOKUNOCH, F., HAGINO, H. and MIYAJIMA,
Electrical Characteristics of High Voltage High Current Gate Turn-Off Thyristor, Mitsubishi Electric Corporation, Japan.

TOSHIBA,
GTO Application Note, Toshiba Corporation, 1983.

UEKA, A., IBAMOTO, M., NARITA, H., HORI, T., TSUBOI, T. and YAMADA, Y.,
GTO Inverter for AC Traction Drives, IEEE Transactions on Industry Applications, Vol. IA-19, No. 8, May/June 1983, pp. 343-347.

UNDELAND, T.,
Snubbers for Pulse Width Modulated Bridge Converters with Power Transistors or GTOs. IPEC - Tokyo, 1983, pp. 313-323.

VITINS, J. and SCHWEIZER, A.,
Use of Power Semiconductors Made Easier by Forward Integration. Brown Boveri Rev. 5, 1984, pp. 216-221.

WARNER, P.,
Suitable and Unsuitable Rotors for Speed-Controlled Induction Motors, Vector, December, 1985.

WILLIAMS, B.W. and PALMER, P.R.,
Drive and Snubber Techniques for GTO's and Power Transistors - Particularly for Inverter Bridges, Imperial College of Science and Technology, U.K.

WOODWORTH, A. and BURGUM, F.
Simple Rules for GTO Circuit Design, Philips Technical Publication 029.

APPENDIX 2.1

DETERMINATION OF AN INDUCTION MOTOR EQUIVALENT CIRCUIT

Below is a detailed explanation for the calculation of the equivalent circuit of an induction motor.

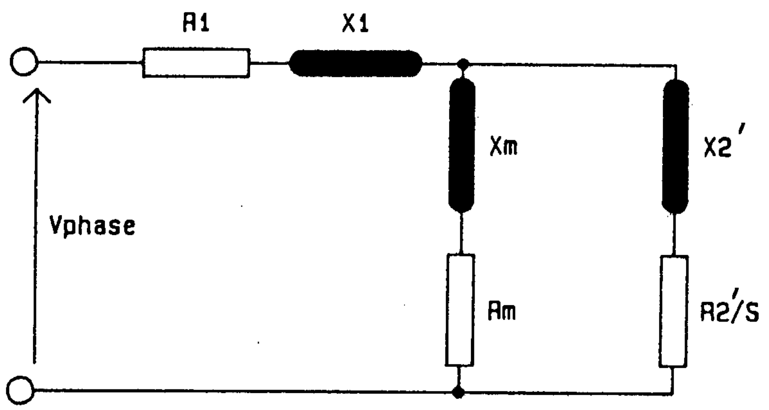

Figure A2.1 Induction Motor Equivalent Circuit

A = Phase volts at no-load
B = Phase current at no-load
C = No-load watts/phase
D = Phase volts at short-circuit
E = Phase current at short-circuit
F = Short circuit watts/phase
G = R1
H = Frequency

Initially $R2' = (F/E^2 - G)$

Assuming $X1 = X2'$ and neglecting Rm and Xm then

$$X_1 = \sqrt{\left[\frac{D^2}{E^2} - \frac{F^2}{E^4}\right]} \times \frac{1}{2}$$

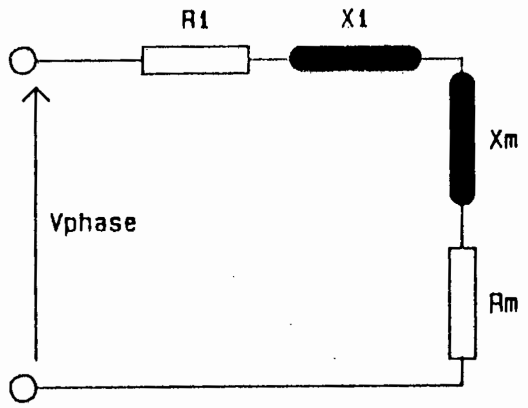

Figure A2.2 Calculating Rm and Xm

Then using the O.C. test results and neglecting R2'/S and X2' as in Fig. A2.2

$$Rm = \frac{C}{B^2} - G$$

$$Xm = \sqrt{\frac{A^2}{B^2} - \frac{C^2}{B^4}} - X1$$

Thus all the initial values of the equivalent circuit in Fig. A2.1 have been calculated

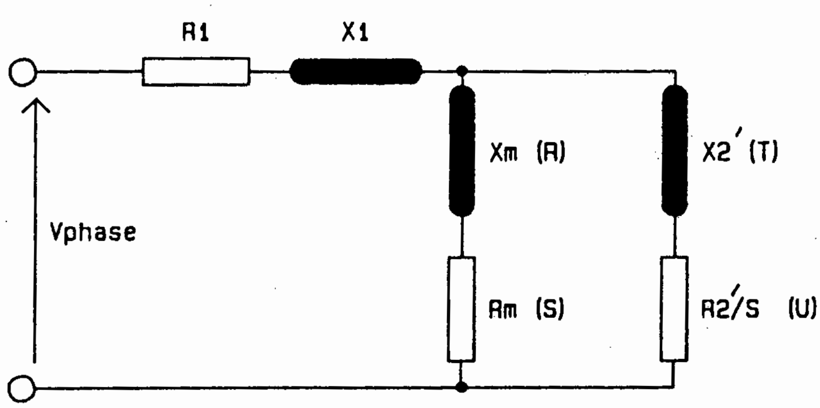

Figure A2.3

The iterative process can now be implemented and an improved value of R2' and X2' can be obtained.

$$Z\angle\phi = \frac{(R + js)(T + ju)}{(R + T) + j(S + u)} = X + jY$$

$$\text{Hence } X1 = \sqrt{\frac{D^2}{E^2} - \frac{F^2}{E^4}} - Y$$

$$\text{and } X1 = X2'$$

Using these new values of X1 and X2' an improved value of R2' can be obtained.

$$|Z| = \frac{\sqrt{R^2 + S^2} \times \sqrt{T^2 + u^2}}{\sqrt{(R + T)^2 + (S + u)^2}}$$

and solving for T

$$T = \frac{-\sqrt{L^2 - (4\ k\ N)} - L}{2K}$$

Where $K = (Z^2 - R^2 - S^2)$

$L = (2RZ^2)$

$N = Z^2(R^2 + (S + u)^2) - U^2(R^2 + S^2)$

The value of Rm remains unchanged and a new improved value of Xm can be calculated.

$$Xm = \sqrt{\frac{A^2}{B^2} - \frac{C^2}{B^4}} - X1$$

After repeating this process of calculating new improved values, until they have stabilised, the exact equivalent circuit is obtained.

A computer program was written so that this method could be implemented efficiently. The listing is given below.

```
10     !*********************************************************************
20     !                                                                    *
30     !  THIS PROGRAM CALCULATES THE EQUIVALENT CIRCUIT OF A 3 PHASE       *
40     !  INDUCTION MOTOR. A NUMERICAL ITTERATION METHOD IS USED TO         *
50     !  OBTAIN THE EXACT EQUIVALENT CIRCUIT VALUES FROM THE APPROXIMATE   *
60     !  ONES.                                                             *
70     !  IT IS ASSUMED THAT (1) THE MOTOR IS STAR CONNECTED                *
80     !                     (2) TOTAL WATTS FOR THE 3 PHASES MUST BE USED  *
90     !                     (3) LINE VOLTAGE VALUES ARE USED i.e. L-N      *
100    !                     (4) LINE CURRENTS ARE USED                     *
110    !  THE RESULTANT SHUNT CIRCUIT VALUES ARE IN SERIES, NOT PARALLEL    *
120    !                                                                    *
130    !*********************************************************************
140    OPTION BASE 0
150    DIM M(5)
160    INPUT "PHASE VOLTS N/L=",A
170    INPUT "AMPS N/L=",B
180    INPUT "TOTAL WATTS N/L=",C
190    INPUT "PHASE VOLTS S/C=",D
200    INPUT "AMPS S/C=",E
210    INPUT "TOTAL WATTS S/C=",F
220    INPUT "R1=",G
230    INPUT "FREQUENCY=",J
240    INPUT "NUMBER OF ITTERATIONS REQUIRED",I
250    PRINTER IS PRT
260    PRINT "FEREQUENCY=";J
270    PRINT "PHASE VOLTS N/L=";A
280    PRINT "AMPS N/L=";B
290    PRINT "WATTS N/L=";C
300    PRINT "PHASE VOLTS S/C=";D
310    PRINT "AMPS S/C=";E
320    PRINT "WATTS S/C=";F
330    PRINT "R1=";G
340    PRINTER IS CRT
350    C=C/3                                    !O/C WATTS/PHASE
360    F=F/3                                    !S/C WATTS/PHASE
370    DISP "CALCULATING EQUIVALENT CIRCUIT "
380    !***************************************************
390    !                                                  *
400    !                 S.C.  TEST  No1                  *
410    !   INITIAL VALUES OF R2',X1 andX2' ARE CALCULATED, *
420    !   NOT TAKING THE VALUES OF Xm and Rm INTO ACCOUNT.*
430    !                                                  *
440    !***************************************************
450    M(2)=(F/E^2)-G                           !M(2)=R2
460    M(0)=(((D^2/E^2)-(F^2/E^4))^.5)/2        !M(0)=X1
470    M(1)=M(0)                                !M(1)=X2
480    !***************************************************
490    !                                                  *
500    !                 O.C.  TEST  No1                  *
510    !       INITIAL VALUES OF Rm and Xm ARE CALCULATED  *
520    !                                                  *
530    !***************************************************
540    M(3)=(C/B^2)-G                           !M(3)=Rm
550    M(4)=(((A^2/B^2)-(C^2/B^4))^.5)-M(0)!M(4)=Xm
```

```
560   !************************************************
570   !                                               *
580   !                 S.C.  TEST  No2               *
590   ! THIS TEST CALCULATES NEW VALUES OF R2´,X1 and X2´ *
600   ! ALLOWING FOR Xm and Rm.                       *
610   !************************************************
620   FOR W=1 TO I STEP 1
630     R=M(3)                            !NEW VARIABLES
640     S=M(4)
650     T=M(2)
660     U=M(1)
670     Z=(((R^2+S^2)^.5)*((T^2+U^2)^.5))/((((R+T)^2)+((S+U)^2))^.5)
680     O=ATN(S/R)+ATN(U/T)-ATN((S+U)/(R+T))
690   !  Z IS IN THE FORM  Z=X+jY
700     X=Z*COS(O)
710     Y=Z*SIN(O)
720   !************************************************
730   !   IMPROVED VALUES OF X1 AND X2                *
740   !************************************************
750     M(0)=(((D^2/E^2)-(F^2/E^4))^.5)-Y    !M(0)=X1
760     M(1)=M(0)                             !M(1)=X2
770   !************************************************
780   !    IMPROVED VALUE OF R2                       *
790   !************************************************
800     U=M(1)
810     Z=((F/E^2-G)^2+((D^2/E^2-F^2/E^4)^.5-M(0))^2)^.5
820     K=(Z^2)-(R^2)-(S^2)
830     L=2*R*(Z^2)
840     N=(Z^2)*(R^2+(S+U)^2)-(U^2*(R^2+S^2))
850     T=(-(L^2-4*K*N)^.5-L)/(2*K)          !R2=T
860     M(2)=T
870   !************************************************
880   !           O.C. TEST No2  USING  NEW VALUE OF X1    *
890   !************************************************
900     M(3)=(C/B^2)-G                         !Rm IS UNCHANGED
910     M(4)=(((A^2/B^2)-(C^2/B^4))^.5)-M(0)   !NEW VALUE OF Xm
920   NEXT W
930   PRINTER IS PRT
940   PRINT
950   PRINT USING """R1="".D.DDDDD";G
960   PRINT USING """R2´="",D.DDDDD";M(2)
970   PRINT USING """X1="",D.DDDDD";M(0)
980   PRINT USING """X2´="",D.DDDDD";M(1)
990   PRINT USING """Rm="",2D.DDDDD";M(3)
1000  PRINT USING """Xm="",3D.DDDDD";M(4)
1010  PRINTER IS CRT
1020  DISP "EXECUTION COMPLETE"
1030  END
```

APPENDIX 2.2

TEST MOTOR AND EQUIVALENT CIRCUIT

Short-Circuit and Open-Circuit tests were performed on a standard GEC DZ160 M Induction motor with a full load current of 16,2 A at 525 V. These tests were performed over a range of frequencies and the results are tabulated in Table A2.2.

Frequency	Test	V_{L-N} (Volts)	I_L (Amps)	Watts (Total)
50 Hz	O.C S.C	303 187	1,33 16,2	324 2950
40 Hz	O.C S.C	242 160	1,33 16,2	204 2755
30 Hz	O.C S.C	182 132	1,32 16,2	144 2590
20 Hz	O.C S.C	121 102	1,19 16,2	152 2425

Table A2.2 Short-Circuit and Open-Circuit Test Results

The armature resistances for each phase were measured.

$R_u = 2,079\ \Omega$

$R_v = 2,074\ \Omega$

$R_w = 2,068\ \Omega$

$R_{AVERAGE} = \underline{2,0737\ \Omega}$

For the O.C test the motor was driven at synchronous speed

APPENDIX 2.3

INDUCTION MOTOR THEORY

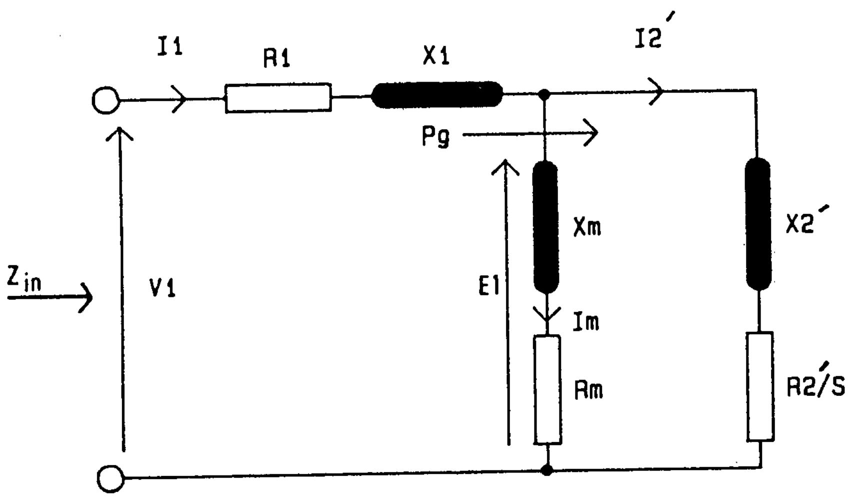

Figure A2.4 Induction Motor Equivalent Circuit

Briefly, for an induction motor the air-gap power, Pg, per phase is given by

$$Pg = V1 \times I1 \times \cos\phi - \text{Stator Loss}$$

but $$Pg = \frac{(I2')^2 \times R2'}{S}$$

therefore the remaining mechanical power

$$Pm = (1 - S) \times Pg = (1 - S) \times \left[\frac{(I2')^2 \times R2'}{S}\right] \text{ watts/phase}$$

but the mechanical torque, Tm, is given by

$$Tm = \frac{3 \times Pm}{Wm} = \frac{3(I2')^2 R2'}{S \times W_s} \quad Nm$$

The above theory is covered in detail by J. Hindmarsh in reference [13] and M. Say in reference [14].

The input impedance is given by

$$Z_{in} = |Z| \underline{\angle \phi}$$

Therefore the power factor is easily obtainable since the input current, I1, is

$$I1 = \frac{V1}{Z_{in}}$$

and

$$P.F. = \cos \phi$$

Efficiency is also obtained easily by

$$EFF = \frac{\text{Power out}}{\text{Power in}}$$

All of the above is implemented in the program which is listed below

```
10     !********************************************************************
20     !                                                                   *
30     !   THIS PROGRAM CALCULATES THE THEORETICAL CHARACTERISTICS OF      *
40     !   THREE PHASE INDUCTION MOTOR CONNECTED IN STAR.                  *
50     !          P=NUMBER OF POLE PAIRS                                   *
60     !          F=FREQUENCY                                              *
70     !          E=LINE VOLTAGE                                           *
80     !          VALUES OF Xm AND Rm ARE SERIES VALUES, NOT PARALLEL      *
90     !********************************************************************
100    OPTION BASE 1                        !ARRAYS START AT ELEMENT 1
110    DIM Z1(2),Z2(2),Z3(2),Eo(2)          !2 ELEMENT ARRAYS
120    DIM A(2),B(2),Result(2)              !FOR COMPLEX SUBROUTINES
130    DIM Zr1(2),Zr2(2),Zr3(2)             !FOR COMPLEX SUBROUTINES
140    DIM Zo(2)                            !INPUT IMPEDENCE
150    DIM Torque(2,101)                    !ALL SLIP AND TORQUE VALUES
160    DIM Powerfactor(2,101)               !ALL SLIP AND POWER FACTOR VALUES
170    DIM Current(2,101)                   !ALL SLIP AND INPUT CURRENT VALUES
180    DIM Efficiency(2,101)                !ALL SLIP AND EFFICIENCY VALUES
190    PRINTER IS CRT !SCREEN
200    INPUT "ENTER THE VALUES FOR Eo,P,F",E,P,F
210    INPUT "R1,R2',X1,X2,Rm,Xm",R1,R2,X1,X2,Rm,Xm
220    Graph(Torque(*),Powerfactor(*),Current(*),Efficiency(*))
                                            !PLOT GRAPHICS AXES
230    Tmax=0
240    FOR I=50 TO 0 STEP -1
250      Slip=I/100                         !SLIP VALUES OF 0 TO 50 P.U.
260      Eo(1)=E/(3^.5)                     !PHASE VOLTAGE
270      Eo(2)=0                            !NO IMAGINARY COMPONENTS
280      Z1(1)=R1
290      Z1(2)=X1
300      IF I>0 THEN
310        Z2(1)=R2/Slip
320      ELSE
330        Z2(1)=1.0E+100                   !FOR R2'/S WHEN S=0 APPROX=INFINITY
340      END IF
350      Z2(2)=X2
360      Z3(1)=Rm
370      Z3(2)=Xm
380    !*****************************************************
390    !                  INPUT IMPEDANCE                   *
400    !              Zo=Z1+(Z3*Z2)/(Z3+Z2)                 *
410    !*****************************************************
420      Complex_mult(Z3(*),Z2(*),Zr1(*))     ! Z2*Z3 STORED IN ZR1
430      Complex_add(Z3(*),Z2(*),Zr2(*))      !Z2+Z3 STORED IN ZR2
440      Complex_div(Zr1(*),Zr2(*),Zr1(*))    !ZR1/ZR2 STORED IN ZR1
450      Complex_add(Z1(*),Zr1(*),Zo(*))      !INPUT IMPEDENCE
460    !*****************************************************
470    !         CALCULATION OF POWER FACTOR                *
480    !*****************************************************
490      O=ATN(Zo(2)/Zo(1))
500      Power=COS(O)                         !POWER FACTOR
510    !*****************************************************
520    !         CALCULATION OF AIR-GAP VOLTAGE             *
530    !*****************************************************
540      Complex_div(Eo(*),Zo(*),Zr1(*))      !I1=Eo/Zo  I1 IN ZR(1)
550      Curr=(Zr1(1)^2+Zr1(2)^2)^.5          !INPUT CURRENT
560      Complex_mult(Zr1(*),Z1(*),Zr1(*))    !I1*Z1
570      Complex_sub(Eo(*),Zr1(*),Zr1(*))     !E1 IN ZR(1)
```

```
580   !*****************************************************
590   !      CALCULATES ROTOR CURRENT AND TORQUE OUTPUT      *
600   !      Torque=3*(I2^2)*R2'/(Slip*Ws)                   *
610   !*****************************************************
620     Complex_div(Zr1(*),Z2(*),Zr1(*))     !I2 IN ZR(1)
630     W=(Zr1(1)^2)+(Zr1(2)^2)              !I2 SQUARED
640     IF I>0 THEN
650       Torq=(3*W*R2*P)/(2*PI*F*Slip)      !TORQUE AT A GIVEN SLIP
660     ELSE
670       Torq=0                             !TORQUE=0 AT Slip=0
680     END IF
690     !***************************************************
700     !           EFFICIENCY CALCULATION                  *
710     !           POWER OUT=Ws*(1-S)*TORQUE               *
720     !***************************************************
730     Powerin=(3^.5)*Curr*E*COS(0)
740     Powerout=(2*PI*F/P)*(1-Slip)*Torq
750     Eff=Powerout/Powerin                 !EFFICIENCY
760     !***************************************************
770     !                  STORE DATA                       *
780     !***************************************************
790     Torque(1,I+1)=I/100                  !SLIP VALUE IN ARRAY
800     Torque(2,I+1)=Torq                   !TORQUE VALUE IN ARRAY
810     Powerfactor(1,I+1)=I/100             !SLIP VALUE IN ARRAY
820     Powerfactor(2,I+1)=Power             !POWER FACTOR IN ARRAY
830     Current(1,I+1)=I/100                 !SLIP VALUEIN ARRAY
840     Current(2,I+1)=Curr                  !INPUT CURRENT IN ARRAY
850     Efficiency(1,I+1)=I/100              !SLIP VALUE IN ARRAY
860     Efficiency(2,I+1)=Eff                !EFFICIENCY VALUE IN ARRAY
870     !***************************************************
880     !                FIND PEAK TORQUE                   *
890     !***************************************************
900     IF Torq>Tmax THEN
910       Tmax=Torq                          !PEAK TORQUE
920       Smax=I/100                         !SLIP AT PEAK TORQUE
930     END IF
940   NEXT I
950   PRINT "Tmax=";Tmax,"Smax=";Smax
960   Graph_plot(Torque(*),Powerfactor(*),Current(*),Efficiency(*))
                                             !PLOT GRAPHS
970   END
980   !*****************************************************************
990   !          C O M P L E X   N U M B E R   S U B R O U T I N E S
1000  !*****************************************************************
1010  SUB Complex_add(REAL A(*),B(*),Result(*))
1020    Result1=A(1)+B(1)      ! Real Components
1030    Result2=A(2)+B(2)      ! Imaginary Components
1040    Result(1)=Result1
1050    Result(2)=Result2
1060  SUBEND
1070  !-----------------------------------------------------------------
1080  SUB Complex_sub(REAL A(*),B(*),Result(*))
1090    Result1=A(1)-B(1)
1100    Result2=A(2)-B(2)
1110    Result(1)=Result1
1120    Result(2)=Result2
1130  SUBEND
1140  !-----------------------------------------------------------------
1150  SUB Complex_mult(REAL A(*),B(*),Result(*))
1160    Result1=A(1)*B(1)-A(2)*B(2)
1170    Result2=A(1)*B(2)+A(2)*B(1)
1180    Result(1)=Result1
1190    Result(2)=Result2
1200  SUBEND
1210  !-----------------------------------------------------------------
1220  SUB Complex_div(REAL A(*),B(*),Result(*))
1230    Result1=(A(1)*B(1)+A(2)*B(2))/((B(1))^2+(B(2))^2)
1240    Result2=(A(2)*B(1)-A(1)*B(2))/((B(1))^2+(B(2))^2)
1250    Result(1)=Result1
1260    Result(2)=Result2
1270  SUBEND
```

APPENDIX 2.4

Program for the calculation of the voltage requirements of an Induction motor driven at variable frequencies.

```
10     !*****************************************************************
20     !      THIS PROGRAM OPTIMIZES TORQUE/SPEED CHARACTERISTICS        *
30     !      FOR A THREE PHASE STAR CONNECTED MOTOR WHEN RUN AT         *
40     !      VARIABLE FREQUENCIES.                                      *
50     !              E=LINE VOLTAGE                                     *
60     !              P=NUMBER OF POLE PAIRS                             *
70     !              F=PRIMARY FREQUENCY                                *
80     !*****************************************************************
90     OPTION BASE 1                                  !ARRAYS START AT ELEMENT 1
100    DIM Z1(2),Z2(2),Z3(2),Eo(2),Eo1(2),Vo(2)       !2 ELEMENT ARRAYS
110    DIM A(2),B(2),Result(2)                        !FOR COMPLEX SUBROUTINES
120    DIM Zr1(2),Zr2(2),Zr3(2)                       !FOR COMPLEX SUBROUTINES
130    DIM Zo(2)                                      !FOR INPUT IMPEDENCE
140    DIM Slip1(2,101),Slip2(2,101),Slip3(2,101),Slip4(2,101),Slip5(2,101)
                                 !FOR ALL TORQUE AND SLIP VALUES
150    DIM Slip(2,101)           !ARRAY FOR TORQUE SUBROUTINE
160    PRINTER IS CRT            !SCREEN
170    INPUT "ENTER R1,R2',X1,X2',Rm,Xm",R1,R2,X1,X2,Rm,Xm
180    INPUT "ENTER E,P,F1",E,P,F1
190    Graph(Slip1(*),Slip2(*),Slip3(*),Slip4(*),Slip5(*))
200    !************************************************
210    !    CALCULATES THE PRIMARY TORQUE/SPEED CURVE     *
220    !************************************************
230    Tmax1=0
240    FOR S=100 TO 0 STEP -1
250      Slips=S/100                      !SLIP VALUES OF 0 TO 100 P.U.
260      Eo(1)=E/(3^.5)                   !PHASE VOLTAGE
270      Eo(2)=0                          !NO IMAGINARY COMPONENTS
280      Z1(1)=R1
290      Z1(2)=X1
300      IF S>0 THEN
310        Z2(1)=R2/Slips
320      ELSE
330        Z2(1)=1.0E+100                 !R2'/S APPROX INFINITY WHEN S=0
340      END IF
350      Z2(2)=X2
360      Z3(1)=Rm
370      Z3(2)=Xm
380    !************************************************
390    !              INPUT IMPEDANCE                     *
400    !            Zo=Z1+(Z3*Z2)/(Z3+Z2)                 *
410    !************************************************
420      Complex_mult(Z3(*),Z2(*),Zr1(*))      !Z2*Z3 STORED IN ZR(1)
430      Complex_add(Z3(*),Z2(*),Zr2(*))       !Z2+Z3 STORED IN ZR(2)
440      Complex_div(Zr1(*),Zr2(*),Zr1(*))     !ZR(1)/ZR(2) STORED IN ZR(1)
450      Complex_add(Z1(*),Zr1(*),Zo(*))       !INPUT IMPEDENCE
460    !************************************************
470    !        CALCULATION OF AIRGAP VOLTAGE             *
480    !************************************************
490      Complex_div(Eo(*),Zo(*),Zr1(*))       !I1=Eo/Zo  I1 IN ZR(1)
500      Complex_mult(Zr1(*),Z1(*),Zr1(*))     !I1*Z1
510      Complex_sub(Eo(*),Zr1(*),Zr2(*))      !E1 IN ZR(2)
520    !************************************************
530    !            CALCULATION OF TORQUE                 *
540    !      Torque=3*(I2^2)*R2'/(Ws*Slip)               *
550    !************************************************
560      Complex_div(Zr2(*),Z2(*),Zr1(*))      !I2 IN ZR(1)
570      W=(Zr1(1)^2)+(Zr1(2)^2)               !I2 SQUARED
580      IF S>0 THEN
590        T1=(3*W*R2*P)/(2*PI*F1*Slips)       !TORQUE AT A GIVEN SLIP
```

```
600     ELSE
610       T1=0                                     !Torque=0 AT SLIP=0
620     END IF
630     !*********************************************
640     !              FIND PEAK TORQUE              *
650     !*********************************************
660     IF T1>Tmax1 THEN
670       Tmax1=T1                                 !PEAK TORQUE
680     END IF
690     !---------------------------------------------
700     Slip1(1,S+1)=(1-Slips)*60*F1/P             !SPEED  VALUE IN RPM IN ARAY
710     Slip1(2,S+1)=T1                            !STORE TORQUE VALUE IN ARRAY
720   NEXT S
730   PRINTER IS PRT
740   PRINT "F=";F1;"(Hz)"
750   PRINT "R2´=";R2;"(Ohms)"
760   PRINT "V=";E;"(Volts)"
770   PRINT "Tmax=";Tmax1;"(Nm)"
780   !*********************************************************
790   !         CALCULATES NEW VOLTAGE FOR THE REQUIRED FREQUENCY  *
800   !         TO GIVE CORRECT PEAK TORQUE OBTAINED FROM THE     *
810   !         PRIMARY FREQUENCY.                                 *
820   !*********************************************************
830   INPUT "ENTER NEW FREQUENCIES  F2,F3,F4,F5",F2,F3,F4,F5
840   INPUT "ENTER R2x,Fx",R2x,Fx            !VALUES AT LOW FREQUENCY TO OBTAIN
                                               LINEAR RESISTANCE RELATIONSHIP
850   DISP "Calculating the values of Torque for frequencies F2,F3,F4,F5"
860   FOR I=2 TO 5
870     SELECT I
880  !************************
890  !  SELECTS A            *
900  !  FERQUENCY=F2         *
910  !************************
920     CASE 2
930       F=F2
940  !************************
950  !  SELECTS A            *
960  !  FERQUENCY=F3         *
970  !************************
980     CASE 3
990       F=F3
1000 !************************
1010 !  SELECTS A            *
1020 !  FERQUENCY=F4         *
1030 !************************
1040    CASE 4
1050      F=F4
1060 !************************
1070 !  SELECTS A            *
1080 !  FERQUENCY=F5         *
1090 !************************
1100    CASE 5
1110      F=F5
1120    END SELECT
1130    GOSUB Torque
```

```
1140  !**************************************************
1150  !         FORMATS DATA INTO CORRECT ARRAYS         *
1160  !**************************************************
1170    SELECT I
1180    CASE 2
1190      MAT Slip2= Slip
1200    CASE 3
1210      MAT Slip3= Slip
1220    CASE 4
1230      MAT Slip4= Slip
1240    CASE 5
1250      MAT Slip5= Slip
1260    END SELECT
1270  NEXT I
1280  PRINTER IS CRT
1290  DISP "EXECUTION COMPLETE"
1300  Graph_plot(Slip1(*),Slip2(*),Slip3(*),Slip4(*),Slip5(*))
                                 !PLOTS TORQUE/SPEED CURVES
1310  STOP
1320  !*******************************************************
1330  !              T O R Q U E   S U B R O U T I N E       *
1340  !*******************************************************
1350 Torque: !
1360  Eo1(1)=Eo(1)*F/50             !FIRST VOLTAGE APPROXIMATION
1370  Eo1(2)=0                       !NO IMAGINARY PART
1380  Z2(1)=(R2x)+(R2-R2x)*(F-Fx)/((50-Fx)^2)^.5
                                 !OBTAINS LINEAR ROTOR VOLTAGE
1390  PRINT "F=";F;"(Hz)"
1400  PRINT "R2'=";Z2(1);"(Ohms)"
1410  Tmax=0
1420  DISP "CALCULATING TORQUE/SPEED CURVE FOR F=";F
1430  !*******************************************************
1440  !  (1)CALCULATES TORQUE FOR A GIVEN FREQUENCY          *
1450  !  (2)CHECKS IF REQUIRED PEAK TORQUE HAS BEEN OBTAINED  *
1460  !  (3)IF NOT, THE LINE VOLTAGE IS INCREMENTED          *
1470  !  (4)IF YES, IT RETURNS TO THE MAIN PROGRAMME         *
1480  !*******************************************************
1490 Increment: !
1500  FOR X=100 TO 0 STEP -1
1510    Slips=X/100                  !SLIP FROM 0 TO 100 P.U.
1520    Z1(1)=R1                     !R1 REMAINS CONSTANT
1530    Z1(2)=X1*F/50                !X1 IS PROPORTIONAL TO FREQUENCY
1540    IF X>0 THEN
1550      Z2(1)=R2/Slips
1560    ELSE
1570      Z2(1)=1.0E+100             !R2'/S TENDS TO INFINITY AT S=0
1580    END IF
1590    Z2(2)=X2*F/50                !X2 IS PROPORTIONAL TO FREQUENCY
1600    Z3(1)=Rm                     !Rm REMAINS CONSTANT
1610    Z3(2)=Xm*F/50                !Xm IS PROPORTIONAL TO FREQUENCY
1620  !**********************************************
1630  !               INPUT IMPEDANCE                *
1640  !             Zo=Z1+(Z3*Z2)/(Z3+Z2)            *
1650  !**********************************************
1660    Complex_mult(Z3(*),Z2(*),Zr1(*))    !Z2*Z3 STORED IN ZR(1)
1670    Complex_add(Z3(*),Z2(*),Zr2(*))     !Z2+Z3 STORED IN ZR(2)
1680    Complex_div(Zr1(*),Zr2(*),Zr1(*))   !ZR1/ZR2 STORED IN ZR(1)
1690    Complex_add(Z1(*),Zr1(*),Zo(*))     !INPUT IMPEDENCE
1691    !
```

```
1692   !
1700  !***********************************************
1710  !      CALCULATION OF AIR-GAP VOLTAGE          *
1720  !***********************************************
1730    Complex_div(Eo1(*),Zo(*),Zr1(*))    !I1=Eo/Zo  I1 IN ZR(1)
1740    Complex_mult(Zr1(*),Z1(*),Zr1(*))   !I1*Z1
1750    Complex_sub(Eo1(*),Zr1(*),Zr1(*))   !E1 IN ZR(1)
1760  !***********************************************
1770  !     CALCULATES ROTOR CURRENT AND OUTPUT TORQUE  *
1780  !     Torque=3*(I2^2)*R2'/(Slip*Ws)              *
1790  !***********************************************
1800    Complex_div(Zr1(*),Z2(*),Zr1(*))    !I2 IN ZR(1)
1810    W=(Zr1(1)^2)+(Zr1(2)^2)             !I2 SQUARED
1820    IF X>0 THEN
1830      T=(3*W*R2*P)/(2*PI*F*Slips)       !TORQUE AT A GIVEN SLIP
1840    ELSE
1850      T=0                               !TORQUE=0 AT  S=0
1860    END IF
1870    !**********************************************
1880    !   FINDS Tmax FOR THIS NEW FREQUENCY AND       *
1890    !   CHECKS TO SEE IF IT IS LESS THAN THE TORQUE *
1900    !   FOR THE PRIMARY FREQUENCY.IF IT IS LESS     *
1910    !   IT INCREMENTS THE VOLTAGE AND REPEATS THE   *
1920    !   CALCULATION.WHEN THIS CONDITION HAS BEEN    *
1930    !   MET IT RETURNS TO THE MAIN PROGRAMME.       *
1940    !**********************************************
1950    IF T>Tmax THEN
1960      Tmax=T                          !FINDS NEW VALUE OF Tmax
1970    END IF
1980    Slip(1,X+1)=(1-Slips)*60*F/P      !SPEED VALUES IN RPM IN ARRAY
1990    Slip(2,X+1)=T                     !STORE TORQUE VALUE IN ARRAY
2000  NEXT X
2010  IF Tmax<Tmax1 THEN                  !COMPARES VALUES OF Tmax
2020    Eo1(1)=1.01*Eo1(1)                !VOLTAGE INCREMENT
2030    GOTO Increment
2040  END IF
2050  PRINT "V=";Eo1(1)*3^.5;"(VOLTS)"
2060  PRINT "Tmax";Tmax;"(Nm)"
2070  PRINT
2080  RETURN
2110  END
2120  !
2130  !*****************************************************************
2140  !               C O M P L E X      S U B R O U T I N E S
2150  !*****************************************************************
2160  SUB Complex_add(REAL A(*),B(*),Result(*))
2170    Result1=A(1)+B(1)      ! Real Components
2180    Result2=A(2)+B(2)      ! Imaginary Components
2190    Result(1)=Result1
2200    Result(2)=Result2
2210  SUBEND
2220  !
2230  !-----------------------------------------------------------------
2240  !
2250  SUB Complex_sub(REAL A(*),B(*),Result(*))
2260    Result1=A(1)-B(1)
2270    Result2=A(2)-B(2)
2280    Result(1)=Result1
2290    Result(2)=Result2
2300  SUBEND
```

```
2310  !
2320  !----------------------------------------------------------------------
2330  !
2340  SUB Complex_mult(REAL A(*),B(*),Result(*))
2350    Result1=A(1)*B(1)-A(2)*B(2)
2360    Result2=A(1)*B(2)+A(2)*B(1)
2370    Result(1)=Result1
2380    Result(2)=Result2
2390  SUBEND
2400  !
2410  !----------------------------------------------------------------------
2420  !
2430  SUB Complex_div(REAL A(*),B(*),Result(*))
2440    Result1=(A(1)*B(1)+A(2)*B(2))/((B(1))^2+(B(2))^2)
2450    Result2=(A(2)*B(1)-A(1)*B(2))/((B(1))^2+(B(2))^2)
2460    Result(1)=Result1
2470    Result(2)=Result2
2480  SUBEND
```

APPENDIX 3.1

A program for the spectral analysis of indeterminate waveforms using Discrete Fourier Transforms

```
10    !***********************************************************
20    !  THIS PROGRAM CALCULATES THE SPECTRUM OF A WAVEFORM        *
30    !  USING A DISCRETE FOURIER SERIES. IT ENTERS THE WAVEFORM   *
40    !  FROM A DATA FILE CALLED "NUMBERS".                        *
50    !***********************************************************
60    OPTION BASE 0
70    INPUT "ENTER THE START ADRESS OF THE WAVEFORM",S
80    INPUT "ENTER THE END ADRESS OF THE WAVEFORM",E
90    ALLOCATE Results(E-S)               !N SAMPLES
100   ALLOCATE Dummy(S-2)                 !ARRAY FOR REDUNDANT DATA
110   ALLOCATE Harmonic(1,30)             !UP TO THE 30th HARMONIC
120   N=E-S+1                             !NUMBER OF DATA POINTS
                                           IN THE WAVEFORM
130   ASSIGN @Path TO "NUMBERS"           !DECLARE I/O PATH
140   ENTER @Path;Dummy(*)                !OBTAIN DATA FROM DATA-FILE
150   ENTER @Path;Results(*)              !   "       "     "     "
160   PRINTER IS CRT
170   !************************************************
180   ! WAVEFORM NOW STORED IN "RESULTS" IN THE FORM   *
190   !             0,1,2,________________,N-1         *
200   !************************************************
210   DEG                                 !DEGREE MODE
220     Mag=0
230     FOR A=0 TO N-1 STEP 1
240     Mag=Results(A)+Mag
250     NEXT A
260     Co=Mag/N                          !D.C. COMPONENT
270     Harmonic(0,H)=Co
280   FOR H=1 TO 29 STEP 2                !ODD HARMONICS UP TO THE 29th HARMONIC
290     DISP "H=";H                       !HARMONIC NUMBER
300     Ah=0
310     Bh=0
320     Ch=0
330     O=360/N                           !ANGLE DIVISION
340     !******************************************
350     !   CALCULATION OF FOURIER CO-EFFICIENTS  *
360     !******************************************
370     Mag=0
380     FOR A=0 TO N-1 STEP 1
390       Mag=Results(A)*COS(O*A*H)
400       Ah=Ah+Mag
410     NEXT A
420     Ah=Ah/(N/2)
430     Mag=0
440     FOR B=0 TO N-1 STEP 1
450       Mag=Results(B)*SIN(O*B*H)
460       Bh=Bh+Mag
470     NEXT B
480     Bh=Bh/(N/2)
490     Ch=SQR(Ah^2+Bh^2)
500     Harmonic(0,H)=H                   !HARMONIC NUMBER INTO ARRAY
510     Harmonic(1,H)=Ch                  !HARMONIC MAGNITUDE INTO ARRAY
520   NEXT H
```

```
530   !*************************************************
540   !      FINDS NORMALIZING CO-EFFICIENT             *
550   !      AND NORMALIZES HARMONICS.                  *
560   !*************************************************
570   Norm=0
580   FOR I=0 TO 30 STEP 1
590     IF Harmonic(1,I)>Norm THEN
600       Norm=Harmonic(1,I)              !NORMALISING MAGNITUDE
610     END IF
620   NEXT I
630   FOR H=0 TO 30 STEP 1
640     Harmonic(1,H)=Harmonic(1,H)/Norm
650   NEXT H
660   GOSUB Graph_plot
670   END
```

APPENDIX 3.3.2

DERIVATION OF FOURIER COEFFICIENTS OF A THYRISTOR INVERTER CURRENT WAVEFORM USING THE SLONIM METHOD

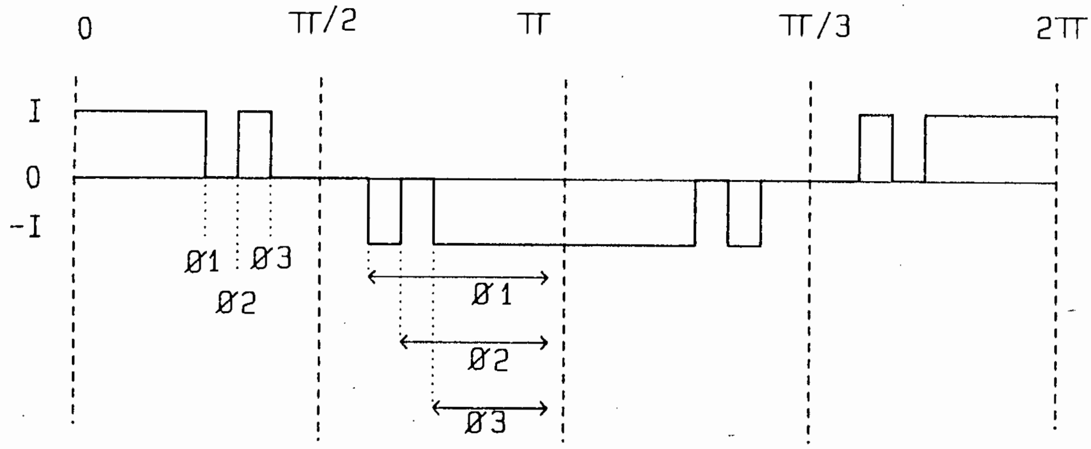

Figure 3.3.2A The Current of a Thyristor Inverter

From the derivation in Chapter 3.3.2A

$$F(k,t) = \frac{I}{jk\pi} \sum_{i=0}^{n-1} \Delta F(t_i) e^{-jkwt_i}$$

Applying this equation to a waveform of the type shown in Fig. 3.3.2A we get

$$\begin{aligned} I(k) = \frac{I}{jk\pi} - \quad & -e^{-jk\phi_1} + e^{-jk\phi_2} - e^{-jk\phi_3} \\ & - e^{-jk(\pi-\phi_3)} + e^{-jk(\pi-\phi_2)} - e^{-jk(\pi-\phi_1)} \\ & + e^{-jk(\pi+\phi_1)} - e^{-jk(\pi+\phi_2)} + e^{-jk(\pi+\phi_3)} \\ & + e^{-jk(3\pi-\phi_3)} - e^{-jk(2\pi-\phi_2)} + e^{-jk(2\pi-\phi_1)} \end{aligned}$$

After adding terms, Factorising and using the fact that

$$e^{-jk(2\pi-\phi_1)} = e^{jk\phi_1}$$

we obtain

$$I(k) = \frac{I(1-e^{-jk\pi})}{jk\pi} \quad e^{jk\phi_1} - e^{-jk\phi_1} + e^{-jk\phi_2} - e^{-jk\phi_2} + e^{jk\phi_3} - e^{-jk\phi_3}$$

$k = 0, 1, 2, 3 \ldots\ldots\ldots$

This can be written more concisely as

$$I(K) = \frac{4I}{k\pi} \quad (\mathrm{Sin}\ k\phi_1 - \mathrm{Sin}\ k\ \phi_2 + \mathrm{Sin}\ k\ \phi_3)$$

$k = 2V + 1;$

$V = 0, 1, 2, 3 \ldots\ldots\ldots$

This implies all even harmonics are zero.

APPENDIX 4.1

DETAILED CIRCUIT INTERCONNECTION DIAGRAM OF COMPLETE SYSTEM

Component Listing

	Part No./Value	Manufacturer
D1 to D6	SKKD 81 14	Semikron
DS1 to D56	D21S1200	AEG
DF1 to DF6	D52SR1200	AEG
D7	Si 250	ASEA
D8	1N4007	
GTO1 to GTO6	G200A 1200/ GG90R 1100	AEG
SCR1	71REB 120	International Rectifier
RS1 to RS6	27Ω 50w	CGS
R1 and R2	7500Ω 50w	
R3	12Ω 50w	
CS1 to CS6	2x0,22μF 1500$V_{D.C.}$/ 3x0,01μF 1500$V_{D.C.}$	
C1 to C4	4000 μF, 450 $V_{D.C.}$	L.C.R.
F1	50A 5SD4	Siemens
F2	1A	
L1	500 μH	
SH	2,64 mΩ	
Speed Reference	10k	
K1	CS3	
K2	CA3-23	
KT1	CZE3	

APPENDIX 4.2

CONTROLLER POWER SUPPLY CIRCUIT DIAGRAM

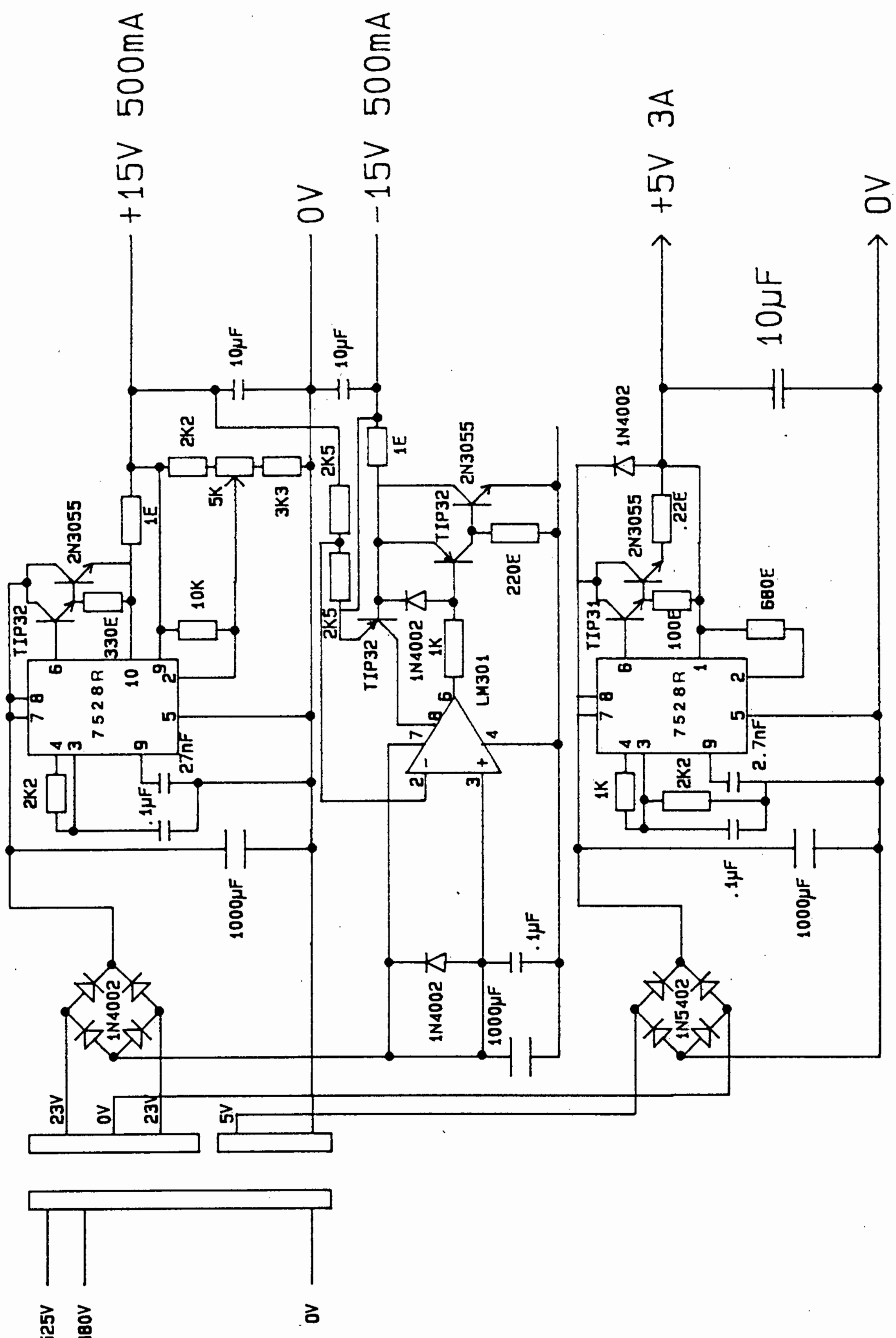

APPENDIX 5.4.1

GTO TECHNICAL SPECIFICATIONS

Electrical properties

	Maximum permissible values			
U_{DRM}	repetitive peak forward off-state voltage	u_{RG} = 5 V oder/or $R_{GK} \le 100\ \Omega$	1200	V
U_{RRM}	repetitive peak reverse voltage		13	V
U_{RGB}	peak reverse gate volatge		13	V
I_{TQRM}	repetitive controllable on-state current	t_{vj} = 125°C; $u_{DP} \le 350$ V; $du_D/dt \le 400$ V/µs; u_{DM} = 0,75 U_{DRM}; u_{LR} = 12 V; L_G = 0,4 µH	200	A
I_{TQSM}	non-repetitive controllable on-state current	t_{vj} = 125°C; $u_{DP} \le 500$ V; $du_D/dt \le 500$ V/µs; u_{DM} = 0,75 U_{DRM}; U_{LR} = 12 V; L_G = 0,4 µH	280	A
I_{TSM}	surge current	t = 10 ms, t_{vj} = 45°C	330	A
		t = 10 ms, t_{vj} = 125°C	300	A
$\int i^2dt$	$\int i^2dt$-rating	t = 10 ms, t_{vj} = 45°C	540	A^2s
		t = 10 ms, t_{vj} = 125°C	440	A^2s
$(di/dt)_{cr}$	critical rate of rise of on-state current	Dauerbetrieb/continuous operation, t_{vj} = 125°C; i_{TM} = 200 A; f_c = 50 Hz; $u_D \le 800$ V; Steuergenerator/pulse generator: i_{FG} = 8 A, di_{FG}/dt = 4 A/µs, $t_{fg} \ge 10$ µs	200	A/µs
$(du/dt)_{cr}$	critical rate of rise of off-state voltage		1000	V/µs
	Characteristc values			
u_T	max. on-state voltage	t_{vj} = 125°C, i_T = 200 A, ohne Steuerstrom/without trigger current	4,1	V
U_{GT}	max. gate trigger voltage	t_{vj} = 25°C, u_D = 12 V, R_A = 1 Ω	1,5	V
I_{GT}	max. gate trigger current	t_{vj} = 25°C, u_D = 12 V, R_A = 1 Ω	600	mA
I_H	typical holding current	t_{vj} = 25°C, u_D = 12 V, R_A = 1 Ω	4	A
I_L	typical latching current	t_{vj} = 25°C, u_D = 12 V, $R_{GK} \ge 20\ \Omega$; Steuergenerator/pulse generator: i_{FG} = 8 A, di_{FG}/dt = 4 A/µs, t_{fg} = 10 µs	6	A
t_{gd}	typical gate controlled delay time	t_{vj} = 25°C; i_{TM} = 20 A; u_D = 800 V; Steuergenerator/pulse generator: i_{FG} = 8 A, di_{FG}/dt = 4 A/µs	1	µs
t_{dq}	typical gate controlled storage time	t_{vj} = 125°C; i_{TM} = 200 A; $u_{DP} \le 350$ V; $du_D/dt \le 400$ V/µs; U_{DM} = 0,75 U_{DRM}; Steuergenerator/pulse generator: u_{LR} = 12 V; L_G = 0,4 µH	4	µs
t_{fq}	typical gate controlled fall time		0,8	µs
t_{gq}	max. gate controlled turn-off time		6,5	µs
I_{RGM}	typical reverse gate current		65	A
I_{TQT}	typical tail current		28	A
t_{tq}	typical tail time		5	µs
	Thermal properties			
R_{thJC}	thermal resistance junction to case	θ = 180°el, trapezförmiger Stromverlauf/trapezoidal current waveform	≤ 0,35°C/W	
	operating temperature		- 40°C…+ 125°C	
	storage temperature		- 40°C…+ 130°C	
	Mechanical properties			
	weight		93 g	

Electrical properties

Maximum permissible values

Symbol	Parameter	Conditions		Value	Unit
U_{DRM}	repetitive peak forward off-state voltage	u_{RG} = 5 V oder/or $R_{GK} \leq$ 300 Ω		1100	V
U_{RRM}	repetitive peak reverse voltage		A:	13	V
			R:	–	V
U_{RGE}	peak reverse gate voltage			13	V
I_{TRMSM}	RMS on-state current			22	A
I_{TQRM}	repetitive controllable on-state current	t_{vj} = 125°C; $u_{DP} \leq$ 350 V; $du_D/dt \leq$ 800 V/μs; u_{DM} = 0,75 U_{DRM}; u_{LR} = 12 V; L_G = 1 μH		90	A
I_{TQSM}	non-repetitive controllable on-state current	t_{vj} = 125°C; $u_{DP} \leq$ 500 V; $du_D/dt \leq$ 800 V/μs; u_{DM} = 0,75 U_{DBM}; U_{LR} = 12 V; L_G = 1 μH		180	A
I_{TAVM}	average on-state current	t_C = 85°C; Θ = 180° el, trapezförmiger Stromverlauf/trapezoidal current waveform		21	A
I_{TSM}	surge current	t = 10 ms, t_{vj} = 45°C		270	A
		t = 10 ms, t_{vj} = 125°C		245	A
$\int i^2 dt$	$\int i^2 dt$-rating	t = 10 ms, t_{vj} = 45°C		365	A^2s
		t = 10 ms, t_{vj} = 125°C		300	A^2s
$(di/dt)_{cr}$	critical rate of rise of on-state current	Dauerbetrieb/continuous operation, t_{vj} = 125°C; i_{TM} = 90 A; f_o = 50 Hz; $u_D \leq$ 800 V; Steuergenerator/pulse generator: i_{FG} = 4 A, di_{FG}/dt = 4 A/μs, $t_{fg} \geq$ 10 μs		200	A/μs
$(du/dt)_{cr}$	critical rate of rise of off-state voltage			**1000**	V/μs

Characteristic values

Symbol	Parameter	Conditions	Value	Unit
u_T	max. on-state voltage	t_{vj} = 125°C, i_T = 90 A, ohne Steuerstrom/without trigger current	3,1	V
$U_{(TO)}$	threshold voltage		1,3	V
r_T	slope resistance		19	mΩ
U_{GT}	max. gate trigger voltage	t_{vj} = 25°C, u_D = 12 V, R_A = 2 Ω	1,5	V
I_{GT}	max. gate trigger current	t_{vj} = 25°C, u_D = 12 V, R_A = 2 Ω	600	mA
I_H	typical holding current	t_{vj} = 25°C, u_D = 12 V, R_A = 2 Ω	1,2	A
I_L	typical latching current	t_{vj} = 25°C, u_D = 12 V, $R_{GK} \geq$ 20 Ω; Steuergenerator/pulse generator: i_{FG} = 4 A, di_{FG}/dt = 4 A/μs, t_{fg} = 10 μs	3,6	A
i_D	max. forward off-state current	t_{vj} = 125°C, u_D = U_{DRM}; u_{RG} = 5 V oder/or $R_{GK} \leq$ 300 Ω	8	mA(A)
			15	mA(R)
t_{dg}	max. gate controlled delay time	t_{vj} = 25°C; i_{TM} = 10 A; u_D = 800 V; Steuergenerator/pulse generator: i_{FG} = 4 A, di_{FG}/dt = 4 A/μs	2	μs
t_{dq}	typical gate controlled storage time	t_{vj} = 125°C; i_{TM} = 90 A; $u_{DP} \leq$ 350 V; $du_D/dt \leq$ 800 V/μs; U_{DM} = 0,75 U_{DRM}; u_{LR} = 12 V; L_G = 1 μH	3,7	μs
t_{fq}	typical gate controlled fall time		0,8	μs
t_{gq}	max. gate controlled turn-off time		6	μs
I_{RGM}	typical reverse gate current		28	A
I_{TQT}	typical tail current		14	A
t_{tq}	typical tail time		5	μs
C_{null}	typical zero capacitance	t_{vj} = 25°C; f = 10 kHz	1,5	nF
U_{ISOL}	insulation test voltage		2,5	kV

Thermal properties

Symbol	Parameter	Conditions		Value
R_{thJC}	thermal resistance, junction to case	Θ = 180°el, trapezförmiger Stromverlauf/trapezoidal current waveform	pro Baustein/per unit	$\leq$ 0,44°C/W
			pro Zweig/per branch	$\leq$ 0,88°C/W
		DC	pro Baustein/per unit	$\leq$ 0,36°C/W
			pro Zweig/per branch	$\leq$ 0,72°C/W
R_{thCK}	thermal resistance, case to heatsink	pro Baustein/per unit		0,1 °C/W
		pro Zweig/per branch		0,2 °C/W
	operating temperature			–40°C . . . + 125°C
	storage temperature			–40°C . . . + 130°C

Mechanical properties

weight	160 g
tightening torques	4 Nm

APPENDIX 5.5

DCCT THEORY AND DESIGN

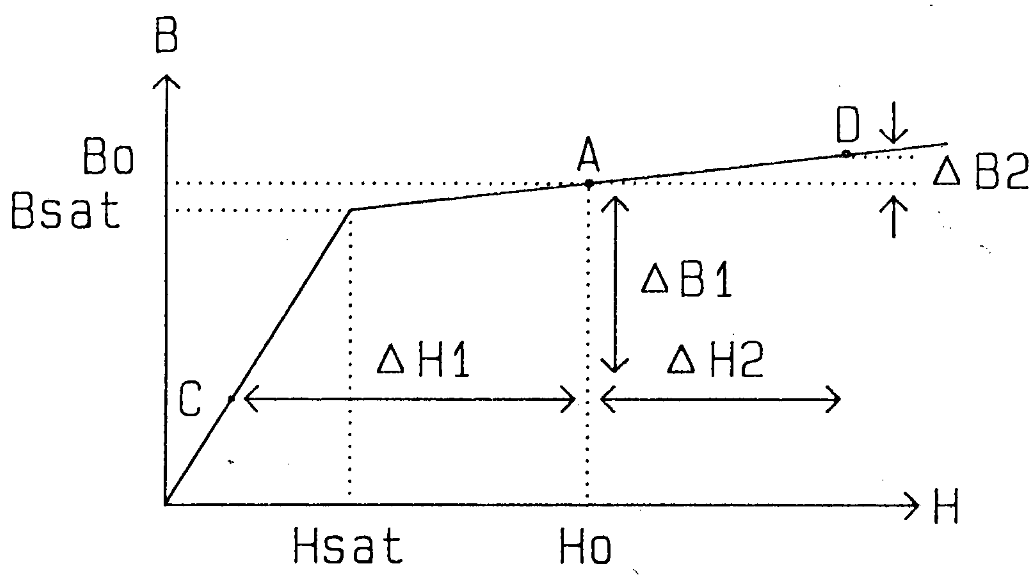

Figure A5.1 Simplified B/H Characteristic

Referring to Fig. 5.1 in chapter 5, the primary current produces a magnetic field strength within each toroid of magnitude.

$$H = \frac{N_p \; I_p}{L_e}$$

Where N_p is the number of primary turns, I_p is the primary current and L_e the toroid effective magnetic path. The magnitude of H sets the operating point "C" on the B/H curve, while the current direction sets the operating quadrant. For simplicity sake the following discussion will assume I_p is a D.C. current and hysteresis is omitted from the B/H curve. This is shown in Fig. A5.1.

By applying a pulsed voltage waveform of known magnitude $V(t)$ there is a resultant change of flux density ΔB

$$\Delta B = \Delta B_1 + \Delta B_2 = \frac{V(t)}{N_s A_e}$$

where A_e is the effective area of the magnetic path of the toroid, N_s is the number of secondary turns/toroid, ΔB_1 is the change in flux density in toroid 1 and ΔB_2 is the change in flux density in toroid 2. ΔB_1 and ΔB_2 are in different directions. Since the two toroids are in series the secondary currents must be equal. Therefore

$$\Delta H_1 = \Delta H_2 = \frac{N_s I_s}{L_e}$$

where I_s is the secondary current in both toroids. This moves the operating point of toroid 2 from point A to point D, which is deeper into saturation region, while toroid 1 becomes unsaturated moving from point A to point C. It is assumed that H_o is much greater than H_{sat} and that the relative permeability, μ_r, is large, then H_o is approximately equal to ΔH_1.
However

$$H_o = \frac{N_p I_{p(o)}}{L_e}$$

where $I_{p(o)}$ is the value of the primary current producing a magnetic field strength H_o, and

$$\Delta H_1 = \frac{N_s I_{s(pk)}}{L_e}$$

Where $I_{s(pk)}$ is the peak value of secondary current which occurs at point C, corresponding to the end of the applied voltage pulse. Therefore

$$\frac{N_p I_{p(o)}}{L_e} = \frac{N_s I_{s(pk)}}{L_e}$$

or $$I_{s(pk)} = \frac{N_p}{N_s} I_{p(o)}$$

The value of the secondary current at the operating point C is therefore proportional to the primary current. The reverse process occurs when the direction of the primary current changes. Thus by detecting the peak value of the secondary current a signal V_o, proportional to the primary current is obtained. Thus a DCCT provides an isolated signal which is proportional to the modulus of the amplitude of the instantaneous current being measured.

For linear operation H_o cannot be less than H_{sat}, so that the minimum value of primary current which can be measured with reasonable linearity is given by

$$I_{p(min)} = \frac{H_{sat} L_e}{N_p}$$

The upper limit on primary current required for linear operation is determined by the need for point C to be in the unsaturated region of the B/H curve. For this requirement it can be shown

$$I_{p(max)} = \left[H_{sat} + \frac{\Delta B}{2\mu_o}\right] \frac{L_e}{N_p}$$

The bandwidth of the DCCT is inversely proportional to the switching frequency. The Sampling Theorem dictates that to resolve a frequency f, requires a frequency of at least 2f. In practice a factor of 10 is used to give reasonable waveform fidelity.

APPENDIX 5.5(b)

DESIGN OF DCCT'S

Fig. A5.2 gives the full DCCT circuit design, including the pulsing circuit. The pulsing circuit which has a switching frequency of 63 kHz. A mark period of 6 μSec and a space period of 11,4 μSec is generated by the pulsing circuit.

Of all the available types, Philips Grade 3E2 Toroids were the most suitable. From the technical data

H_{sat}	=	300	(A/m)
B_{sat}	=	360	(m/T)
ΔB	=	250	(mT)
μ_o	=	$1,257 \times 10^{-6}$	(H/m)
L_e	=	57 mm	
Inner diameter	=	14 mm	
Outer diameter	=	23 mm	

The calculation of the operating range and the number of turns for both primary and secondary is very much governed by physical constraints. The physical size of the toroid is generally the limiting factor. The operating range is determined by trying values of primary current and calculating winding the requirements.

Using $12 \leq I_p \leq 30$ amps

$$I_{s(max)} = 0,2 \text{ amps}$$

$$\delta = \frac{\text{Mark period of pulse the waveform}}{\text{total period of pulse the waveform}}$$

$$= \frac{6}{17,4} = 0,345$$

the number of turns on the primary and secondary can be calculated

$$Np \geq \frac{H_{sat}\,L_e}{I_{p(min)}} = 1,42$$

Taking Np = 1

$$N_s = \frac{N_p}{I_s} \times \sqrt{\delta} \times I_{p(max)} = 88 \text{ Turns}$$

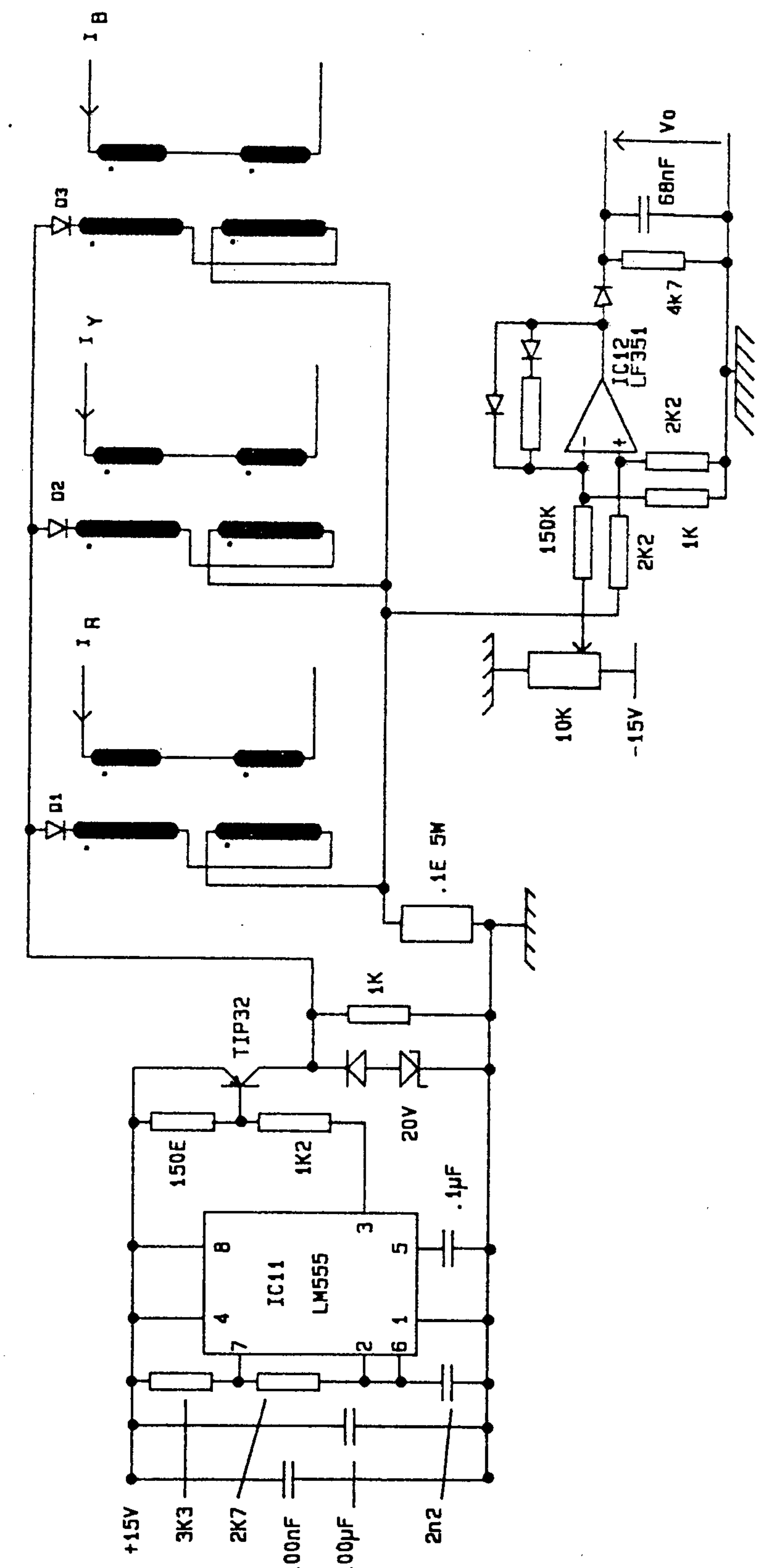

Figure A5.2 Complete DCCT Circuit Diagram

APPENDIX 6.5

CONTROL BOARD 1

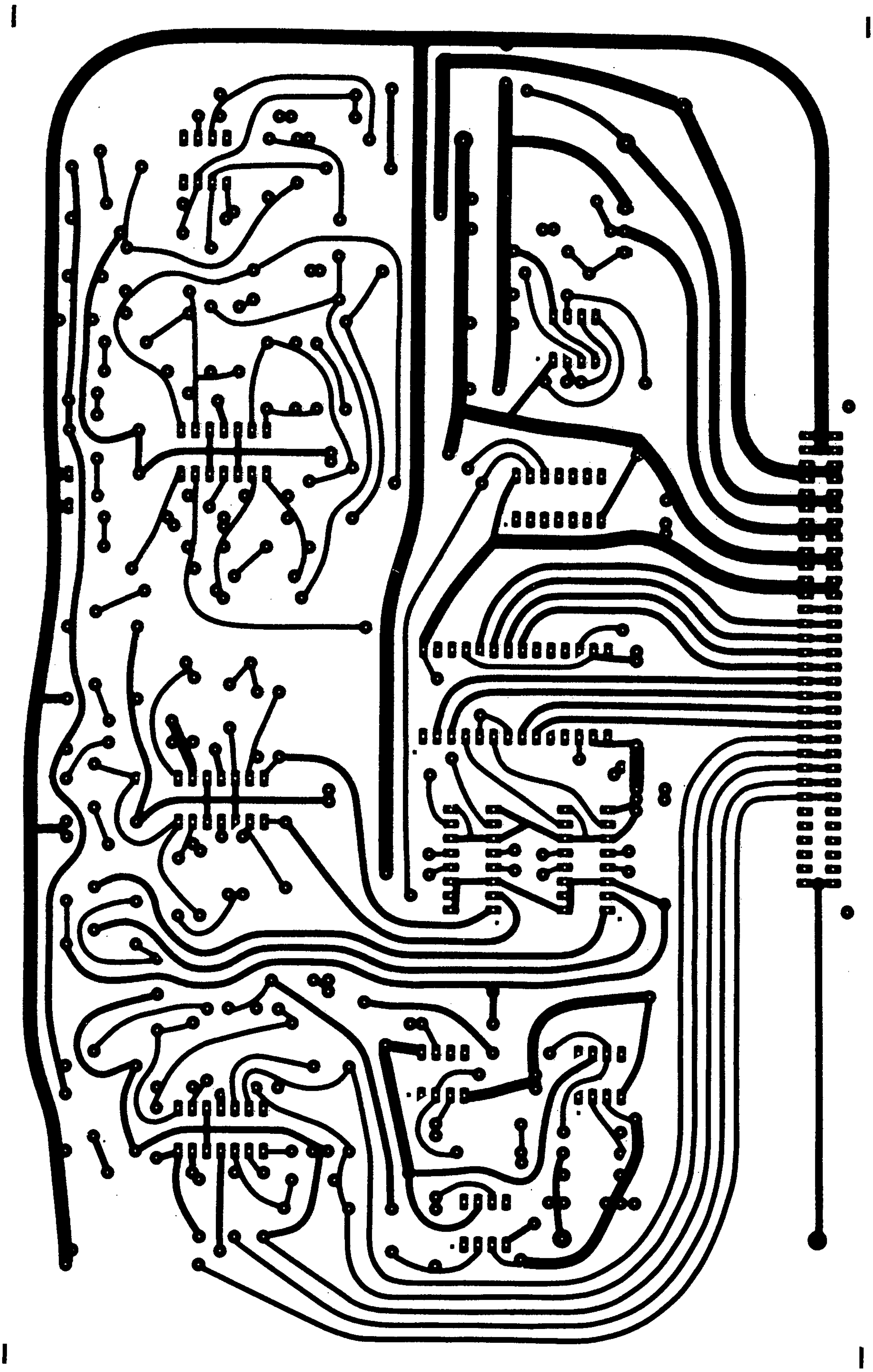

CONTROL BOARD 1 Printed Circuit Board Layout

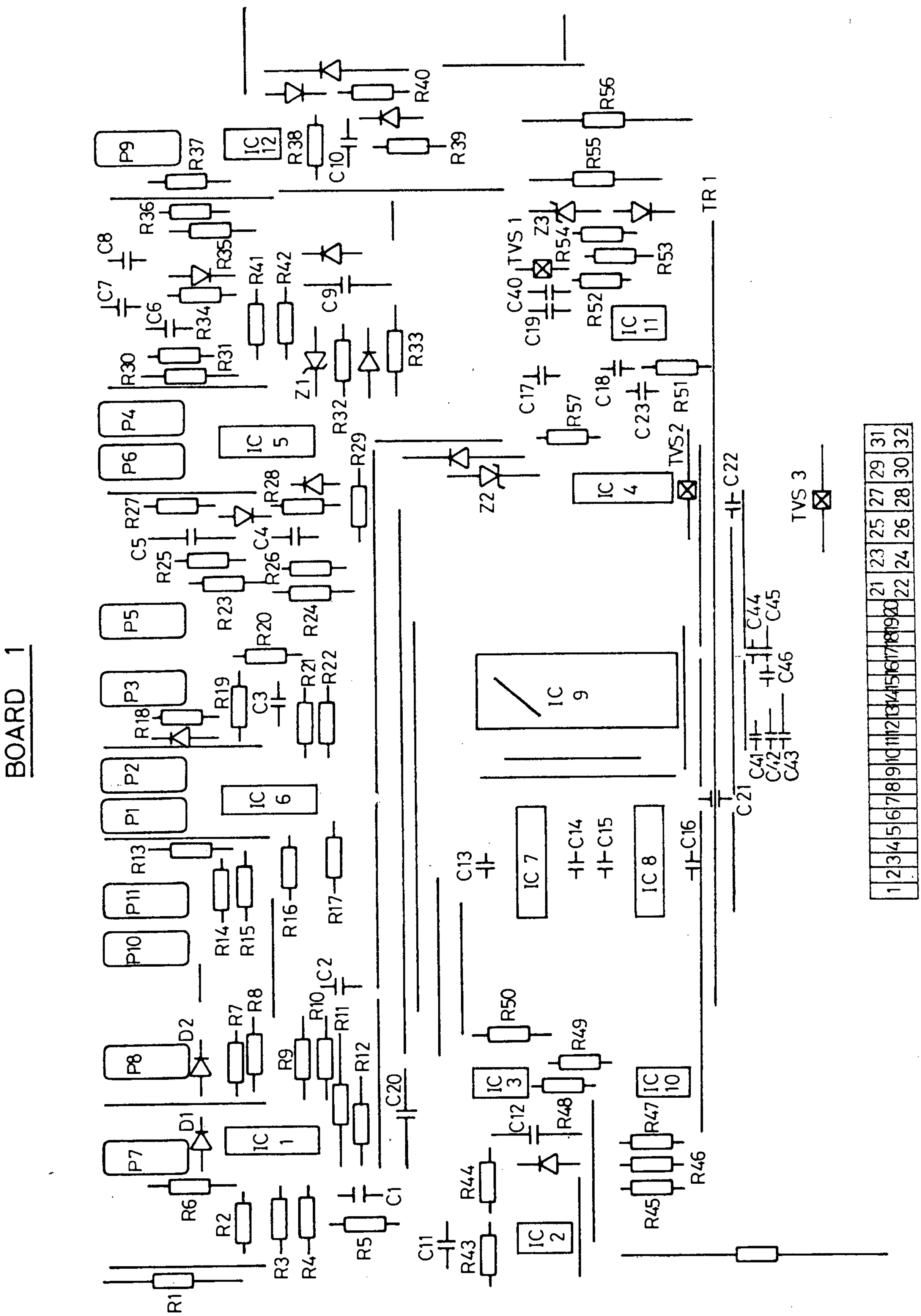

CONTROL BOARD 1 Component Layout

CONTROL BOARD 1 Edge Connector

Pin Number	Connection	
1	V_{cb}	
7	1	
8	2	10K Speed Potentiometer
9	3	
10	A1	
11	A2	
12	ORM2	
13	ORM1	
14	OBM1	
15	OBM2	
16	OYM2	
17	OYM1	
18	RSYN	
19	Enable	
21 and 22	+ 5 Volts	
23 and 24	0 Volts	
25 and 26	DC1	
27 and 28	DC2	
29 and 30	- 15 Volts	
31 and 32	+ 15 Volts	

CONTROL BOARD 1 Component Listing

R1	12K	R31	330K	TR1	TIP32C
R2	10K	R32	560K	TVS1	15V
R3	10K	R33	820K	TVS2	5V
R4	10K	R34	330K	TVS3	15V
R5	10K	R35	2K2		
R6	10K	R36	1K	Z1	5,1V
R7	10K	R37	150K	Z2	5,1V
R8	10K	R38	4K7	Z3	20V
R9	10K	R39	2K2		
R10	2M2	R40	10K		
R11	10K	R41	33K		
R12	10K	R42	33K		
R13	10K	R43	2M2		
R14	10K	R44	10K		
R15	10K	R45	2K7		
R16	18K	R46	10K		
R17	22K	R47	10K		
R18	10K	R48	10K		
R19	10K	R49	33K		
R20	10K	R50	1K		
R21	33K	R51	2K7		
R22	10K	R52	3K3		
R23	33K	R53	1K2		
R24	33K	R54	150Ω		
R25	330K	R55	1K		
R26	330K	R56	0,1Ω 5W		
R27	330K	R57	47K		
R28	330K				
R29	560K				
R30	33K				

All resistors are ¼w unless otherwise stated

C1	0,47 µf	IC1	LF347N
C2	0,47 µF	IC2	LF357N/MC34001P
C3	0,47 µF	IC3	LM311N
C4	0,47 µF	IC4	7404N
C5	0,22 µF	IC5	LF347N
C6	0,47 µF	IC6	LF347N
C7	20 µF Tant	IC7	74LS629N
C8	20 µF Tant	IC8	74LS629N
C9	0,68 µF	IC9	HEF4752VD
C10	68 nF	IC10	LF351/MC34001P
C11	0,47 µF	IC11	LM555CN
C12	0,68 µF	IC12	LF351N
C13	680 pF		

C14	1,2 nF	P1	10K	Region of Base-Boost
C15	680 pF	P2	10K	Base-Boost
C16	620 pF	P3	10K	100% modulation setting
C17	100 µF	P4	10K	$I_{M(ref)}$
C18	2,2 nF	P5	10K	$I_{g(ref)}$
C19	100 nF	P6	10K	$V_{cb(ref)}$
C20	0,68 µF	P7	10K	Deceleration
C21	10 nF	P8	10K	Acceleration
C22	10 µF tant	P9	10K	DCCT Zero offset
C23	100 nF	P10	10K	OCT
		P11	10K	RCT
C40	15 µF tant			
C41	47 pF			
C42	47 pF			
C43	47 pF			
C44	47 pF			
C45	47 pF			
C46	47 pF			

APPENDIX 6.9

CONTROL BOARD 2

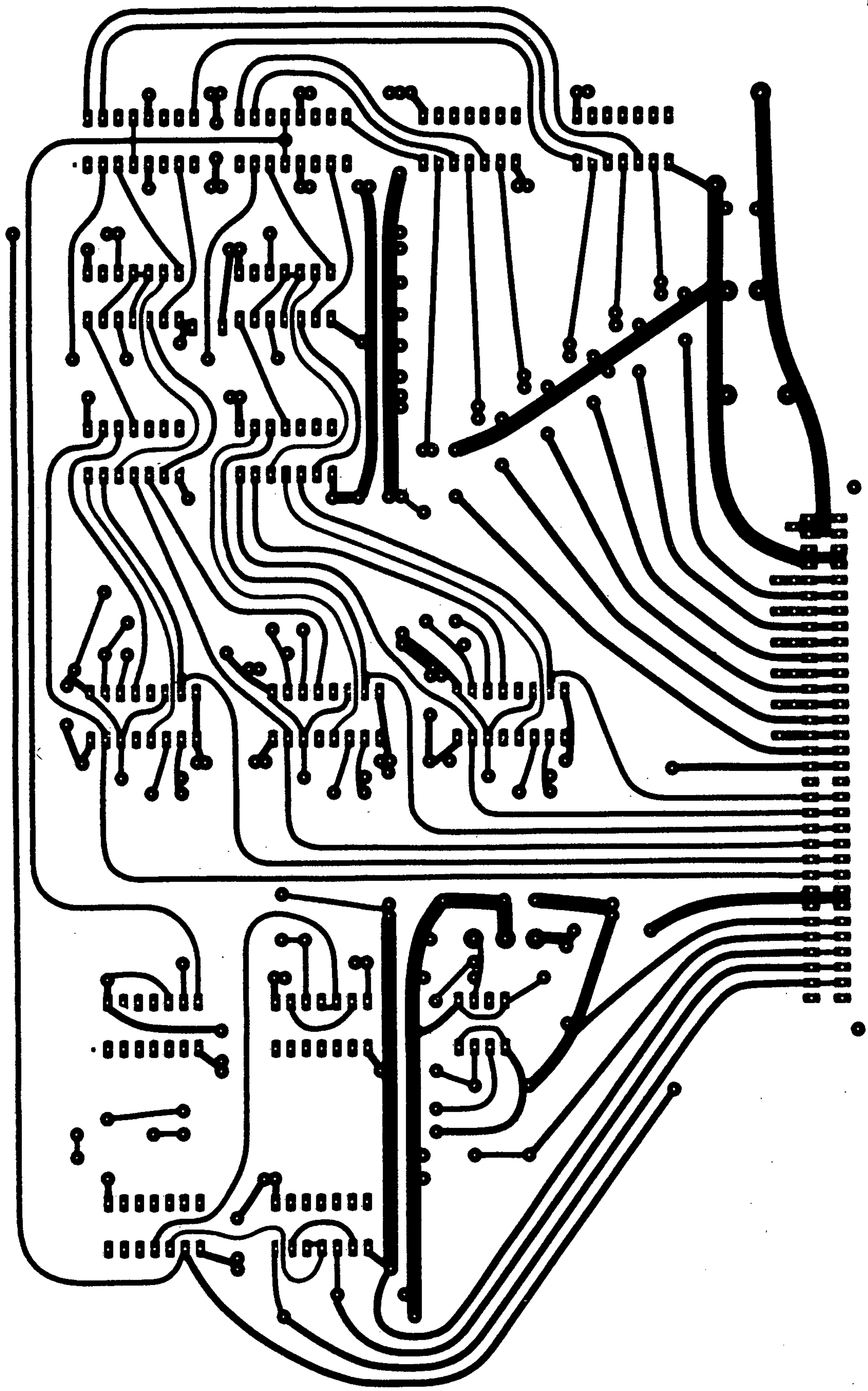

CONTROL BOARD 2 Printed Circuit Board

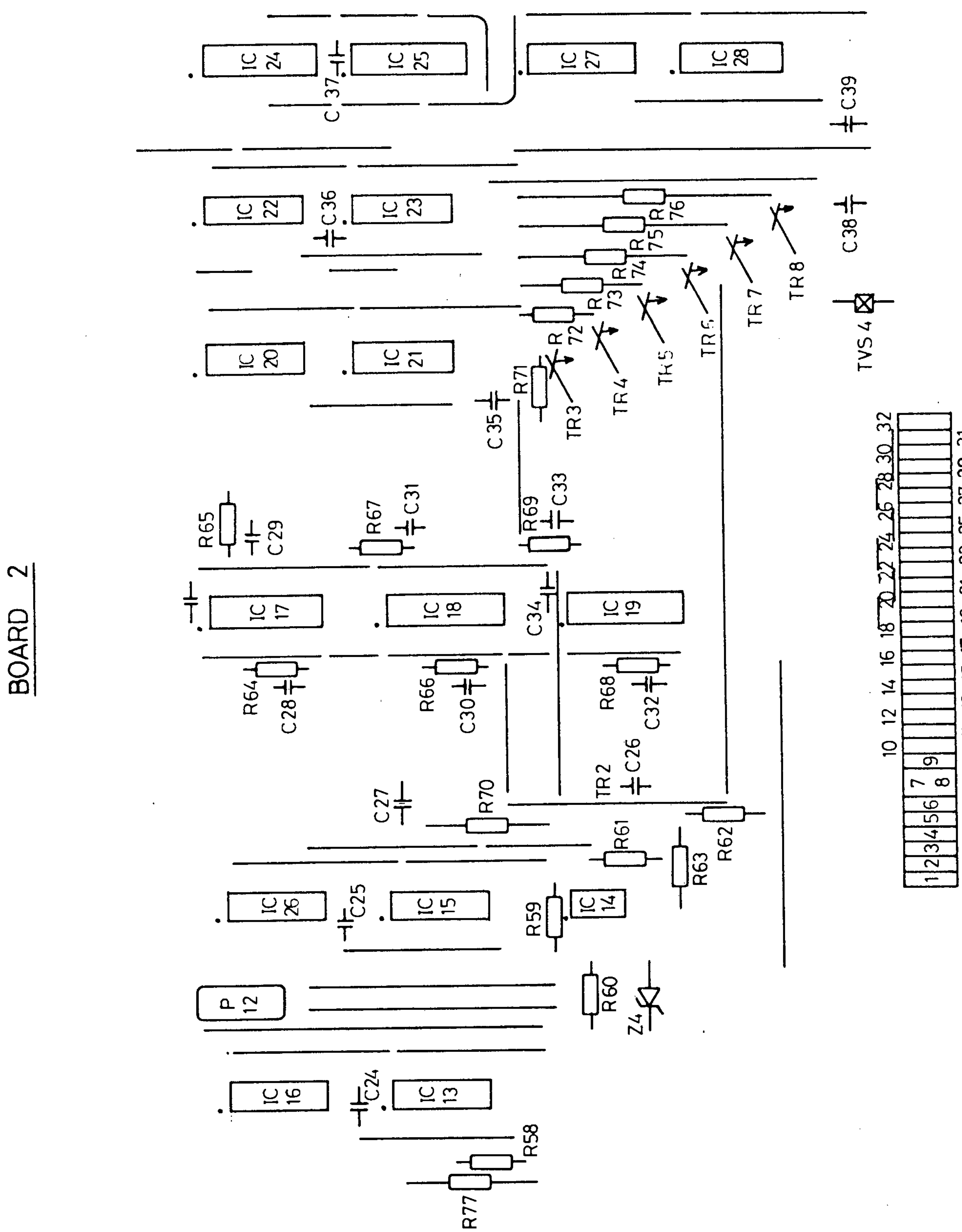

CONTROL BOARD 2 Component Layout

CONTROL BOARD 2 Edge Connector

Pin Number	Connection
2	A
3	C Start relay
4	B
5	S1
6	S2 Shunt connection
7 and 8	Crowbar Thyristor Gate
9	IRM2
10	IRM1
11	IBM1
12	IBM2
13	IYM2
14	IYM1
16	ENABLE
17	- Y1
18	+ Y1
19	- Y2
20	+ Y2
21	- B2
22	+ B2
23	- B1
24	+ B1
25	- R1
26	+ R1
27	- R2
28	+ R2
29 and 30	0 Volts
31 and 31	+ 5 Volts

CONTROL BOARD 2 Component Listing

R 57	1K	C24	10nF
R58	1K	C25	10nF
R59	10K	C26	15 μF Tant
R60	100Ω	C27	10 μF
R61	560 Ω	C28	10nF
R62	10 Ω ½W	C29	10nF
R63	100 Ω ½W	C30	10nF
R64	4K7	C31	10nF
R65	4K7	C32	10nF
R66	4K7	C33	10nF
R67	4K7	C34	10nF
R68	4K7	C35	15 μF Tant
R69	4K7	C36	10nF
R70	120 Ω	C37	10nF
R71	820 Ω	C38	100 μF
R72	820 Ω	C39	15 μF Tant
R73	820 Ω		
R74	820 Ω		
R75	820 Ω	Z4	5V
R76	820 Ω	TVS4	5V

All resistors ¼w unless stated

P12. 10k (Crowbar trip threshold)

TR2	TIP 31C
TR3	2N2222C
TR4	2N2222C
TR5	2N2222C
TR6	2N2222C
TR7	2N2222C
TR8	2N2222C

IC 13	7400N
IC 14	LM 311
IC 15	7402N
IC 16	7408N
IC 17	74221N
IC 18	74221N
IC 19	74221N
IC 20	7432N
IC 21	7432N
IC 22	7408N
IC 23	7408N
IC 34	7475N
IC 25	7475N
IC 26	7486N
IC 27	7417N
IC 28	7417N

APPENDIX 7.5

GATE DRIVE CIRCUIT

GATE DRIVE CIRCUIT COMPONENT LISTING

R1	22K	C_1	1000 μF 25V
R2	200 Ω	C_2	1000 μF 25V
R3	5K6	C_3	10 nF
R4	1K5	C_4	10 nF
R5	10K	C_5	2,2 μF 25V
R6	15K	Z_1	3V
R7	10K	Z_2	3V
R8	100K		
R9	100K	D_1	IN 4007
R10	30K	D_2	IN 4007
R11	5K1	D_3	IN 4007
R12	300 Ω	D_4	IN 4007
R13	300 Ω	D_5	IN 4007
R14	51K		
R15	10 Ω 5w OC1		4N25
R16	66K		
R17	33K	BR1	PK 80F
R18	4K7		
R19	47 Ω	SCR1	S600 8D
R20	10 Ω		
R21	10K	L_6	1 μH
R22	5,1Ω		
R23	100 Ω	F	2A
R24	22 Ω 5w		
R25	3,3 Ω 5w		

All resistors are ¼ w unless otherwise stated

Q_1	2N3703	Q_9	2N6292
Q_2	2N3704	Q_{10}	2N6292
Q_3	2N3704		
Q_4	2N3704		
Q_5	2N3704		
Q_6	2N3704		
Q_7	MPSA56		
Q_8	MPSA12		

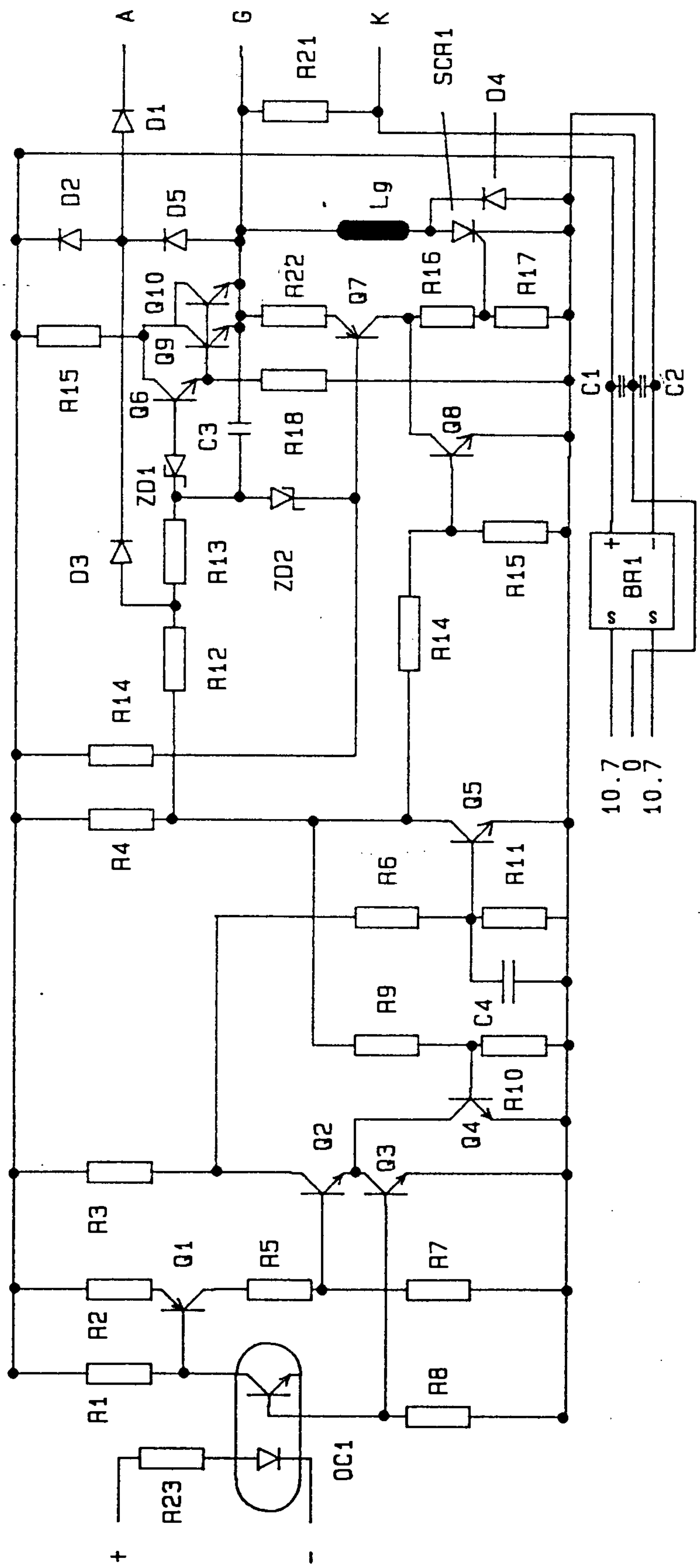

Narrow Pulse Gate Drive Circuit

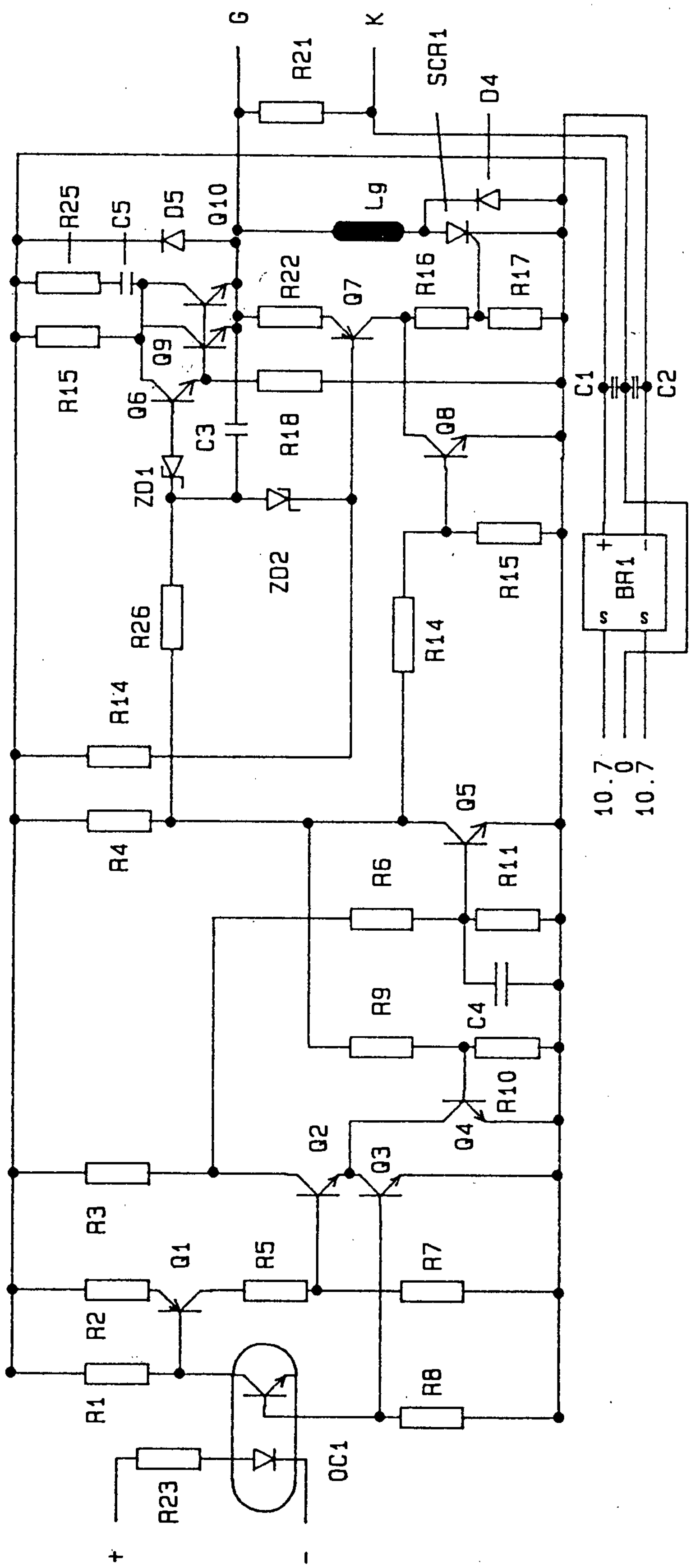

Block Firing Gate Drive Circuit

15 DEC 1986